Some studies of donor-acceptor systems and the ortho-parahydrogen conversion on transition metal salts.

A thesis presented for the

Degree of Doctor of Philosophy

in the

Faculty of Science

by

MICHAEL FRANCIS FARMER

University of Leicester

October 1967

ProQuest LLC
789 East Eisenhower Parkway
P.O. Box 1346
Ann Arbor, MI 48106-1346

STATEMENT

The experimental work in this thesis has been carried out by the author in the Department of Chemistry of the University of Leicester between October 1964 and October 1967 under the supervision of Dr. K. M. C. Davis. This work has not been presented and is not being concurrently presented for any other degree.

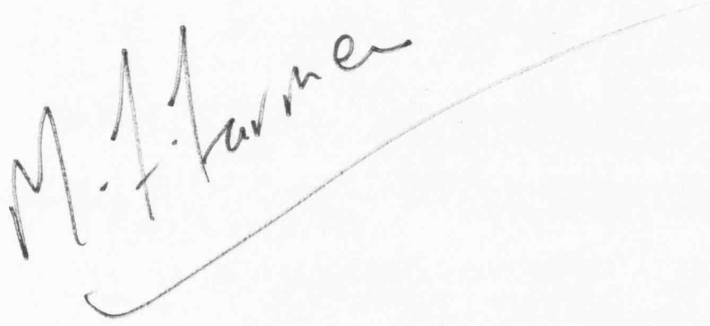

October 1967.

ACKNOWLEDGEMENTS

Firstly my sincere thanks go to my supervisor, Dr. K. M. C. Davis, for his constant help, patience, guidance and encouragement throughout this work.

I should like to extend my thanks to all those who have helped to make this thesis possible and especially to the members of the Department of Chemistry, University of Leicester, for their interest and assistance. In particular I am grateful to the technicians of the Department in the engineering and glass-blowing workshops for their continual patience. I also extend my thanks to Mr. Brivati for supplying the Brivastat.

I am very grateful to Mrs.J. Kempston and my mother for the many hours spent typing this thesis.

Finally, I would like to thank the Science Research Council for a maintenance grant enabling me to carry out this research.

DEDICATION

I would like to dedicate my thesis to my vacuum rig which obliged me by staying in one piece for a period long enough to obtain some results and also to the numerous science fiction authors who have kept me sane during the last three years.

SUMMARY

This thesis is presented in two parts. Part one deals with a study of donor-acceptor systems in both the solid and solution phases using spectroscopic techniques and part two contains an investigation of the catalytic properties of the first row transition metal salts towards the ortho-parahydrogen and hydrogen-deuterium exchange reactions.

An introduction to donor-acceptor complexes and the theoretical treatments of such complexes has been included. It has been suggested that in solid complexes in which there is a strong donor (D) and strong acceptor (A) of electrons that the neutral species DA and the dative species $D^{+}A^{-}$ can exist simultaneously. This postulate has been tested using complexes of N,N,N',N'-tetramethyl-p-phenylenediamine with a series of strong acceptors and found to be false, and the explanation of why the DA and $D^{+}A^{-}$ species do not exist together in the solid state is discussed.

The use of halogenomethanes as acceptors in donor-acceptor complexes has been examined using aromatic amines and condensed hydrocarbons as donors. The general belief that these "contact" donor-acceptor complexes should give characteristic absorption peaks is criticised. The results obtained show that instead of

a new absorption peak characteristic of the complex there is a broadening of one of the donor peaks which could lead to an incorrect interpretation of the spectra. The merits of the Benesi-Hildebrand equation when applied to weak donor-acceptor complexes is discussed with special reference to the role of the solvent in complex formation and an attempt has been made to establish the true nature of the interaction in these donor-acceptor systems.

An investigation of the catalytic properties of the first row transition metal divalent sulphates and chlorides to the ortho- parahydrogen conversion using thermal conductivity and mass spectroscopic techniques has shown that the conversion over the temperature range 77°-300°K is purely physical in nature. The theoretical treatments for this type of conversion are thoroughly discussed and a mechanism for the conversion on the salts examined is suggested. Calculations based on the suggested mechanism have been made and found to favourably fit the experimental results obtained.

C O N T E N T S

PART ONE

Some studies of the ultra-violet and visible absorption spectra of donor-acceptor systems in the solid state and in solution.

PART TWO

An investigation of the catalytic properties of the first transition metal salts to the ortho-para hydrogen conversion.

P A R T O N E

SOME STUDIES OF THE ULTRA-VIOLET AND VISIBLE ABSORPTION SPECTRA OF DONOR-ACCEPTOR SYSTEMS IN THE SOLID STATE AND IN SOLUTION.

C H A P T E R O N E

Donor-Acceptor Complexes

1·1 Historical Introduction

As early as 1920 it was recognised that certain aromatic species could undergo combination with other aromatic compounds with the apparent violation of existing rules of chemical bonding. Since then many attempts have been made to describe the nature of the ground state bonding of the complexes formed.

Early theories favoured a covalent bond linkage between the two components of a complex. Although this idea was upheld for some time it was discarded when X-ray diffraction studies of the complex established that the distance between the two components far exceeded normal covalent bond lengths. Briegleb[1] suggested that the molecular complexes were products of an interaction resulting from electrostatic attractions between molecules with permanent dipoles and non-polar molecules which are then subject to polarisation through induction. It was, however, at that time difficult to explain how these bonding forces could produce sufficient electron transfer between interacting components to account for the marked increase in light absorption which usually accompanied complex formation.

Gibson and Loeffler[2] and Hammick and Yule[3] interpreted the increase in light absorption on complex formation as the result of electronic interchange between components during normal collisions. These theories were later dispelled when it was found possible to

isolate stable solid complexes and also detect infrared absorption bands characteristic of true complexes.

It had been recognised for some time[4] that the complexes formed were products of the interaction of an electron donor (D) and an electron acceptor (A). Weiss,[5] developing this idea, described aromatic donor-acceptor complexes in terms of the transfer of a single electron from donor to acceptor.

$$D: + A \rightarrow [D\cdot]^{+} + [\cdot A]^{-}$$

This description was not however compatible with the low heats of interaction of the components, Brackmann[6] modified Weiss's theory by introducing a resonance interaction which only required partial ionic character for the complex. This theory was more in accord with the known properties of molecular complexes, and was a formalised expression of the ideas of Hammick and Yule,[3] and Gibson and Loeffler.[2]

Spectroscopic studies of aromatic donor-acceptor complexes had shown that in addition to the absorption bands characteristic of the free donor and acceptor there was the formation of a new absorption band in the visible or near ultra-violet region of the spectrum which could not be attributed to either component of the complex. Mulliken[7,8,9] developed the ideas of Weiss and Brackmann and applied a quantum mechanical description to this new absorption band. This treatment gave the basis to the present day theories on the

nature of the ground state bonding of donor-acceptor molecular complexes.

1·2 Donor-Acceptor Complexes

Mulliken[7,8,9] in his quantum mechanical approach to the interaction of donors and acceptors considered the ground state of the complex to be a resonance interaction between a non-bonded state (D,A) and a polar excited state (D^+A^-). This gives a stabilised ground state having the wave function,

$$\psi_N \simeq a\ \psi_0\ (D,A) + b\ \psi_1\ (D^+A^-) \qquad (1\cdot1)$$

the excited state he similarly described as,

$$\psi_E \simeq a^*\ \psi_1\ (D^+A^-) - b^*\ \psi_0\ (D,A) \qquad (1\cdot2)$$

where $a^* \simeq a$, $b^* \simeq b$ and $a^2 >> b^2$

The ground state can therefore be considered as a resonance hybrid receiving a major contribution from the non-bonded state, while the excited state is mainly dative in character with the D^+A^- species being the main contributor. The observed charge transfer band is then associated with the electronic transition

$$\psi_N \longrightarrow \psi_E$$

Mulliken[10] later revised his theory to include internal excitation of the donor and acceptor, and excited states of the D^+ and A^- ions. If these are included, equation (1·1) can be rewritten as,

$$\psi_N = a\ \psi_0\ (DA) + \sum b_i\ \psi_{1i}\ (D^+A^-) + \sum c_j\ \psi_{2j}\ (D^-A^+) + \cdots \qquad (1\cdot1a)$$

In simple cases only the first term and one or two terms of the first summation are important. Among the excited states are some where the main term corresponds to the internal excitation of the donor and acceptor, while in others the main term is usually one of the ψ_{1i} $(D^{+}A^{-})$, i.e. a charge transfer state. A typical excited state could be

$$\psi_{v}(D,A) = a^{*}\ \psi_{11}\ (D^{+}A^{-}) - b^{*}\ \psi_{0}(D,A) + d^{*}\ \psi_{31}\ (D^{*}A) + \cdots\cdots \qquad (1\cdot2a)$$

The coefficient, b (whose square is a measure of the amount of charge transfer), in equation (1·1) is given by,

$$b = c\ S_{DA}\ (W_1 - W_0)$$

Where c is approximately a constant, W_1 and W_0 are the energies of a hypothetically pure dative and pure non-bonded wave function ψ_1 and ψ_0 and S_{DA} is the overlap integral between the donor orbital Φ_D out of which an electron has been donated and the acceptor orbital Φ_A of the negative ion of the acceptor molecule into which the same electron has been accepted

$$S_{DA} = \int \Phi_D \quad \Phi_A \ \partial\tau$$

For a true molecular complex Mulliken[11] suggested that S, the orbital overlap, must be greater than zero, and the partners of the complex will tend to assume a relative orientation such that S is a maximum. This is termed the overlap and orientation principle. Although the new absorption bandcharacteristic of a complex can undoubtedly

be considered to be due to electron transfer from donor to acceptor as described above, several criticisms of Mulliken's description of the ground state of a molecular complex have been made. Dewar[12] suggests that it is feasible in some donor-acceptor systems for electron transfer to occur between the two components of a complex if they were held together by only Van der Waals forces. He criticises Mulliken's generalization that a dative species D^+A^- contributes to the ground state of all molecular complexes.

For charge transfer to occur it is only necessary that the two components of the complex be close together. Earlier work by Briegleb[13] had shown that the heats of formation of many π complexes were in the order of that to be expected by considering Van der Waals forces to be a major factor in the ground state bonding of such complexes. Dewar[12] divides Van der Waals forces into three contributions,

(a) Electrostatic interaction, as between polar molecules,

(b) Electrostatic polarisation; such as the interaction betwwen a polar and non-polar molecule,

(c) Heitler London dispersion forces; instantaneous electrostatic attractions due to electron correlations, which could be obtained in a system where neither molecule is polar.

He showed that if first and second order perturbation theory was applied to the ground state of a donor-acceptor complex equivalent terms for (a),(b) and (c) could be derived. Dewar suggests that

using this treatment it is not necessary in some cases to invoke the use of a D^+A^- species to describe the stability of a complex.

In both the treatments of Mulliken and Dewar the contribution of a dative structure to the ground state of the complex is either negligible or non-existent. Weiss[14], however, puts forward the idea that the ground state of a molecular complex can be more adequately described in terms of the transfer of a single electron from donor to acceptor.

$$D: + A \rightarrow [D.]^+ + [.A]^-$$

Where in solvents of high dielectric constant the resulting ions are stabilised by solvation giving D_s^+ and A_s^- species, and in solvents of low dielectric constant the donated electron remains coupled to the positive hole of the donor giving an electron-hole pair state.

It is obvious from this discussion that the nature of the ground state bonding between two components of a donor-acceptor complex is still a very controversial subject. For systems in which the donor has a very low ionisation potential and the acceptor a high electron affinity evidence for the existence of a D^+ and A^- species in solvents of high dielectric constant has been found, which would suggest that Weiss's arguments could well be valid. It has been suggested[33] that in these cases the formation of the ionic species is preceded by the neutral complex DA which then undergoes ionisation. It does not seem feasible that Weiss's argument would fit a system in which the

ionisation potential of the donor is high and the electron affinity of the acceptor low. In such a system Van der Waals forces would be expected to play an important role in the bonding of the complex and either Mulliken's or Dewar's description of the ground state would seem more reasonable.

1·3 Charge Transfer Absorption

The electronic transition in a molecular complex is from the donor to the acceptor, therefore the energy of such a transition should be a function of both the ionisation potential of the donor and electron affinity of the acceptor. The energy of the transition can be given as a first approximation by the expression,[15]

$$h\gamma_{CT} = I_D - E_A - W \qquad (1\cdot6)$$

in which h is Planck's constant, I_D the donor ionisation potential, E_A the acceptor electron affinity and W the dissociation energy of the charge transfer excited state. A more detailed consideration of the energetics of the charge transfer absorption for complexes with a common acceptor gives an alternative equation,[16]

$$h\gamma_{CT} = I_D - C + 2\beta^2 / (I_D - C) \qquad (1\cdot7)$$

where C and β are approximately constant. This equation is that of a parabola and it has been suggested that the straight line of equation (1·6) may be part of the curve.

Recently a molecular orbital treatment has been successfully applied to a number of donor-acceptor systems[17,18] with a single

acceptor and series of donors for which direct calculations could be made,

$$E_\pi = A_j - D_i + \text{const.} \qquad (1\cdot8)$$

Where E_π is the charge transfer interaction energy, A_j and D_i being the energies of the j th. orbital on the acceptor and the i th. orbital on the donor respectively. This treatment in a modified form has also been applied to complexes with polycyclic aromatic donors.[19] The energy of a filled orbital of a polycyclic aromatic is given by the Huckel molecular orbital treatment and is,

$$\alpha + X_i\beta$$

where α is the coulomb integral for carbon, X_i a quantity calculated theoretically for the i th. orbital of the hydrocarbon and β is the carbon-carbon resonance integral. From (1·8)

$$E_\pi = A_j - (\alpha + X_i\beta) \qquad (1\cdot9)$$

This further leads to the prediction that E_π values for complexes of a given acceptor should be linearly dependent on the $\pi - \pi^*$ transition energies of the donors.[19] Consider an internal transition,

$$E_D = D_j - D_i$$

If the donor is polycyclic the transition is from the highest filled to the lowest unfilled orbital. The energy of the lowest unfilled orbital is,

$$D_j = \alpha - X_i\beta$$

$$\therefore \quad E_D = \alpha - X_i\beta - (\alpha + X_i\beta)$$

$$= -2X_i\beta$$

From (1·9) $\quad E_\pi = A_j - \alpha + (E_D/2)$

Therefore the charge transfer energy is related to the internal transition.

1·4 Stability of Complexes.

(i) Equilibrium Constants.

Several different experimental procedures exist to investigate the equilibria established between the two components of a molecular complex. Such methods have been reviewed[20] and include solubility, distribution measurements and spectrophotometric techniques. Only the spectrophotometric determinations of equilibrium constants will be considered here.

For a 1:1 molecular complex in solution, at a given wavelength the optical density of the solution, assuming obedience of Beer's Law, is given by,

$$d = \log_{10} Io/I = \varepsilon_D c_D \, l + \varepsilon_A c_A \, l + \varepsilon_{DA} c_{DA} l \qquad (1·10)$$

I and Io are the intensities of the incident and emergent light, ε_D, ε_A and ε_{DA} are the extinction coefficients of the donor, acceptor and complex respectively, c_D, c_A and c_{DA} are the concentrations of the donor, acceptor and complex respectively and l is the length of light

path through the solution. If the donor is in large excess of the acceptor, and an acceptor-free solution which contains the donor at the same concentration as in the solution of the complex is used as a blank, d', the measured optical density is given by,

$$d' = d - \varepsilon_D l \sum D = c_A \varepsilon_A l + c_{DA} \varepsilon_{DA} l \qquad (1\cdot11)$$

Now $\sum D >> \sum A$ and $\sum D - c_{DA} \simeq D$ (1·12)

where $\sum D = c_D + c_{DA}$ and $\sum A = c_A + c_{DA}$

Thus the apparent extinction coefficient ε_a is,

$$\varepsilon_a = d'/l \sum A \qquad (1\cdot13)$$

For a 1:1 complex the simple mass action law can be applied to the complex equilibrium

$$A + D \rightleftharpoons AD \qquad (1\cdot13)$$

$$K_c = \frac{[AD]}{[A]\,[D]} \quad 1.\text{mole}^{-1} \qquad (1\cdot14)$$

From this using (1·11), (1·12) and (1·13)

$$\frac{1}{\varepsilon_a - \varepsilon_A} = \frac{1}{K_c c_D (\varepsilon_{DA} - \varepsilon_A)} + \frac{1}{\varepsilon_{DA} - \varepsilon_A} \qquad (1\cdot15)$$

A straight line should therefore be obtained by plotting $1/\varepsilon_a - \varepsilon_A$ versus $1/c_D$, and on determining the slope and intercept of the line ε_{DA} and K_c can be evaluated. If it is assumed that ε_A is negligible compared to ε_a or ε_{DA} then we arrive at the Benesi-Hildebrand equation

$$\frac{1}{\varepsilon_a} = \frac{1}{K_c c_D \varepsilon_{DA}} + \frac{1}{\varepsilon_{DA}} \qquad (1\cdot16)$$

(ii) Contact Charge Transfer

Mulliken[8] predicted that the increase in K_c which normally resulted when examining a series of complexes with a common acceptor as the ionisation potential of the donor decreased, should be accompanied by an increase in the oscillator strength and quantum mechanical dipole of the charge transfer transition. Certain anomalies to this prediction are apparent, for example, with iodine and a series of donors with decreasing ionisation potential, the intensity of the charge transfer band decreases.

In an attempt to explain these anomalies Mulliken[23] and Orgel[21] suggested that in these systems complications arise due to the presence of several 1:1 complexes with different orientations and to "contact" charge transfer. Contact charge transfer arises from random encounters of the donor and acceptor in solution. Such a transfer can occur when the donor's outermost molecular orbital (M.O.) overlaps with an "acceptation" M.O. of the acceptor. The "acceptation" M.O. is not one which is normally associated with the acceptor, but is a M.O. which is occupied only in the negative ion of the acceptor. Such an overlap can occur at distances beyond the Van der Waals distance of approach, therefore during normal random contact of the two species transitions to a charge transfer excited state can occur.

The application of the Benesi-Hildebrand treatment to pure contact charge transfer spectra gives $\varepsilon = \infty$ and $K_c = 0$. The simultaneous presence therefore of a normal charge transfer process

and a contact charge transfer process for a donor-acceptor complex in solution can lead to misleading results. The ε_{DA} value obtained will be the sum of the ε values for the normal and contact charge transfer process,

$$\varepsilon_{DA} = \sum \varepsilon_i$$

thus misleading equilibrium constants will be obtained.

Mulliken and Orgel[22] introduced an expression giving the concentration of "contact" pairs [DA] as,

$$[DA] = \alpha' [D][A] \qquad (1\cdot17)$$

where α' is the number of sites for a D molecule around an A molecule. The optical density, d, of the solution being given by,

$$d = [DA]\, l\, \varepsilon_{DA}$$

they then obtained the expression

$$\frac{c_A l}{d} = \frac{1}{\alpha' \varepsilon_{DA}} \cdot \frac{1}{c_D}$$

thus for a mixture of normal and contact charge transfer species K can be obtained from,

$$c_A l/d = 1/K\varepsilon_{eff} \cdot 1/c_D + 1/\varepsilon_{eff} \qquad (1\cdot18)$$

where

$$\varepsilon_{eff} = \varepsilon_c + \frac{\alpha'[DA]}{K} \qquad (1\cdot19)$$

where ε_c is the extinction coefficient of the complex.

(iii) Dependence of Equilibrium Constants on Solvent

The derivation of equilibrium constants from spectrophotometric data by the Benesi-Hildebrand treatment, or modifications thereof, has undergone severe criticism. The main shortcoming of the treatment is that it ignores the role of the solvent in complex formation.

Early treatments [25,26,27] of the effect of solvation on complex formation considered the solvent to be a competing donor.

$$A + D = \text{Complex 1 } (C_1) \qquad K_1 = [AD]/[A][D]$$

$$A + S = \text{Complex 2 } (C_2) \qquad K_2 = [AS]/[A][S]$$

An analysis similar to the derivation of Benesi and Hildebrand yields the relationship,

$$\frac{[A]\,l}{d_{AD}} = \frac{1 + K_2}{\varepsilon \cdot K_1} \cdot \frac{1}{[D]} + \frac{1}{\varepsilon}\left(1 - \frac{K_2}{K_1}\right) \qquad (1\cdot20)$$

From equation (1·15) the equilibrium constant K_0 and extinction coefficient ε_o of the complex is given by,

$$\frac{[A]\,l}{\log I_o/I} = \frac{1}{K_o\varepsilon_o} \cdot \frac{1}{[D]} + \frac{1}{\varepsilon_o}$$

therefore $K_o = \dfrac{K_1 - K_2}{1 + K_2}$ and $\varepsilon_o = \dfrac{K_1}{K_1 - K_2}\,\varepsilon$

Thus the contribution of the solvent can be determined. Murrell *et al.*[24] developing on these ideas assumed the free donor, free acceptor, and complex to occur in solution each with a well defined solvent shell,

$$A\,S_n + D\,S_m = (DA)\,S_p + qS \qquad (1\cdot21)$$

where $q = n + m - p$, whence it can be shown that

$$K_{exp.} = K_{true} - \frac{q\ (m + 1)}{S_o} \qquad (1\cdot22)$$

and

$$\varepsilon_{exp} = \varepsilon_{true}\ \frac{K_{true}}{K_{exp}} \qquad (1\cdot23)$$

where $K_{exp.}$, $\varepsilon_{exp.}$ are the experimental values of K_c and ε by the Benesi-Hildebrand treatment or a modification, K_{true} is the equilibrium constant for (1·21) and S_o is the total solvent concentration. Murrell et al.[24] criticise the Mulliken/Orgel[22] concept of contact charge transfer and suggest that for weak complexes the anomalies in the behaviour of K_c can be explained by considering a competition between solvation and complexing as described above, without the necessity of introducing a new species of complex.

The relative importance of solvation effects on the formation of complexes is still in some doubt. Foster et al.[28] considered the term (1·22) in Murrell's treatment:

$$K_{exp.} = K_{true} - q\ \frac{(m + 1)}{S_o}$$

As K decreases, the term $q(m + 1)/S_o$ should become more important. This however is not the case, for ε tends to remain remarkably constant. Foster also criticised the basic assumptions of equations (1·15) and

(1·16), that of the constancy of Beer's Law, in the determination of equilibrium constants. Although Beer's Law is valid in many instances its use is based on the assumption that large variations in ε are not expected on varying solvent. It seems reasonable to assume some variation,[29] then if ε varies as some function (f) of the component in excess,

$$\varepsilon = \varepsilon_o f \quad [D]$$

where ε_o is the value of ε for an infinitely dilute solution. Assuming the variation to be linear,

$$\varepsilon = \varepsilon_o \quad (1 + \alpha\,[D])$$

from (1·14) $$K = \frac{d/\varepsilon}{([A]-d/\varepsilon)\,[D]}$$

hence $$\frac{[A]}{d} = \frac{1}{[D]}\,\frac{1}{K_c \varepsilon} + \frac{1}{\varepsilon}$$

Plotting this for a given set of results gives a straight line, and on introducing the new factor into the equation an equivalent straight line with identical gradient but different intercept is obtained. Thus different values of the equilibrium constant result. Foster et al.[28] suggest that this factor could be obtained by determining equilibrium constants by methods other than by spectrophotometric means and comparing the results.

(iv) Thermodynamic Constants

The interaction of donors and acceptors in solution is accompanied by only small changes in enthalpies and entropies. The constants determined for many complexes have usually been obtained from a Bernesi-Hildebrand or similar treatment and then substituted into the Gibbs-Helmholtz equation,

$$\frac{d \ln K}{d/(1/T)} = \frac{-\Delta H^{o}}{R}$$

thus

$$2.303 \log \frac{K_{T_2}}{K_{T_1}} = 2.303 \log \frac{\text{Slope } T_1}{\text{Slope } T_2} = \frac{\Delta H^{o}}{R}\left(\frac{1}{T_2} - \frac{1}{T_1}\right)$$

This application is based on the assumption that extinction coefficients do not change with change in temperature. In the presence of more than one type of 1:1 complex ΔH should show temperature dependence unless all the complexes have the same heats of formation.

C H A P T E R T W O

The visible absorption spectra of some solid molecular complexes.

2·1 Introduction

It has been shown[45,33] that 1:1 molecular complexes in solution may consist of a mixture of neutral and ionic species as the donor and acceptor strengths or the solvent polarity are varied. Some workers[38] have also suggested that if the donor and acceptor strengths are varied in a similar way then solid molecular complexes may show the same behaviour, their structures varying progressively from one containing all neutral molecules to one containing all radical ions. Foster and Thomson[33] have shown that the visible absorption spectra of the solid molecular complexes of N,N,N',N'-tetramethyl-p-phenylene-diamine (T.M.P.D) with weak electron acceptors gives a single absorption peak in the visible region corresponding to an intermolecular charge transfer transition of a loose "outer" molecular complex, whereas the spectrum of complexes with acceptors of relatively high electron affinity suggested that ionisation by complete transfer of an electron from the donor to acceptor has occurred in the ground state. Their results, however, failed to give conclusive evidence on the simultaneous existence of the neutral and ionic charge transfer species in the solid state. This work attempts to clarify the picture by re-examining the same series of complexes as used by Foster and Thomson, in diluted and undiluted forms, using improved instrumentation.

2·2 Experimental

(i) Materials

The acceptors used in this study are listed below

I 2,4-dinitrotoluene

II 1,3-dinitrotoluene

III 2,6-dichloro-p-benzoquinone

IV Chloranil

V Bromanil

VI Tetracyanoethylene (T.C.N.E.)

VII 7,7,8,8-tetracyanoquinodimethane (T.C.N.Q)

VIII 2,3-dichloro-5,6-dicyano-p-benzoquinone

Acceptors I to V were obtained commercially and recrystallised thrice from an appropriate solvent. Acceptor VI was purified by sublimation, 110°/1 mm, Melting point 199°C. Acceptors VII and VIII were used without further purification, 7,7,8,8-tetracyanoquinodimethane was supplied by courtesy of Dr. Benson of DuPont.

N,N,N',N'-tetramethyl-p-phenylenediamine

The free base was obtained from the dihydrochloride salt. To an oxygen free aqueous solution of the salt was added dilute NH_4OH. The white precipitate obtained was dried in a vacuum desiccator over P_2O_5 and purified by sublimation in vacuo. Melting point 51°C.

(ii) Preparation of complexes

For acceptors I - V the complexes were prepared by addition of

a benzene solution of the acceptor to a benzene solution of the donor. The solid complex which precipitated out was washed with benzene and anhydrous ether. The last traces of solvent were removed in a vacuum dessicator over P_2O_5. The complex was then stored in a dry nitrogen atmosphere until used for optical measurements. Complexes with acceptors VI, VII and VIII were similarly prepared from acetone solutions. All the complexes were studied within 12 hrs. of preparation. It was noted that in all cases there was a period of induction prior to precipitation of the complex from the mixture of the components. After precipitation the solvent residue was slightly coloured.

A number of complexes were examined in a diluted form. All of these diluted complexes were prepared by intimately grinding together the complex and diluent in a dry nitrogen atmosphere. The ratio of diluent to complex in all cases was 1 mol : 0·05 mol.

(iii) Preparation of alkali metal salts of acceptor ions

The solid anions of acceptors III-IV, V, VI and VIII were prepared from the acetone solution of the acceptors by the action of sodium or potassium iodide.[31] Excess acetone was evaporated off and the precipitate obtained was dried in a vacuum dessicator. The anion of the acceptor VII was prepared from an acetonitrile solution.

(iv) Spectra

Spectrophotometric studies, reflectance and absorption, were

made with a Beckmann DK2A recording spectrophotometer incorporating a reflectance attachment. The reflectance unit consists of an integrating sphere coated with magnesium oxide. The incident radiation enters the sphere and is alternatively reflected from the sample and reference (MgO) surfaces onto the sphere walls. The walls then reflect the sample beam back and forth until it reaches the detector.

The cells used for examining the spectra of the molecular complexes were a modified version of those supplied with the instrument. They incorporated a quartz "window" which rested over the sample. This window served a dual purpose.

(a) It prevented the sample from being contaminated by atomospheric moisture.

(b) It prevented trace quantities of the sample damaging the reflectance sphere of the spectrophotometer.

For trace samples of the complex it was found possible to obtain a spectrum by depositing the complex onto a 4.25 cm. diameter filter paper and placing the filter paper in the sample port of the spectrophotometer.

The absorption bands of the solid complex were usually found to be broad and values quoted may only be significant in some cases to $\pm$ 10 $m\mu$.

2·3 Results

(i) Undiluted Complexes

The maxima in the visible and ultra-violet region of the spectra of the solid complexes of T.M.P.D. and the Na^+A^- salts for the acceptors I-VIII are given in TABLE 2·1. For comparison, results obtained by Foster and Thomson[32,34] for the same complexes in both the liquid and solid state are given in TABLE 2·2. The acceptors in both tables are placed in order of increasing electron affinity as measured by the position of the charge transfer band of the corresponding hexamethybenzene complexes. The spectra obtained for the complexes of T.M.P.D with acceptors III to VIII and the spectra of the corresponding Na^+A^- salts are shown in FIG. 2·1 to 2·6.

The spectra of the complexes of T.M.P.D with the weak acceptors I and II, give only one broad maximum, denoted by λ_8, in the visible region. This band is attributed to an intermolecular charge transfer as described by Mulliken. No evidence for the presence of an A^- or D^+ species was found.

Complexes of acceptors III to VIII with T.M.P.D show a remarkable contrast in behaviour when compared with complexes of acceptors I and II. At least five absorption bands occur in the region 400 to 1300 mμ. These results also differ considerably from those obtained by Foster and Thomson for the same complexes (TABLE 2·2). The position of the bands λ_2 (610 ± 10 mμ) and λ_3 (565 ± 10 mμ) is consistent throughout

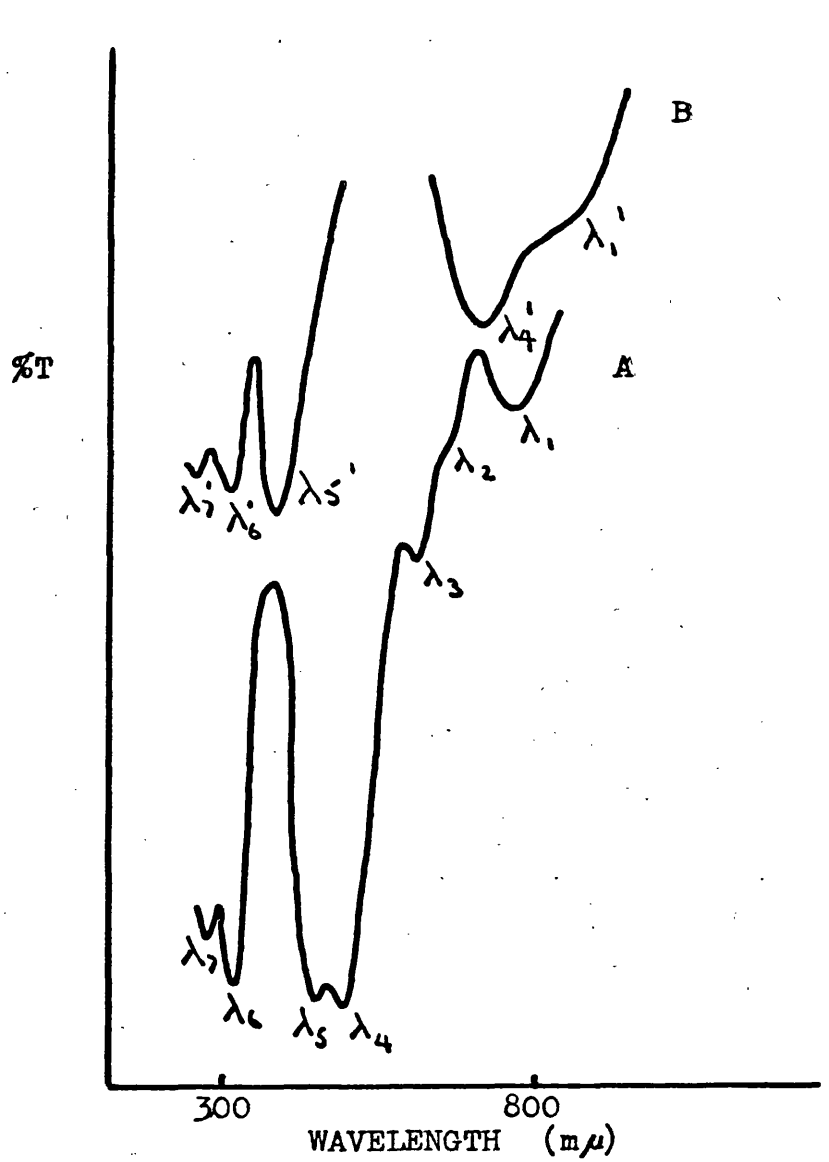

Fig. 2.2. A Chloranil / T.M.P.D. complex
B Chloranil negative ion.

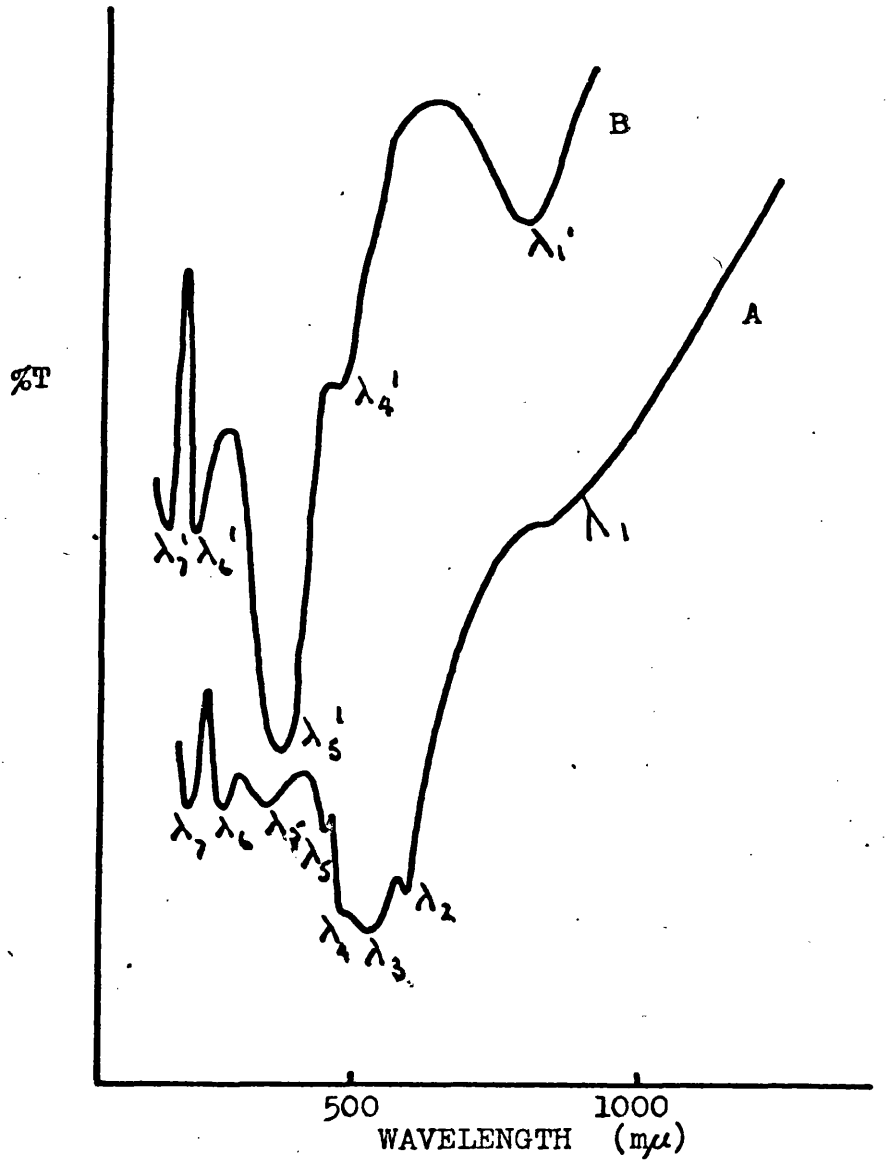

Fig. 2.1. A 2,6-dichloro-p-benzoquinone / T.M.P.D. complex.
B 2,6-dichloro-p-benzoquinone negative ion.

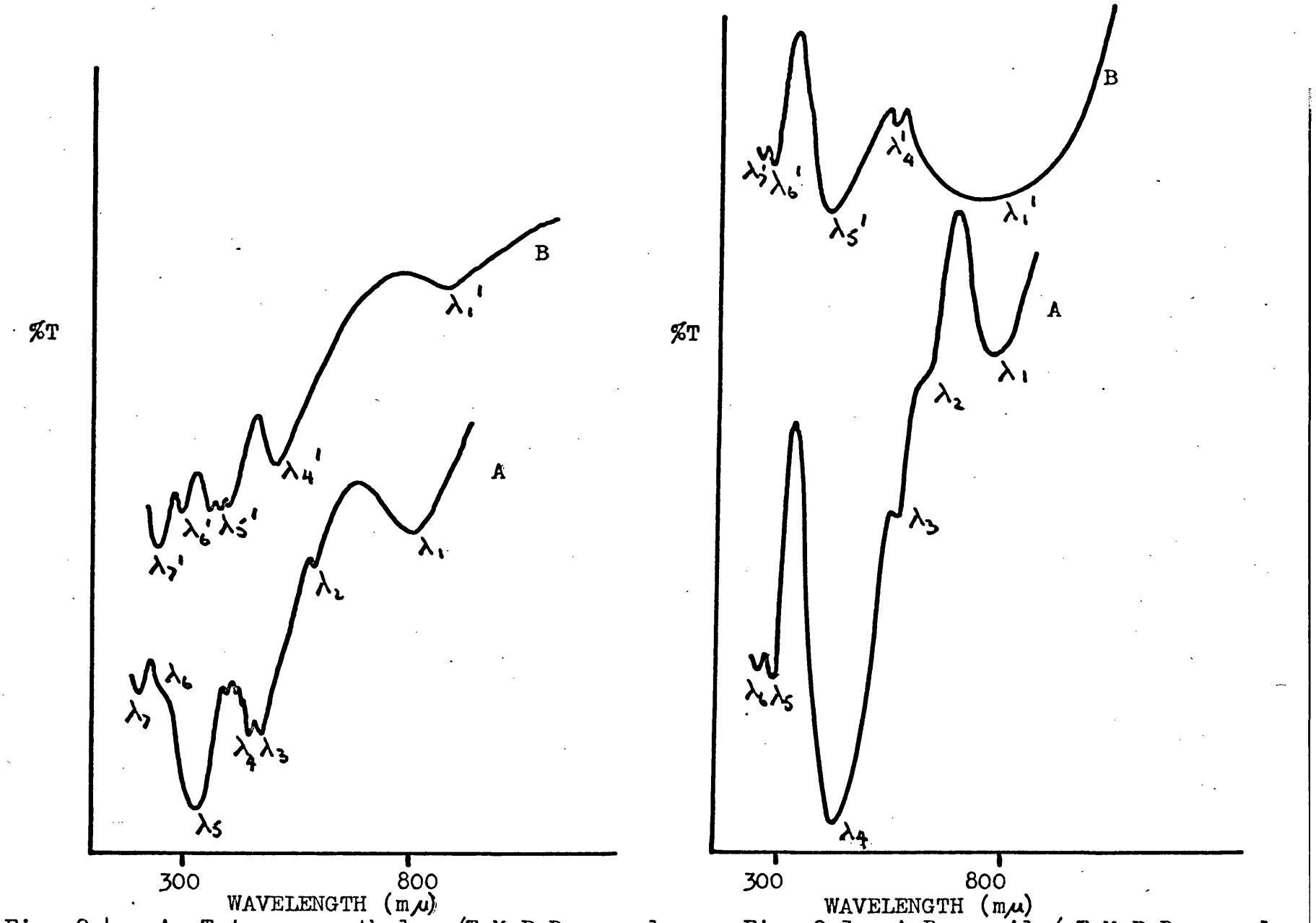

Fig. 2.4. A Tetracyanoethylene/T.M.P.D. complex.
B Tetracyanoethylene negative ion.

Fig. 2.3. A Bromanil / T.M.P.D. complex.
B Bromanil negative ion.

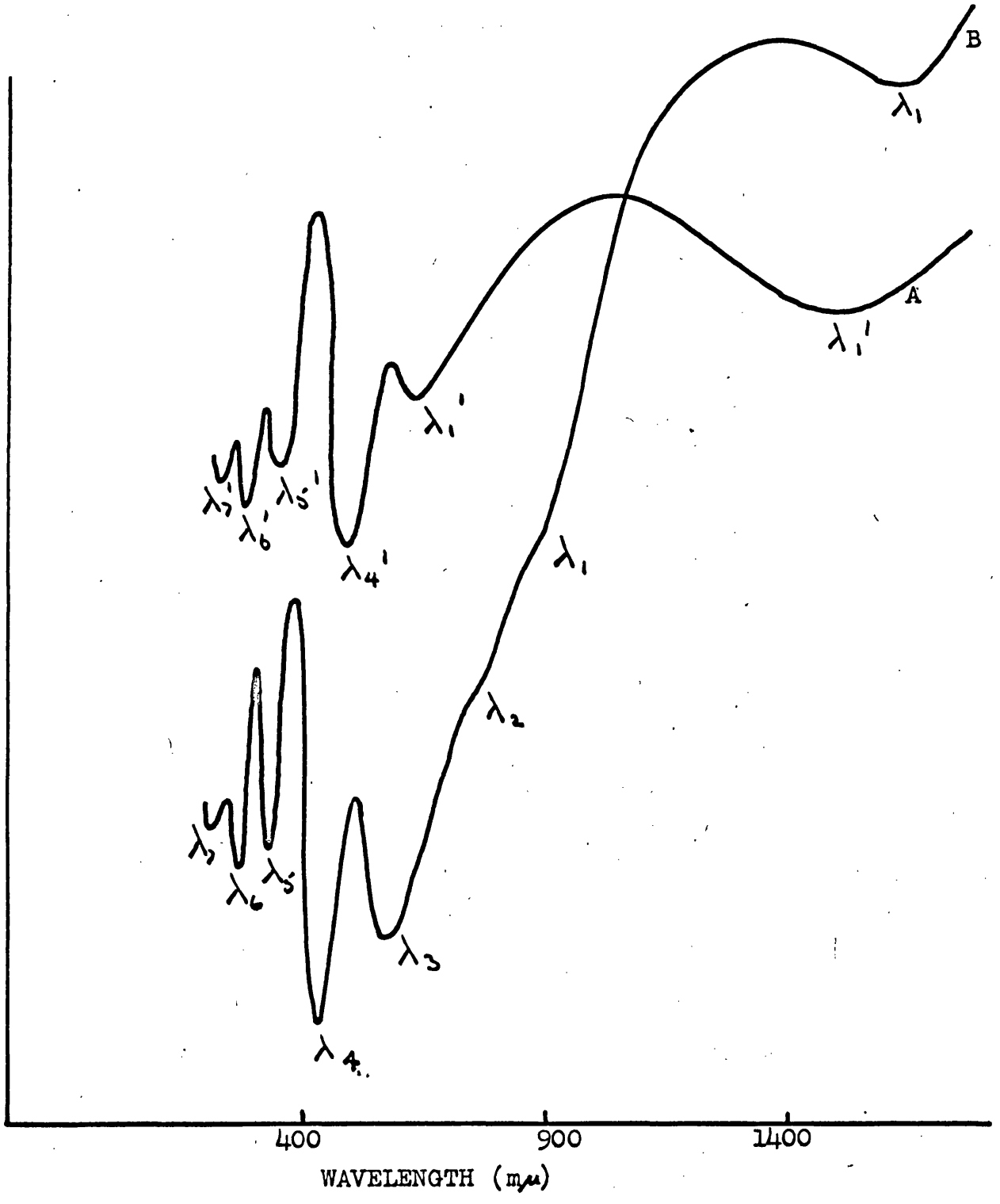

Fig. 2.5. A T.C.N.Q. / T.M.P.D. complex.
B T.C.N.Q. negative ion.

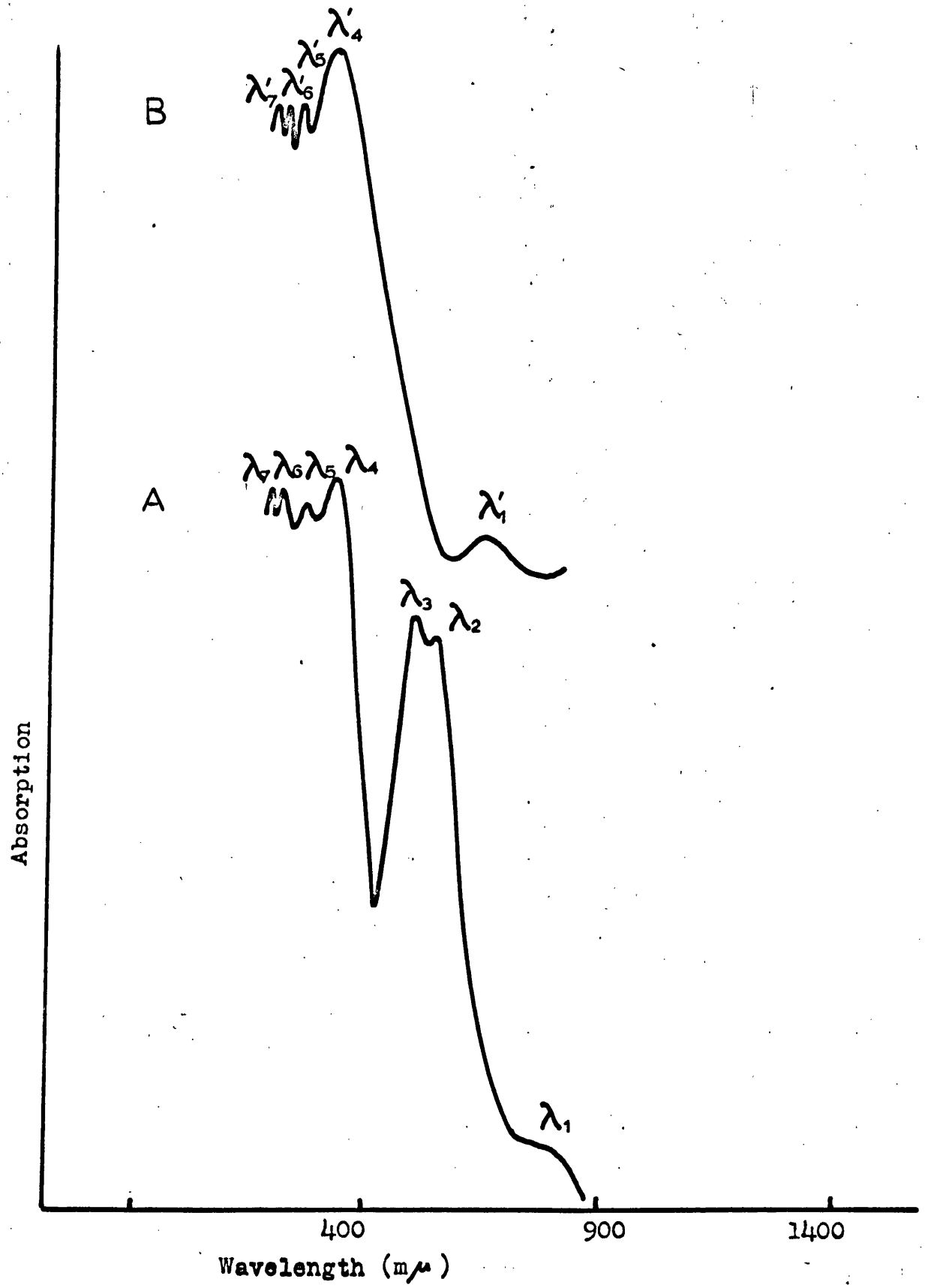

Fig.2.6. A. 2,3-dichloro-5,6-dicyano-p-benzoquinone / T.M.P.D. complex.

B. 2,3-dichloro-5,6,-dicyano-p-benzoquinone

TABLE 2·1 Data obtained from present work.

Acceptor	Band maxima of solid complexes								Band maxima of A^- ion				
	λ_1	λ_2	λ_3	λ_4	λ_5	λ_6	λ_7	λ_8	λ_1'	λ_4'	λ_5'	λ_6'	λ_7'
2,4-Dinitrotoluene								480					
1,3-Dinitrobenzene								510					
2,6-Dichloro-p-benzoquinone	885	610	560	510	472 360	322	260		940	485	390	280	
Chloranil	735	620	670	447	410	278	240		847	650	360	283	235
Bromanil	800	615	560	430		285	248		775	463	358	280	
T.C.N.E.	810	610	560	520	390	290	210		850	500	385 405	250	220
T.C.N.Q.	1475 760	620	610	465	353	275	210		1400 670	525	390	309 250	
2,3-Dichloro-5,6-dicyano--p-benzoquinone	875	600	555	380	328	258	208		730	535	385	260	208

TABLE 2·2 Data obtained by Foster and Thomson[33,34]

Acceptor	Solid complex band maxima			Band maxima of A^- ion		Band maxima of complexes in methanol						Band maxima of A^- ion in solution		
	σ_1	σ_2	σ_8	σ_1'	σ_2'	π_2	π_3	π_4	π_5	π_1	π_8	π_1'	π_2'	π_3'
2,4-Dinitrotoluene			479								424			
1,3-Dinitrobenzene			512								454			
2,6-Dichloro-p-benzoquinone	440	550		382	880	616	568	445			(770)		426	452
Chloranil	440	554		393 440	889	616	568	452	426		(870)		426	451
Bromanil	463	550		396	820	616	568	455	430		(876)		429	455
T.C.N.E	435	580		402	618	616	568	polybanded 370–470			(980)		400	418
T.C.N.Q	410	555		608		617	570			844 744	(1163)	740	760	842
2,3-Dichloro-5,6-dicyano--p-benzoquinone	422	590 647		449	493	618	568	396						424

the series of acceptors III to VIII. These two bands are very close to the bands $\pi_2(616)$ and $\pi_3(568)$ of the corresponding complexes in an ionising solvent (TABLE 2·2). Foster and Thomson have attributed π_2 and π_3 to the T.M.P.D$^+$ ion and it seems reasonable to assign λ_2 and λ_3 in the solid complexes to the same ion. On the basis of this assignment the presence of bands corresponding to λ_2 and λ_3 would not be expected to be present in the spectra of the solid Na^+A^- salts. It is found that for these salts no absorption peaks occur in the region 610 ± 10 mμ, 565 ± 10 mμ.

The results obtained for the Na^+A^- salts of the acceptors show some consistency with the results of Foster and Thomson[33] in giving a long wavelength band λ'_1, which is not detectable in the solution spectra of these salts with ionising solvents. It is suggested[33] that this is a new transition of A^- permitted by the ionic environment of the solid. For the solid molecular complexes a similar long wavelength band, λ_1, is detected. If this band is due to charge transfer it would be expected to vary as the acceptor varies in the same manner as π_8 in TABLE 2·2, moving to lower energy as the electron affinity of the acceptor increases. The band λ_1, in fact, remains remarkably constant as the acceptor varies. It seems reasonable, therefore, to assign λ_1 of the solid complexes to the A^- species. Some small shift in the band maxima of λ_1 compared to that of λ'_1 would be expected because of the change in environment on going from Na^+A^- to D^+A^-, the D^+ ion differing in size to the Na^+ ion.

The bands denoted by λ_4,λ_5 , λ_6 and λ_7 for the solid complexes are close to the λ'_4, λ'_5, λ'_6 and λ'_7 bands of the corresponding salt and it is tempting to assign these to the A^- ion. The A^- bands in the visible region for the complex will be affected by the absorption of the T.M.P.D$^+$ ion in addition to the environmental change on going from Na^+ to T.M.P.D$^+$. The effect of the T.M.P.D$^+$ absorption should diminish as the ultraviolet region of the spectrum is approached. This assists in explaining why the bands denoted by λ_1, λ_6 and λ_7 have maxima in closer agreement to the corresponding bands in the salt than the bands λ_4 and λ_5 .

None of the bands in the complexes of acceptors III to VIII with T.M.P.D could be attributed to a Mulliken type intermolecular charge transfer.

(ii) Diluted Complexes

Due to poor instrumentation it is sometimes not possible to obtain the spectra of complexes of intense colour. The usual procedure in these cases is to "dilute" them with an inert compound which does not absorb or transmit radiation in the region to be studied. The possible effects of diluting such complexes has been examined using the solid complex of T.M.P.D with chloranil and bromanil. These two complexes were intimately mixed with a number of diluents and the resulting spectra examined.

The effects noted were

(a) A diminution of band intensity, particularly the weak bands of the undiluted complex.

(b) The band maxima of the diluted complex shifted relative to the band maxima of the undiluted complex; the direction and magnitude of the shift depending on the diluent used.

(c) There was a marked increase in the susceptibility of the diluted complex to atmospheric moisture relative to the undiluted complex.

For the chloranil - T.M.P.D complex the effect of changing the cation of the diluent while keeping the anion constant was examined; the position of the observable band maxima are given in TABLE 2·3. For the bromanil - T.M.P.D complex the effect of changing the anion of the diluent while keeping the cation constant was examined; the position of the observable band maxima being given in TABLE 2·4.

TABLE 2·3

Band Maxima

Diluent	λ_2	λ_3	λ_5	λ_6	λ_7
Undiluted	620	570	410	278	240
LiF	600	558	315	258	206
NaF	490	435	320	260	210
KF	470	400	330	265	225

TABLE 2·4

Band Maxima

Diluent	λ_3	λ_4	λ_5	λ_6	λ_7
Undiluted	560	430		285	248
LiF	549	440	306	255	200
LiCl	535	440	306	255	200
LiBr	510	440	306	255	200

Constant anion/changing cation

The results in TABLE 2·3 show that on changing the cation from Li to K the T.M.P.D$^+$ ion bands, designated λ_2 and λ_3, move to higher energies while the bands assigned to the chloranil$^-$ ion move to lower energies as the size of the cation increases. The fluorides are all ionic in character, thus if these ionic salts are mixed intimately with the complex the D^+ and A^- ions will experience a change in environment. Such a change could affect the excitation energies of the ions. It is not surprising that a shift of the band maxima of the chloranil$^-$ ion is observed on changing the cation of the diluent. This ion will experience a change in polarisation as the size of the cation increases and the energy of its ground and excited states will change. The reason why there is a shift to higher energies of the band maxima of the T.M.P.D$^+$ ion on altering the diluent is not at first obvious because the anion of the diluent remains the same. However, on going from LiF to KF the orbital overlap of the cation with the anion increases, and this will alter the polarising power of the F^- ion and subsequently alter the energy levels of the T.M.P.D$^+$ ion.

Constant cation/changing anion

The results obtained for this system are given in TABLE 2·4. Only the band designated, λ_3, shifts on changing the anion from F to Br. This band due to its position can be assigned to the T.M.P.D$^+$ ion while

λ_4, λ_5, λ_6 and λ_7 are assigned to the Bromanil$^-$ ion. If this assignment is true then λ_3 would be expected to move to higher energy on increasing the size of the anion while the remaining bands would be expected to exhibit no shift at all, which is in fact what is observed. This is of course only a crude explanation as it assumes that the excited state remains constant while the ground state moves to lower energy, there being no justification for this.

Effect of water

The possible effects of atmospheric moisture on a diluted complex was examined using NaI as a diluent and the solid molecular complex of T.M.P.D with chloranil. The band maxima examined were those in the visible region i.e. 600, 500 and 424 mμ. It was observed that the bands at 600 mμ and 500 mμ moved to lower energies, while the band at 400 mμ moved to higher energy on exposure to atmospheric moisture. The colour of the complex was also noticed to change from brown to blue over the same period. This colour change suggests that the complex is breaking down from distinct D^+A^- units to separate D^+ and A^- species each of which is being hydrated.

2·4 Discussion

The existence of a dative charge transfer complex, D^+A^-, in solution is well established. Visible absorption[36,33] and electron spin resonance[37] spectroscopy has shown that for complexes between donor molecules of low ionisation potential and acceptor molecules of high electron affinity the D^+A^- species can readily be obtained in solvents of high ionising power. In such a solvent the resulting ions would be strongly stabilised by solvation and it has been suggested[35] that in these cases Weiss's[14] description of the ground state of the molecular complex is more suitable than the generally accepted Mulliken[7] description. Foster and Thomson[33] have investigated a series of complexes of T.M.P.D with different acceptors and found that for complexes in which the components have greatly differing electron affinities the complex varied from neutral to ionic on varying the ionising power of the solvent. They suggest that the formation of the dative species might be preceded by the formation of a Mulliken type complex

$$A + D \rightleftharpoons (AD) \rightarrow A^- + D^+$$

the extent to which the neutral species breaks down depending on the ionising power of the solvent.

Studies using electron spin resonance[38] and conduction measurements[39,40,41] on solid molecular complexes in which the components have greatly differing electron affinities have detected a certain percentage of free radical character which suggests an ionic

contribution to the structure. Kainer et al.[38] using electron spin resonance techniques on a variety of donor-acceptor systems noticed that the percentage free radical character appeared to increase as the donor or acceptor strength of the appropriate component increased. This evidence suggested that the solid molecular complexes were showing a similar behaviour to that of complexes in solution by varying from neutral to ionic as the medium changed, thus implying that at one stage both the ionic and neutral species of the complex are present. Such a viewpoint has been severely criticised[42,43].

Weiss[14] has postulated that the ground state of a solid molecular complex is the dative species $D^{+}A^{-}$. This is formed by electron transfer which leads to an ionic molecule in which the electron remains coupled to the positive hole of the donor giving an electron-hole pair state. Such a species will not give any electron spin resonance absorptions. Light absorption then leads to a bound electron-hole pair state somewhat similar to the case of an exciton. Such a description appears feasible as there are two similar types exciton[44] known in the crystalline state.

(i) Where the electron and hole are at the same lattice cell

(ii) The electron and hole are separated by a distance that is large compared with the lattice constant.

If these excitons existed in solid molecular complexes it is possible that they could act as electron sources or traps, thus

creating low concentrations of separate anions and cations. Electron spin resonance and conduction techniques could therefore give misleading results.[42] It is also possible that these or similar defects could exist in low concentrations in a Mulliken type donor-acceptor complex thus giving similar misleading results.

Electronic spectra can be considered as a better criteria for deciding whether a solid is ionic or neutral than electron spin resonance and conduction experiments. It has the advantage of being far less sensitive to the perturbing effects of adjacent radicals than electron spin resonance. The detection of the ionic species by studying the visible absorption of a solid molecular complex was suggested by the results of Kainer and Uberle[36] who examined the magnetic susceptibility of some solid complexes of T.M.P.D with various acceptors. Foster and Thomson[33] and Davis and Symons[42] examined a similar system of solid complexes using visible absorption spectroscopy and found that there was a definite contrast in the spectra of the complexes with acceptors of high electron affinity. They concluded that this contrast was due to the presence of the $D^{+}A^{-}$ species.

Davis and Symons[42] noticed that on mixing the donor and acceptor in a non-polar solvent (benzene) the complex DA was immediately formed in high concentration, then, a few seconds later the solid complex precipitated out leaving only a very small concentration of the complex in solution. A similar sequence of events was noted in this work.

They considered that a situation where there exists simultaneously D^+A^- species together with the neutral complex DA in the solid crystalline complex to be energetically unfavourable. The ion pair D^+A^- gains little from any stabilisation offered by the "medium" which if it contains a high concentration of the neutral complex DA can be compared with a solvent of low ionising power. Thus if this is the case the excited state D^+A^- will revert to the neutral condition DA. If however, there is a catastrophic process by which all the DA species simultaneously become D^+A^- then the ion pair under consideration is now in an ionic medium and is therefore stabilised. Thus if the stabilisation is sufficient an ionic complex is favoured. Such a situation would explain the formation of an ionic solid from a solution of the neutral complex and the period of induction before precipitation. A chance gathering of many neutral complex molecules is then required before nucleation of the ionic crystals can take place.

A catastrophic process as described above in which all the DA species simultaneously become D^+A^- is much more energetically favoured in the crystalline state than in the solution or gaseous states, for the energy required to form a positive or negative ion is considerably less. This energy is reduced by two effects; first the electrostatic field of one excited ion will polarize the surrounding molecules and secondly there will be some overlap of

the wave functions of the ion with those of the surrounding molecules, the electron (or positive hole) will therefore be partly delocalized.

The results obtained in this work suggest that the picture as suggested by Davis and Symons[42] is correct, for in the complexes examined in no instance were the neutral and ionic species of the charge transfer complex found to exist simultaneously.

C H A P T E R T H R E E

Complex formation between halogenomethanes and aromatic donors.

3·1 Introduction

Attempts to measure directly the electron affinities of carbon tetrachloride and chloroform[46-48] have led to values higher than those of powerful π-acceptors such as p-benzoquinone. Studies of electron donor-acceptor complex formation involving halogenomethanes,[49 53] on the other hand, show them to be weak electron acceptors. This has been attributed[47] to the halogenomethanes having σ-acceptor properties rather than the π-acceptor properties of the aromatic species. In all cases the association constants, K, for complex formation, derived from the Benesi-Hildebrand equation, have been small with a maximum value of ~0·1 litres $mole^{-1}$. In this present work the validity of such association constants are discussed and an attempt has been made to establish the true nature of the interaction between halogenomethanes and aromatic donors.

3·2 Experimental

(i) Materials

N,N,N',N'-tetramethyl-p-phenylenediamine (T.M.P.D) was prepared as previously described (page 18).

N,N-dimethylaniline (D.M.A) was obtained commercially and purified by reduced pressure distillation in a dry nitrogen atmosphere, b.p. 193-195°C. The condensed aromatics were all obtained commercially. Naphthalene and anthracene were purified by recrystallising thrice from benzene, tetracene by sublimation in vacuo and perylene and pentacene were used without further purification.

Spectroscopic grade carbon tetrachloride, chloroform, dichloromethane and all the other solvents used in this work were dried over 5A molecular sieve and purged with dry nitrogen to remove oxygen and prevent oxidation of the donor. Solutions of the donor were prepared in dry oxygen-free n-hexane and kept in the dark until use. The complexes were prepared by mixing the n-hexane solution of the donor with a n-hexane solution of the halogenomethane.

(ii) U.v. Spectra.

All the u.v. spectra were obtained using a Beckmann DK-2A recording spectrophotometer. The 1 cm., stoppered silica cells were accommodated in a specially constructed copper block fitting into

into the sample compartment of the spectrophotometer. Water from a precision, constant temperature bath was rapidly circulated through the block. Temperature control was ± 0.01°C. Pure n-hexane was used as the reference except where the halogenomethane began to absorb radiation in the region studied. The reference in these cases was an appropriate mixture of n-hexane and the respective halogenomethane.

3·3 Results

(i) Halogenomethanes with aromatic amines

FIG. 3·1, 3·2 and 3·3 show the u.v. spectra of T.M.P.D at a fixed concentration with increasing proportions of carbon tetrachloride, chloroform and dichloromethane respectively. FIG. 3·4, 3·5 and 3·6 show the spectra obtained for D.M.A. under the same conditions on adding halogenomethanes. On addition of the halogenomethane a new absorption band appears to develop under the long wavelength region of the amine absorption which in turn reduces the resolution of the amino bands. Tocheck that this apparent absorption was not due to solvent shifts of the high energy amine band, the amine spectrum was studied in a number of different solvents, dioxan, methanol, cyclohexane, isopropyl alcohol and 1,2-dichloromethane. No relative shift of the two bands was observed and there was no development of an apparent new absorption or marked

FIGURE 3.1.

Absorption spectra of T.M.P.D (2.5×10^{-4}M) in n-hexane with added CCl_4: (A) none (B) 1.08M (C) 2.16M (D) 3.24M (E) 4.32M (F) 5.4M

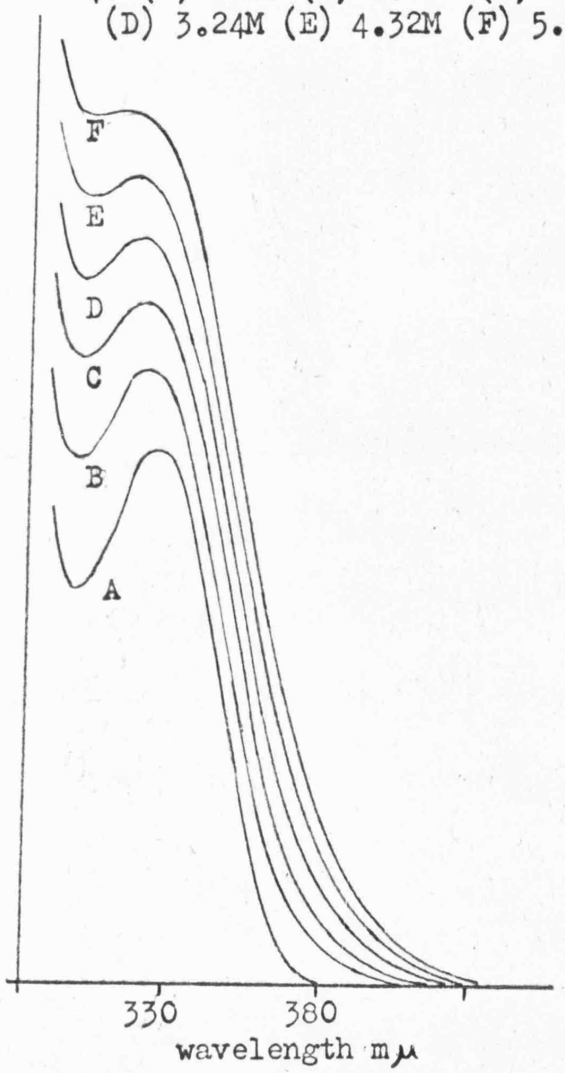

FIGURE 3.2. Absorption spectra of T.M.P.D (2.5×10^{-4}M) in n-hexane with added $CHCl_2$: (A) none (B) 1.39M (C) 2.78M (D) 4.17M (E) 6.95M.

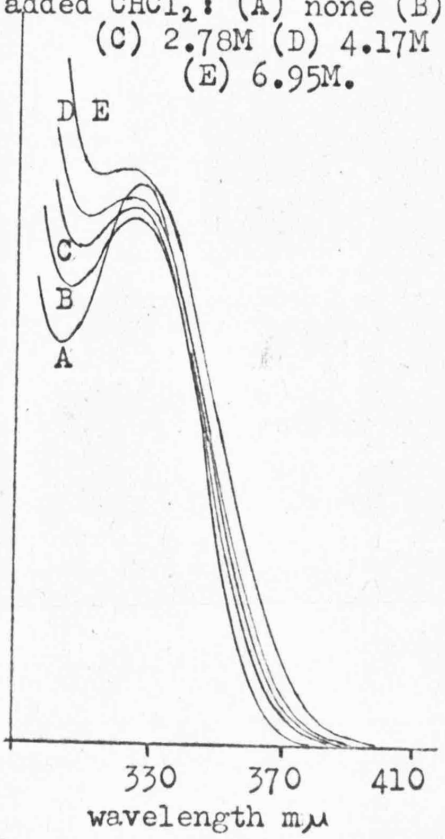

FIGURE 3.3.

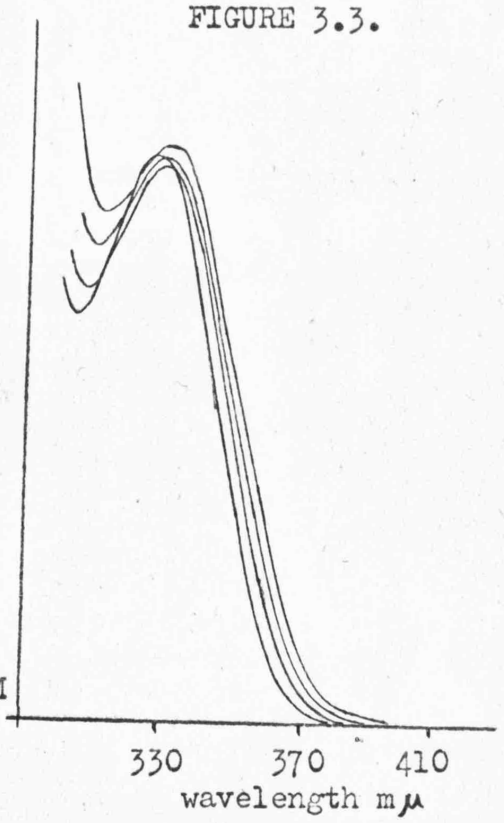

Absorption spectra of T.M.P.D (2.5×10^{-4}M) in n-hexane with added CH_2Cl_2: (A) none (B) 1.96M (C) 5.88M (D) 9.80M.

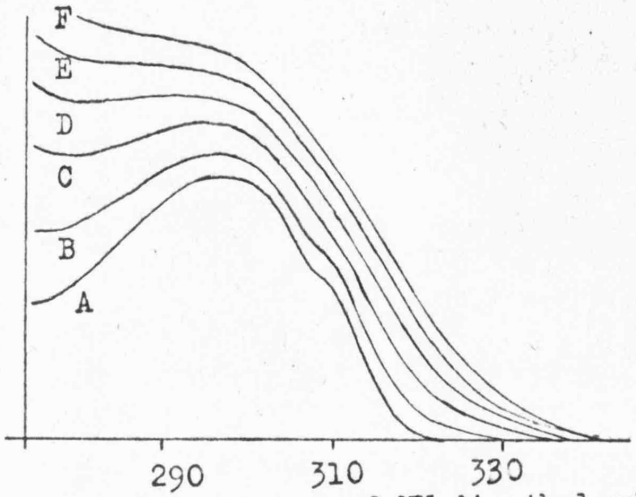

FIGURE 3.4. Absorption spectra of NN-dimethyl-aniline (1.8×10^{-3} M) in n-hexane with added carbon tetrachloride.
(A) none (B) 1.08M. (C) 2.16M. (D) 3.24M. (E) 4.32M. (F) 5.4M.

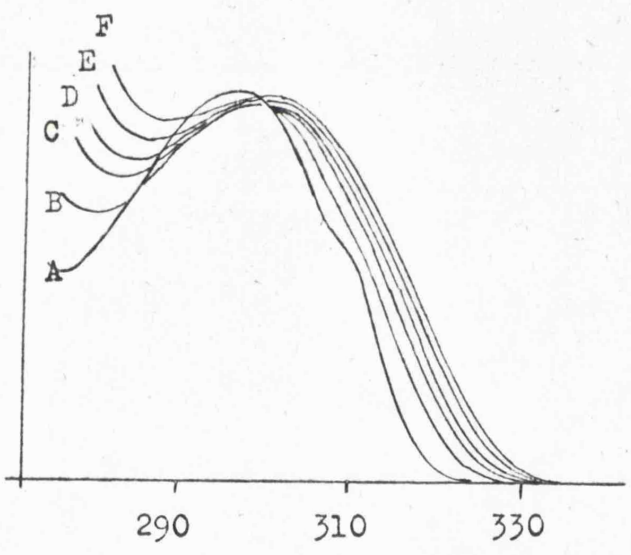

FIGURE 3.5. Absorption spectra of NN-Dimethylaniline (1.8×10^{-3}) in n-hexane with added chloroform. (A) none. (B) 1.39M.
(C) 2.78M. (D) 4.17M. (E) 5.56M. (F) 6.95M.

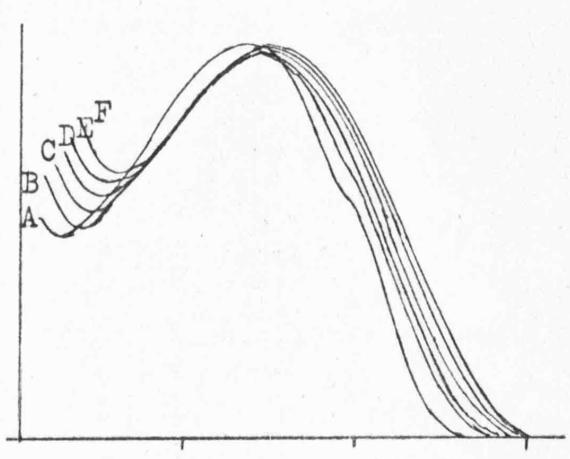

FIGURE 3.6 Absorption spectra of D.M.A. (1.8×10^{-3}) in n-hexane with added CH_2Cl_2 (A) none (B) 1.96M (C) 3.92M (D) 5.88M (E) 7.84M

decrease in resolution as was observed with the addition of the halogenomethanes. It is possible that this apparent absorption could be due to a broadening of the high energy amine band. It was, however, not possible to determine whether this was the case because of the absorption of the halogenomethane in the region of the high energy band of the amine. Attempts were made to isolate the new absorption band by using a reference solution containing the donor at the same concentration as in the sample, this should eliminate the amine bands in the sample spectrum and leave the absorption band of the complex. This technique is usually successful when employed for strong complexes, in this case, however, after initial absorption there was a very large negative absorption which made it difficult to characterise any new absorption band.

By examining the apparent absorption in the low energy region of the amine spectrum estimates were made of the association constants for the equilibrium $A + D \rightleftharpoons AD$ by using the Benesi-Hildebrand[21] equation in the form (for 1 cm. cells)

$$\frac{1}{O.D.} = \frac{1}{K\varepsilon_c b} \quad \frac{1}{a} + \frac{1}{\varepsilon_c b}$$

where O·D. is the optical density due to the complex only, i.e., corrected for the absorption of the donor, K is the association

constant, ε_c the extinction coefficient of the complex at the wavelength of measurement, b is the low fixed concentration of the donor and, a, the high variable concentration of the acceptor. A plot of 1/O.D. versus 1/a gives a straight line of gradient $1/K\varepsilon_c b$ and intercept $1/\varepsilon_c b$ from which K and ε may in principle be determined. The Benesi-Hildebrand plots obtained for the T.M.P.D./halogenomethane system at 305 mμ are shown in FIG. 3·7 and those for the D.M.A./halogenomethane system at 275 mμ in FIG. 3·8. Estimates of ΔH, the heat of association of the complex were made from

$$\Delta H = 2{\cdot}303 \frac{RT_1T_2}{T_2-T_1} \log\left(\frac{(\varepsilon b/O.D._1) - 1}{(\varepsilon b/O.D._2) - 1}\right)$$

where $O.D._1$ and $O.D._2$ are the complex optical densities at temperatures T_1 and T_2 °K. This analysis assumes ΔH and ε to be constant over the temperature range employed, which is probably valid for weak complexes. Values of K and ΔH are given in TABLE 3·1.

FIGURE 3.7

Benesi-Hildebrand plots of 1/O.D. versus 1/a for T.M.P.D/halogenomethane systems at 305 mμ and 23.7°C.

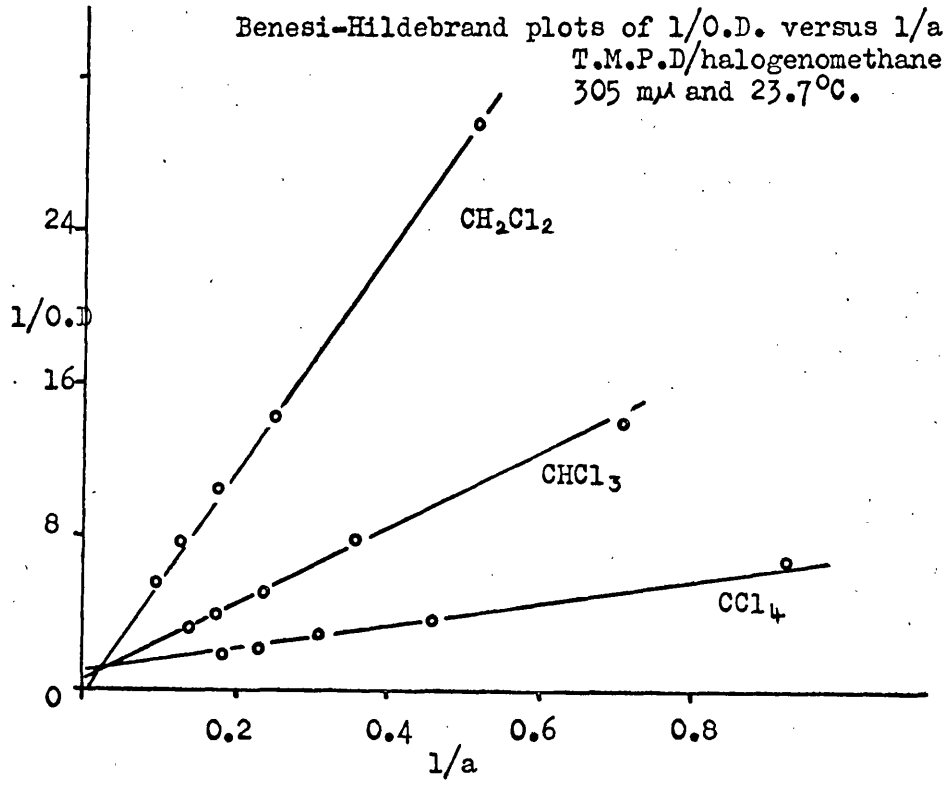

FIGURE 3.8.

Benesi-Hildebrand plots of 1/O.D. versus 1/a for D.M.A/halogenomethane systems at 275 mμ and 23.7°C.

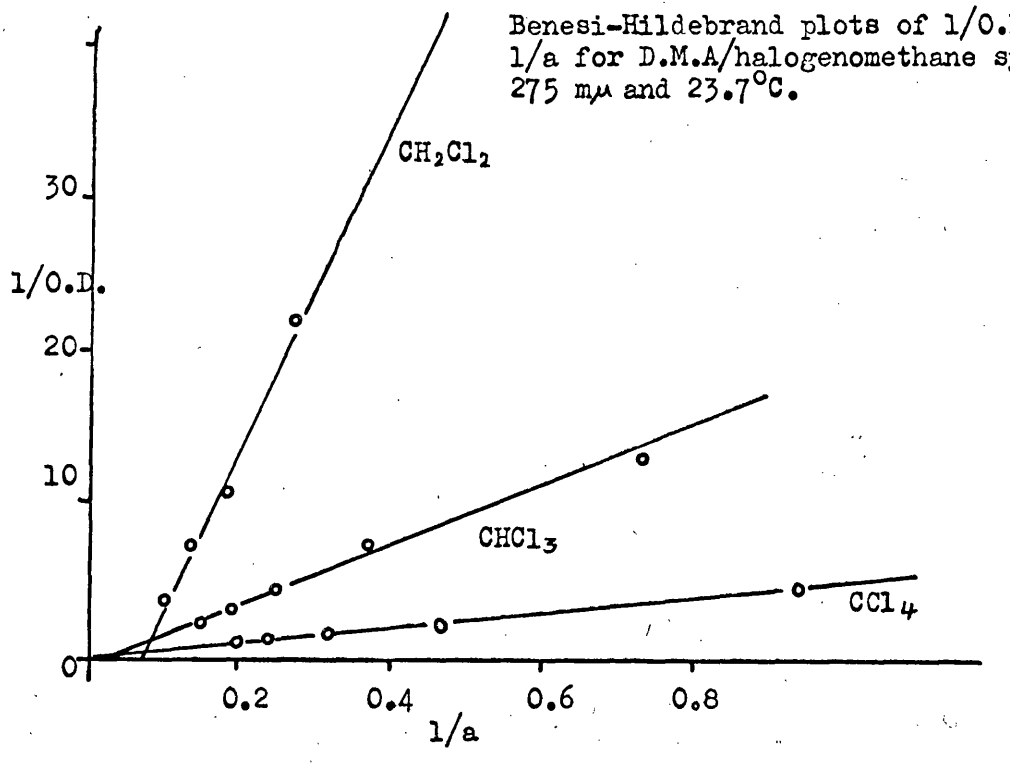

TABLE 3·1 Association constants K and heats of association, ΔH, for the complexes of N,N-dimethylaniline and N,N,N',N'-tetramethyl-p--phenylenediamine with the halogenomethanes, derived from the least-squares analysis of the Benesi-Hildebrand plots.

	NN-Dimethylaniline		N,N,N',N'-tetramethyl-p-phenylene diamine	
	$K(l \cdot mole^{-1})$	ΔH(cal.)	$K\ (l \cdot mole^{-1})$	ΔH(cal.)
CCl_4	0·00	-500	0·13	-1200
$CHCl_3$	Intercept ∿0	-	0·007	0
CH_2Cl_2	Negative	-	Intercept ∿0	-

Solutions of the amines in pure carbon tetrachloride were unstable to light. NN-dimethylaniline formed a brown oil and N,N,N',N'-tetramethyl-p-phenylenediamine reddish brown crystals.

(ii) Halogenomethanes with condensed aromatics

The condensed aromatics give three types of absorption bands in the visible and ultraviolet region of the spectrum. These bands have been classified into three types[45,46] and will be referred to as types 1, 2 and 3.

Type 1. Weak bands often possessing a complicated vibrational structure. The first band of the spectrum is often of this type, or if such a band appears to be absent, then it is assumed to underly the more intense bands which are present.

Type 2. Moderately intense bands, which usually show a very regular vibrational structure.

Type 3. Strong bands with rather less vibrational structure than either of the previous bands.

The effect on the spectrum of a condensed aromatic on adding a halogenomethane differs according to the type of band observed.

Anthracene-halogenomethane system

Anthracene exhibits types 2 and 3 bands. The spectra of anthracene at a fixed concentration with increasing proportions of carbon tetrachloride and chloroform are shown in FIG. 3·9 and 3·10. Both these figures show the effect of added halogenomethane on the long wavelength tail of the type 3 band of anthracene. The tail appears to move out to longer wavelengths, and there appears to be

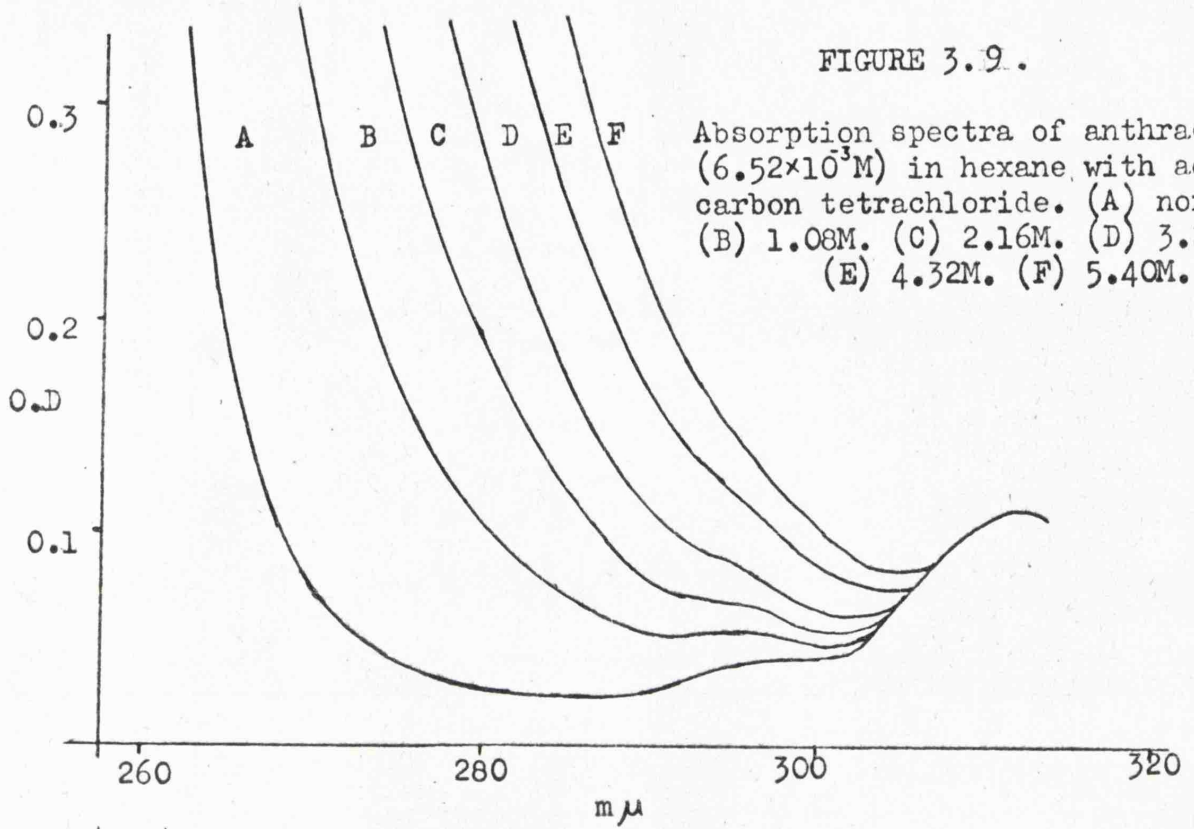

FIGURE 3.9.

Absorption spectra of anthracene (6.52×10^{-3}M) in hexane with added carbon tetrachloride. (A) none. (B) 1.08M. (C) 2.16M. (D) 3.24M. (E) 4.32M. (F) 5.40M.

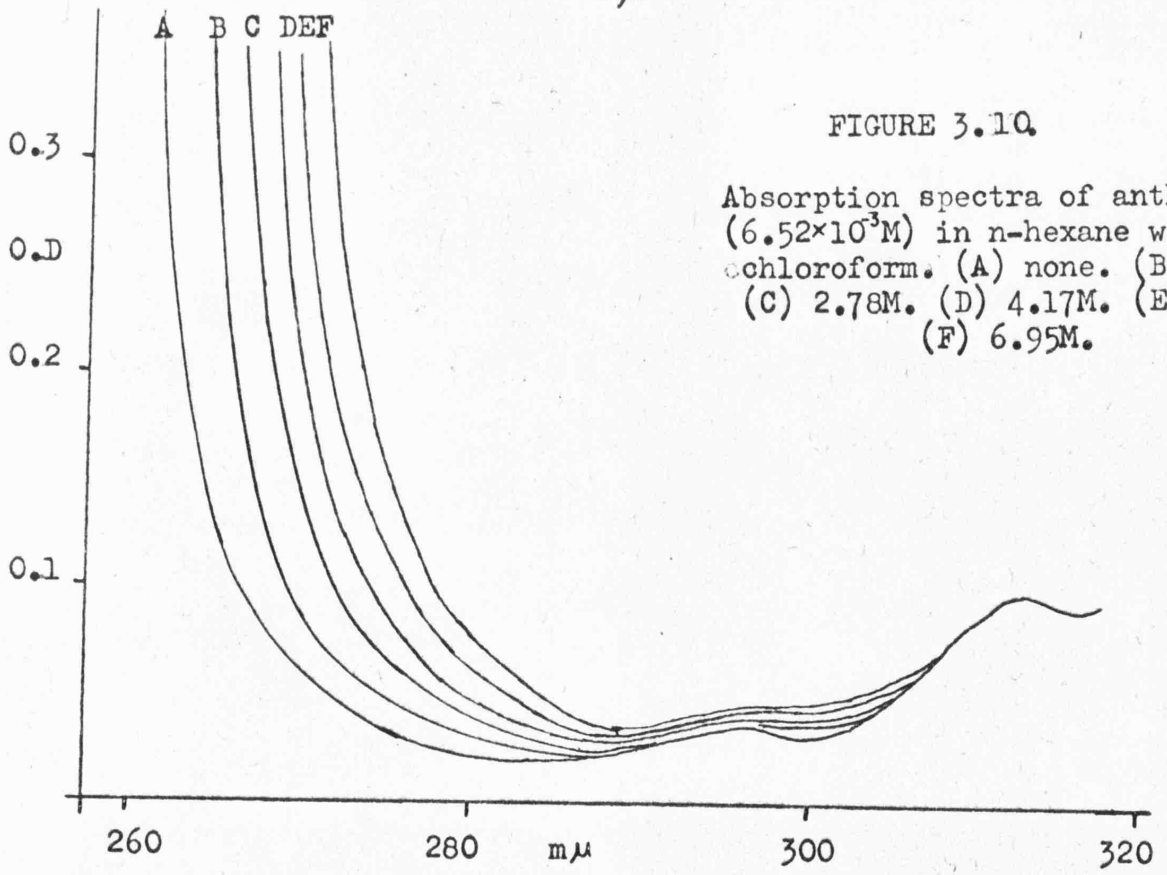

FIGURE 3.10.

Absorption spectra of anthracene (6.52×10^{-3}M) in n-hexane with added chloroform. (A) none. (B) 1.39M. (C) 2.78M. (D) 4.17M. (E) 5.56M. (F) 6.95M.

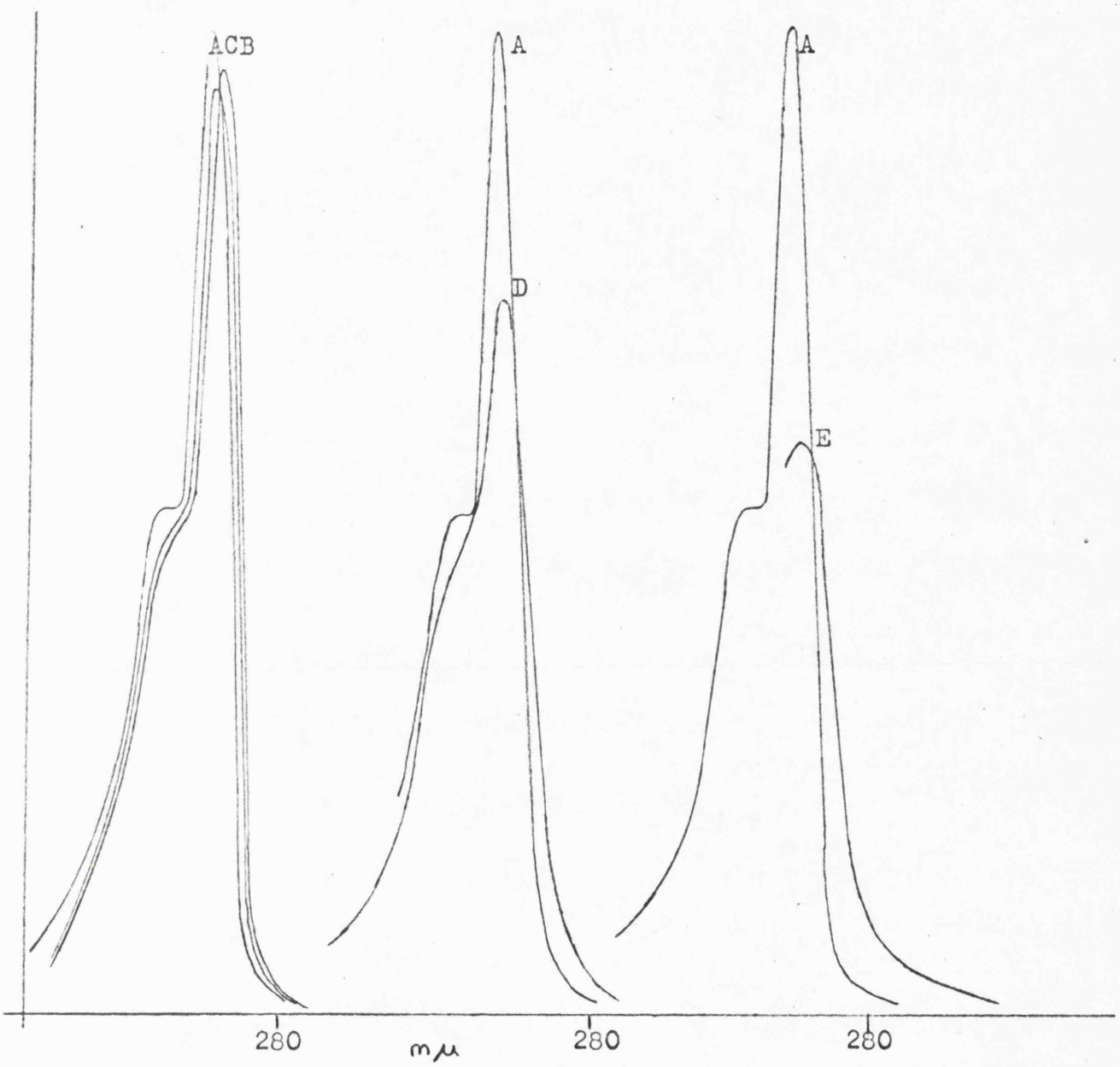

FIGURE 3.11.

A comparison of the effect of various solvents on the type 3 band of a fixed concentration of anthracene.

(A) 1ml. of anthracene 5ml. n-hexane.
(B) ,, ,, 5ml. dioxan.
(C) ,, ,, 5ml. iso-propyl alcohol.
(D) ,, ,, 5ml. chloroform.
(E) ,, ,, 5ml. carbon tetrachloride.

a new absorption growing under it, which could be attributed to complex formation between the anthracene and halogenomethane. This is not a simple solvent shift as was demonstrated by examining the behaviour of the band on addition of solvents, dioxan, isopropyl alcohol, 1,2-dichloroethane, acetonitrile and methanol, (FIG. 3·11.) In these cases a simple shift of the type 3 and 2 bands was observed as is shown in FIG. 3·12 where dioxan is added to a fixed concentration of anthracene in n-hexane. This shift is attributed to normal solvation.

A further investigation of the type 3 band revealed that, if the concentration is changed to permit observation of the peak, although the long wavelength tail of the band increases in intensity, the band maximum decreases drastically in intensity on addition of halogenomethane (FIG. 3·11). This suggests that the increase in intensity of the tail of the type 3 band of anthracene is due to a broadening effect rather than the formation of a new band. Further investigations of this point were not possible with anthracene due to the halogenomethane absorption rendering it impossible to resolve the high energy portion of the band.

Attempts to isolate any new absorption band which might be growing under the type 3 band, by using a reference solution containing anthracene at the same concentration as in the sample solution gave similar results to those reported for the aromatic

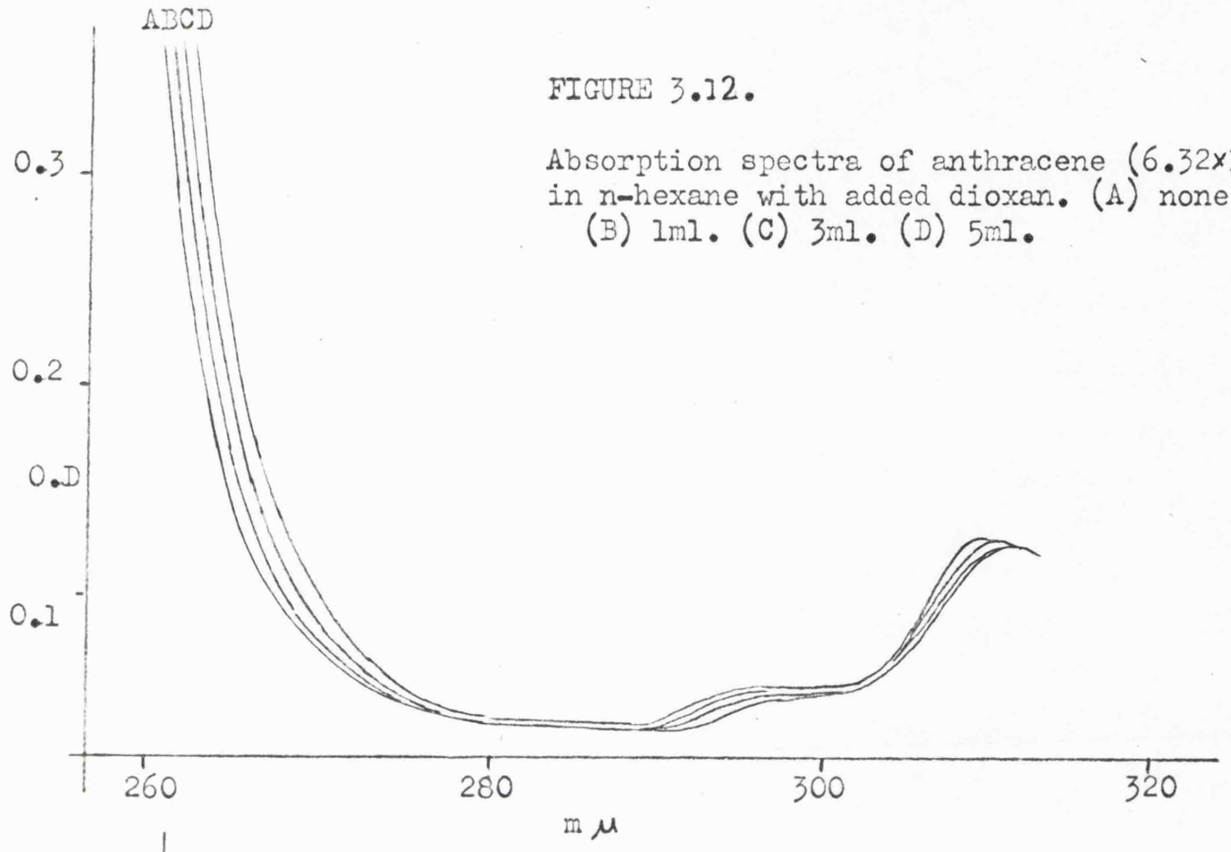

FIGURE 3.12.

Absorption spectra of anthracene (6.32×10^{-3} M) in n-hexane with added dioxan. (A) none. (B) 1ml. (C) 3ml. (D) 5ml.

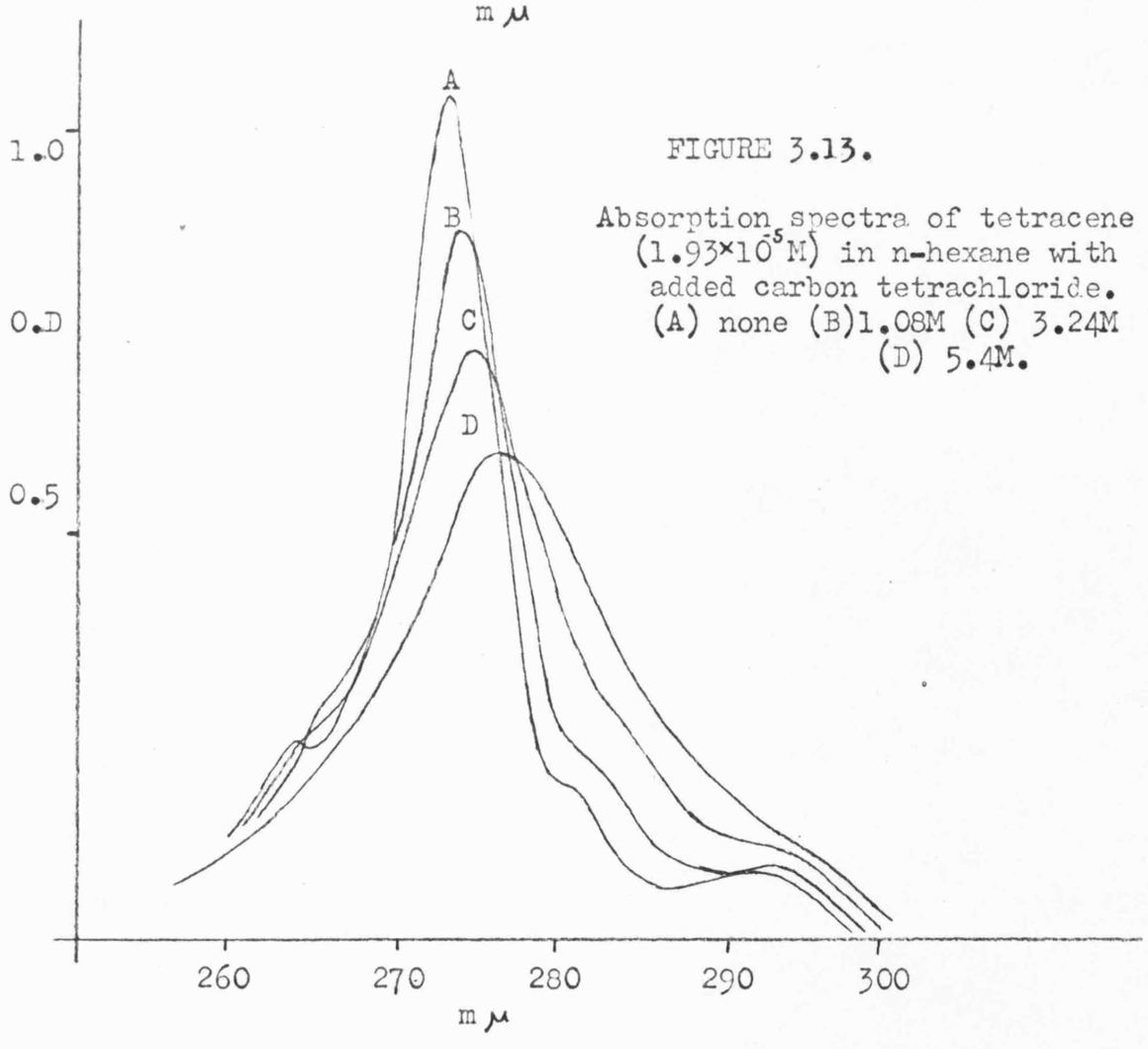

FIGURE 3.13.

Absorption spectra of tetracene (1.93×10^{-5} M) in n-hexane with added carbon tetrachloride. (A) none (B) 1.08M (C) 3.24M (D) 5.4M.

amine halogenomethane systems, i.e. an initial absorption and then a large negative absorption. Such results are explained if the effect of the halogenomethane on the donor is to broaden the absorption band which is being investigated.

Tetracene - halogenomethane system

Tetracene exhibits types 2 and 3 bands. The spectra of the type 3 band of tetracene in n-hexane at a fixed concentration with increasing proportions of carbon tetrachloride is shown in FIG. 3·13. A similar behaviour is shown to that of anthracene. The intensity of the type 3 band diminishes and the peak broadens while the intensity of the type 2 band remains unaffected, and only suffers a slight solvent red shift. Again addition of dioxan and 1,2-dichloroethane (FIG. 3·14) caused no marked diminution in peak intensity or broadening of the band although some loss of fine structure was observed which is normal for a change to a more polar solvent.

To check that the effect was not caused by a chemical reaction the spectrum of a solution of tetracene in n-hexane was obtained. The hexane was evaporated off and the solid was redissolved in carbon tetrachloride to give the same concentration as in the hexane solution. The spectrum exhibited the broadening and diminution of peak height observed previously. Finally the carbon tetrachloride

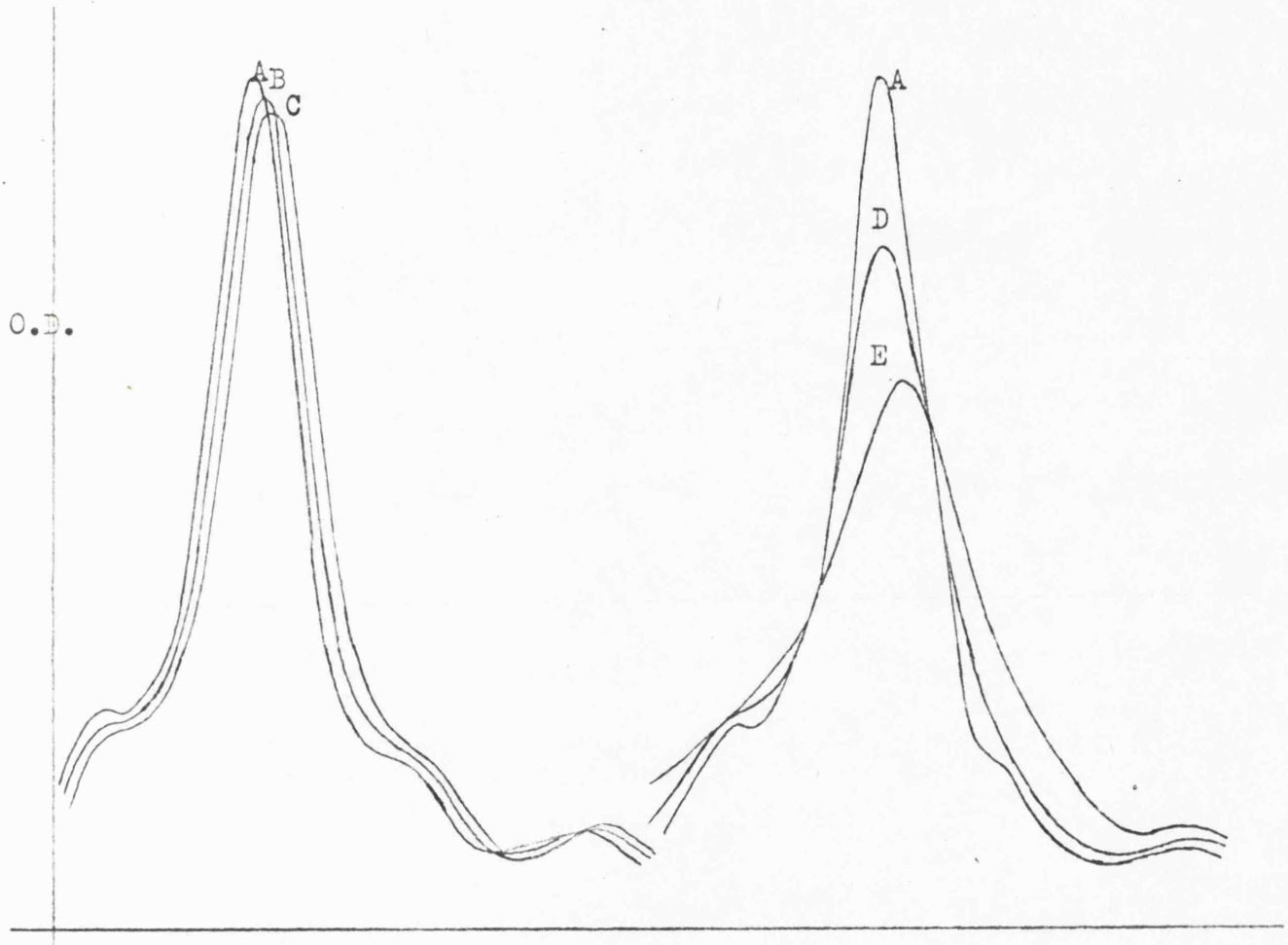

FIGURE 3.14.

A comparison of the effect of various solvents on the type 3 band of tetracene.

A	1ml. of tetracene in	n-hexane,	5ml. n-hexane.
B	,, ,,	,,	5ml. dioxan.
C	,, ,,	,,	5ml. 1,2 dichloroethane.
D	,, ,,	,,	5ml. dichloromethane.
E	,, ,,	,,	5ml. chloroform.

was evaporated off and the solid redissolved in n-hexane again at the same concentration as previously. The spectrum obtained was identical to that of the original n-hexane solution.

Measurements of the integrated intensity of the type 3 band for a fixed concentration of tetracene with varying proportions of halogenomethane showed that although there was a diminution and broadening of the peak the integrated intensity remained constant.

Naphthalene - halogenomethane system.

Naphthalene exhibits types 1, 2 and 3 bands. The spectra of the types 1 and 2 bands of a fixed concentration of naphthalene with varying proportions of carbon tetrachloride is shown in FIG. 3·15. An apparent increase in absorption was observed under the types 1 and 2 bands. It was not possible to examine the type 3 band due to halogenomethane absorption. In naphthalene the types 1 and 2 bands are closer in proximity to the type 3 band than in anthracene and tetracene and consequently there is a good deal of overlap. A broadening of the type 3 band could therefore cause an apparent increase in absorption under the types 1 and 2 bands.

Perylene - halogenomethane system.

Perylene exhibits types 2 and 3 bands. The spectra of a fixed concentration of perylene in n-hexane on addition of carbon tetrachloride

FIGURE 3.15.

Absorption spectra of napthalene (2×10^{-4}M) in n-hexane with added carbon tetrachloride.
(A) none. (B) 1.08M. (C) 2.16M. (D) 3.24M.
(E) 4.32M. (F) 5.4M.

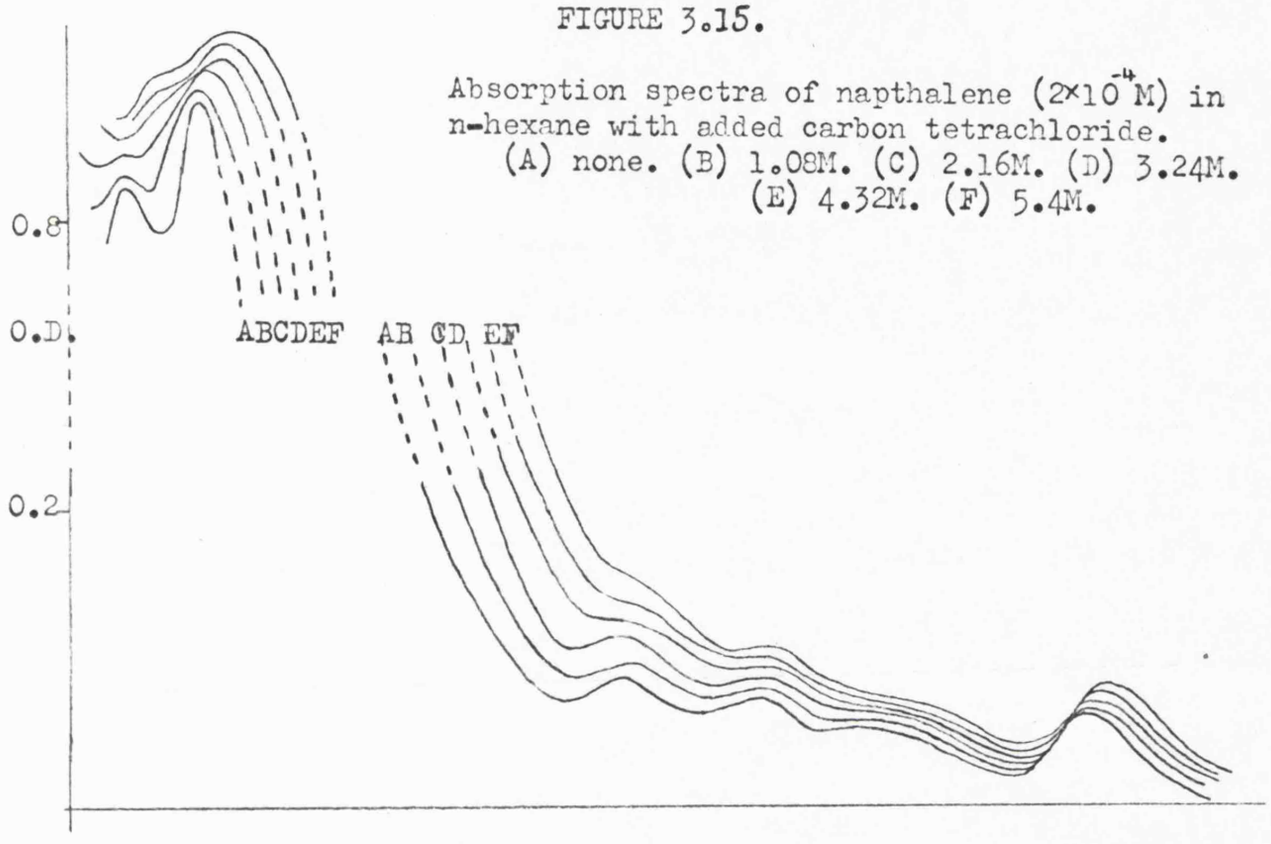

FIGURE 3.16.

Effect of the addition of carbon tetrachloride to a fixed concentration of perylene.

(A) none.

(B) 5ml.

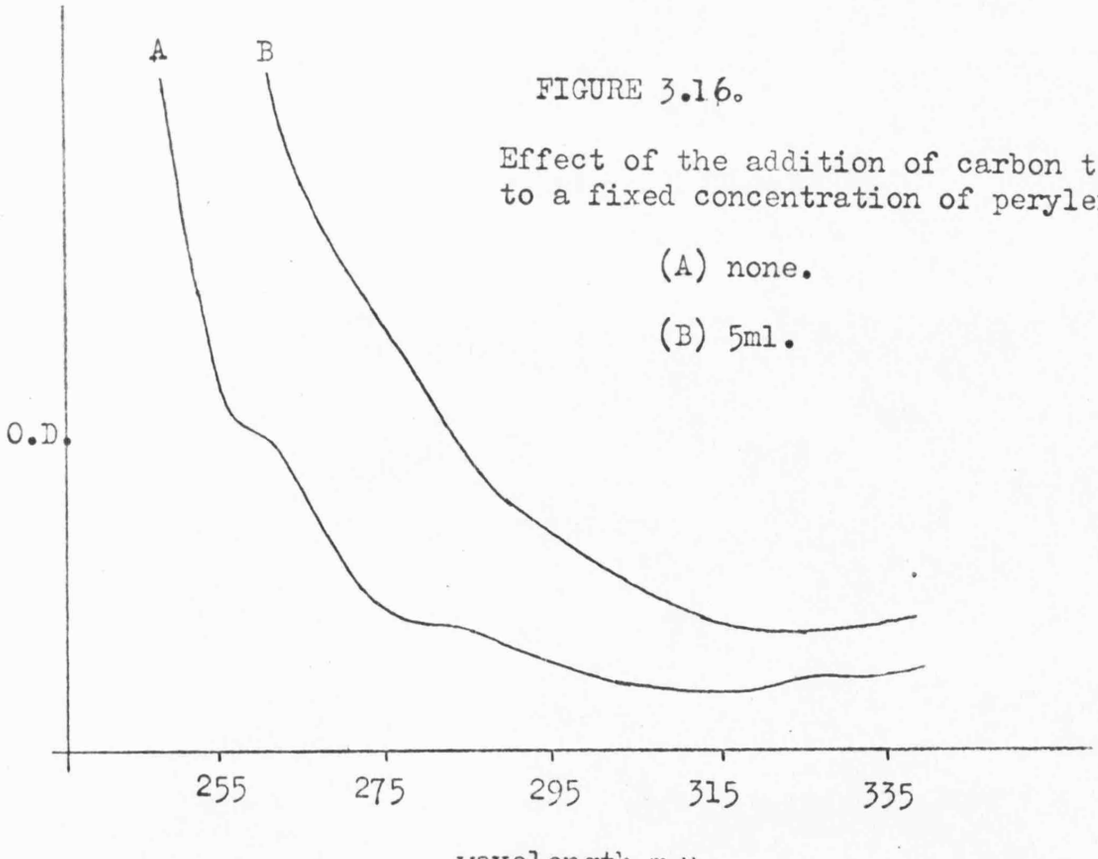

is shown in FIG. 3·16. Similar behaviour is observed to that of the other condensed aromatics studied. The type 3 band appears to broaden while the type 2 band at longer wavelengths remains unaffected.

In all cases the peak broadening and diminution was most marked with carbon tetrachloride and decreased with chloroform and dichloromethane, although they were still marked in these cases.

Applying the Benesi-Hildebrand equation to the apparent absorption under the low energy tail of the type 3 band gave results typified by those in FIG. 3·17, similar to those obtained for halogenomethane - aromatic amine systems. Only in the case of tetracene - carbon tetrachloride was a positive intercept observed giving a computed value for K of 0·15 $1.mole^{-1}$. In all the other cases the intercept was either zero or negative.

3·4 Discussion

(i) Association constants

It is obvious from the plots in FIG. 3·7, 3·8 and 3·17, that the Benesi-Hildebrand equation is unsatisfactory in dealing with the weak complex formation of the halogenomethanes with aromatic donors. Even in those cases where a positive intercept and thus a positive value of K was obtained, it is probable that the value is not accurate. The standard Benesi-Hildebrand equation gives no explanation for zero and negative intercepts. Orgel and Mulliken[22] have suggested that a

FIGURE 3.17 Benesi-Hildebrand plots of 1/O.D. versus 1/a for (A) anthracene/carbon tetrachloride in n-hexane at 270 mμ. b= 6.52×10^{-3}M; (B) anthracene/chloroform at 270 mμ, b=6.52×10^{-3}M; (C) tetracene/carbon tetrachloride at 286.25 mμ, b=1.93×10^{-5}M.

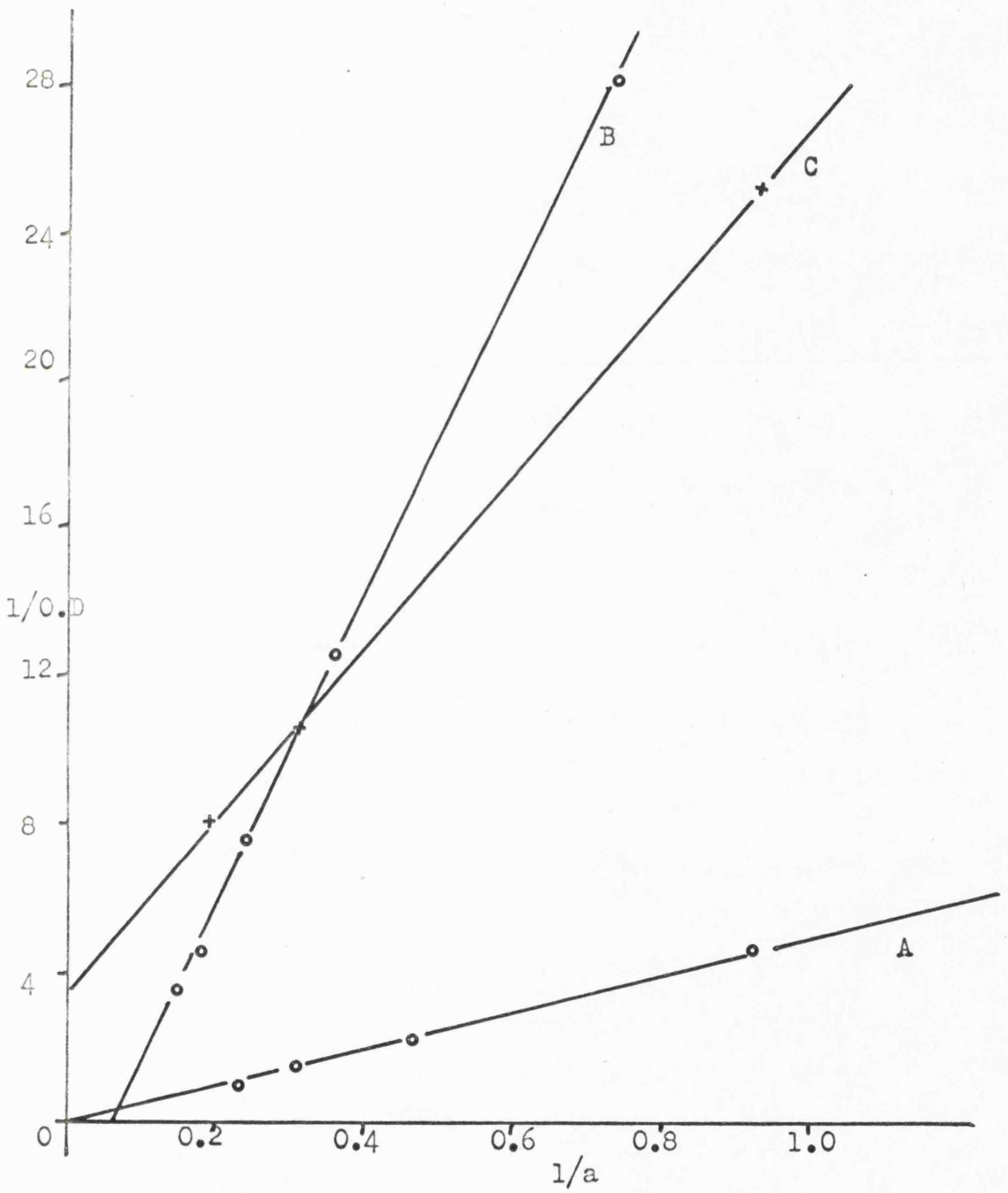

value of K of zero by application of the Benesi-Hildebrand equation such as that found previously in the n-heptane-iodine complexes, may be explained by "contact" charge transfer between molecules in collision. Later is was suggested by Carter et al.[24] that the true equilibrium can be considered as

$$AS_n + DS_m = (DA)S_p + qS \qquad (3\cdot1)$$

where n, m and p are the number of solvent molecules[49] associated with the species A, D, and DA respectively, and n + m-p = q, where it may be shown that

$$K_{B-H} = K_{true} - q(m + 1)/S_o \qquad (3\cdot2)$$

and

$$\varepsilon_{B-H} = \varepsilon_{true} \; K_{true}/K_{B-H}$$

where K_{B-H} is the association constant derived from the Benesi-Hildebrand equation and K_{true} is the association constant for the reaction (3·1). S_o is the solvent concentration in the absence of the donor. They suggest values for the term q(m + 1) of the order 1-3 l mole^{-1} giving errors in the estimation of K for weak complexes (K=1) in the order of 100% or more. They predict that for weak complexes where $q(m + 1)/S_o > K_{true}$ then the Benesi-Hildebrand equation will lead to a negative intercept. This could provide an explanation for the Benesi-Hildebrand plots obtained in this work. Complexes of carbon tetrachloride with tetracene and both amines and chloroform with T.M.P.D give small positive intercepts, those of chloroform with D.M.A, carbon tetrachloride

with anthracene and dichloromethane with T.M.P.D give an intercept of approximately zero, and those of chloroform with anthracene and dichloromethane with D.M.A give a negative intercept. A solvent interaction as suggested above would be expected to be weak with solvents such as n-hexane and therefore this explanation of the negative and zero intercepts may not be conclusive.

Foster et al.[28] have criticised the above theory on the basis that whereas K_{B-H} is often found to be markedly solvent-dependent, ε_{B-H} is often relatively solvent insensitive. They attribute anomalies in K to non-obedience of Beer's Law. Departures from Beer's Law, however, would have to be quite large to explain zero and negative intercepts in the Benesi-Hildebrand plots.

The estimates in TABLE 3·1 are in good qualitative agreement with the value of Stevenson and Coppinger[49] of 0·09 $l mol^{-1}$ for the triethylamine - carbon tetrachloride complex and the value of Dörr and Buttgereit[50] of 2×10^{-2} $l\ mole^{-1}$ for the hexamethyl benzene - carbon tetrachloride complex. Also the value obtained for the carbon tetrachloride-tetracene complex of 0·15 $l\ mole^{-1}$ is in the same range as that obtained by Prausnitz and Anderson[51] of 0·113 $l\ mole^{-1}$ for the mesitylene-carbon tetrachloride complex although the value of 0·64 $l\ mole^{-1}$ obtained by Prausnitz and Weiner for hexamethylbenzene - carbon tetrachloride is considerably higher than any of the K values determined in this work.

Some agreement in the results quoted above is to be expected since all the values for K were determined in n-hexane solutions so that any solvation errors which might be present in the estimation of K are similar.

Wavelength variations in K were found in the present work, and this, coupled with the dependence of K on carbon tetrachloride concentration[52] could indicate some contribution from 2:1 or higher complexes and could explain discrepancies between the results of different workers. It has been suggested that dependence of K on wavelength can be attributed to non-obedience of Beer's Law by the complex absorption peak.[28]

(ii) Heats of Association.

Estimates of ΔH for carbon tetrachloride with the aromatic amines are small and exothermic in contrast to the value for the heat of mixing of aniline and carbon tetrachloride of +300 calories.[55] There is a sharp drop on going from T.M.P.D to D.M.A which is a weaker electron donor and this trend would presumably continue with aniline. With aniline the thermodynamic endothermic heat of mixing must outweigh the small exothermic contribution due to complex formation; that this may be so is borne out by the asymmetrical form of the heat of mixing versus mole fraction curve for aniline in carbon tetrachloride, which is suggestive of complex formation. Aniline will also be self-associated to some extent whereas the methylated amines will not.

This could lead to a larger endothermic contribution to the heat of mixing for aniline.

(iii) Solvent effects of K_{B-H}

If a halogenomethane is used as a solvent in the evaluation of association constants of a molecular complex the results obtained in this work suggest that the halogenomethane may compete with the acceptor for available donor. This will lead to K_{B-H} being underestimated. Merrifield and Phillips have discussed[25] such competitive complexing in terms of the equilibria

$$D + A \underset{}{\overset{K_1}{\rightleftharpoons}} DA$$

$$D + S \underset{}{\overset{K_2}{\rightleftharpoons}} DS$$

whence they derive a dependence of K_{B-H} on K_2, the association constant of the solvent-donor complex

$$K_{B-H} = \frac{K_1 - K_2}{1 + K_2} ; \quad \varepsilon_{B-H} = \frac{K_1}{K_1 - K_2} \cdot \varepsilon \qquad (3\cdot3)$$

The error in estimating K will be greatest for the weak complexes as shown in TABLE 3·2. This table shows the effect on association constants of various values of using a competing solvent such as carbon tetrachloride. Values of K_2 of 0·1 and 0·5 are chosen as most of the association constants reported for various donors with carbon tetrachloride lie in this region.

TABLE 3·2

Effect on the values of K_{B-H} of considering solvent donor complex formation with an association constant K_2 ; K_1 is the corrected association constant of the complex in the presence of the competing solvent.

	K_2 = 0·1	K_2 = 0·5
K_{B-H}	K_1	K_1
0·1	0·21	0·65
0·5	0·65	1·25
1·0	1·20	2·0
10·0	11·10	15·5

TABLE 3·2 shows that quite drastic modifications of K_{B-H} can result. This specific interaction may be additive to the solvent effect of equation (3·2) since in the former the site of the donor is blocked by complex formation and in the latter the acceptor must remove part of the solvation shell attached by rather weaker forces to those donor molecules not involved in a specific complex. In the limit of very weak complexes these two effects may be indistinguishable. Bayliss and Brackenridge[56] have suggested that for weak complexes the absorption spectra may well be interpreted in terms of solvent

perturbations of the donor excited state, or acceptor bands as by 1:1 complex formation.

(iv) Nature of the interaction

From the results obtained for the interaction between aromatic hydrocarbons and amines with the halogenomethanes it is obvious that this interaction is different from the "normal"solvation effects exhibited by other solvents.

The nature of this specific interaction is not however immediately apparent. It is tempting, particularly if the low energy tail of the donor absorption only is observed, to assign the apparent increase in intensity to a new band characteristic of a charge transfer complex. This explanation has been proposed to explain similar results obtained with benzene derivatives[50-52] and amines[50,53]. If this is the case then if the technique of using the donor solution as a reference is used it should be possible to obtain a peak due to the new absorption. Employing this technique on the systems studied in this work only produced a spurious peak due to the broadening and shifting of the donor peak in the sample cell compared with the unchanged donor absorption in the reference cell. This could explain some of the results published previously. Other evidence for the existence of a specific complex in solution is inconclusive. Quadrupole resonance studies[57] on the systems

p-xylene-carbon tetrachloride and p-xylene-carbon tetrabromide showed little evidence of complex formation but the same technique also failed to produce evidence for the well established complex, hexamethylbenzene-chloranil. The X-ray crystal structure[58] of p-xylene-carbon tetrabromide on the other hand shows an alternate structure characteristic of donor-acceptor complexes, the structure consisting of "zig-zag" strings of alternate carbon tetrabromide and p-xylene molecules. Also quite well defined complexes crystallise out from a solution of methylbenzenes in carbon tetrachloride on lowering the temperature and this method may be used to effect a separation of the methylbenzenes.[59] Only with the complexes of carbon tetrachloride with the amines and tetracene, and chloroform with T.M.P.D, in the present work, could a positive value for the association constant be determined from spectrophotometric data using the Benesi-Hildebrand equation and even those values were too small to be definitely ascribed to a complex. It would appear that although there is considerable evidence for complexes of some form in the solid phase, the evidence for solution complexes is inconclusive.

All this underlines the difficulties arising in analysing the spectrophotometric data to obtain association constants and other thermodynamic data. The assumption has to be made if the peak

ascribed to a complex overlaps the component absorption peaks, that these peaks remain unaltered in position, intensity and width in the complexing medium. In this particular case and in other systems which have been examined in a similar way[60] this would seem to be an invalid assumption.

It has already been discussed in 3·4(i) that the evidence for complex formation from Benesi-Hildebrand plots is hardly conclusive. From the plots obtained for the systems examined it is difficult to distinguish between the three possibilities of real complex formation with perhaps solvent competition (positive, zero or negative plots); contact charge-transfer (zero intercept); and a physical interaction of some kind, presumably an intermediate interaction between normal solvation and specific complex formation.

If the spectra are considered, particularly those of the halogenomethane-aromatic hydrocarbon systems, the fact that the total integrated intensity of the donor absorption band remains constant would seem to rule out the presence of a charge-transfer band, although the possibility remains that such a band could be present at higher energies and that the effect observed on the donor absorption peak is a secondary effect caused by complex formation. However the ease of evaporating off the halogenomethane leaving the spectra unchanged seems to be against the existence of a specific complex of any strength.

If no specific complex is formed under the conditions used then we are left with contact charge-transfer or physical perturbation due to a specific form of solvation and it is extremely difficult to distinguish between these alternatives. Previous measurements which have been ascribed to contact charge-transfer have been obtained for such systems as oxygen with various organic molecules[61] and iodine with saturated hydrocarbons.[22] Many of the features of such spectra are similar to the spectra of the systems studied in the present work. In all cases the common feature has been an absorption rising steeply into the region where the components absorb, with no observation of an absorption peak.

Contact charge-transfer occurs when two molecules are in chance contact with one another, when a transition to a charge transfer excited state becomes possible. To account for the intensity of such transitions Murrell[62] postulated that intensity was 'borrowed' by admixture of a donor excited state with a charge transfer state. Such an admixture is helped by the two states belonging to the same group theoretical species and also by the fact that the overlap integral between these states will be quite large due to the excited state orbitals involved being larger than the ground states thus favouring electron transfer via the donor excited states. For contact charge-transfer one therefore has a ground state consisting of a donor in contact with an acceptor. The interaction in the

ground state will be weak with little or no stabilisation. One may then view two transitions, one from a donor to a donor excited state, the other from a donor in contact with a halogenomethane molecule to an excited state which is an admixture of donor excited state and charge transfer state. These two excited states may not differ greatly in energy and since the ground state perturbation is small the two transitions may not differ greatly in wavelengths. The effect of say a halogenomethane on the donor spectrum may then be simply a redistribution of intensity caused by admixture of charge-transfer state into the donor excited state causing a broadening of the particular absorption peak.

Alternatively one may describe the interaction as a physical perturbation of the donor causing a redistribution of vibrational component intensities. Either of these explanations would be consistent with the observation of broadening with maintenance of integrated intensity.

(v) Reactions of the halogenomethanes

The broadening and resultant fall in peak intensity explains the quenching effect of halogenomethanes on aromatic molecules,[63,64] as with a standard exciting intensity the population of the excited state and consequently the emission intensity will fall in the presence of the halogenomethane. In addition quenching may also be caused by intersystem crossing from the donor excited state to a

charge transfer excited state followed by radiationless transition to the ground state.

Solutions of amines and hydrocarbons in carbon tetrachloride are photochemically unstable and this may be interpreted as decomposition via the excited state of the charge transfer complex.

PART ONE

REFERENCES

The references are arranged so that the authors names in alphabetical order are followed by the journal, the volume of the journal underlined, the page number and the year of publication in brackets.

1. Briegleb;
Z.physik.Chem., B16,249,(1932).

2. Gibson and Loeffler;
J.Am.Chem.Soc., 62,1324,(1940).

3. Hammick and Yule;
J.Chem.Soc., 1539,(1940).

4. Bennett and Willis;
J.Chem.Soc.,256,(1929).

5. Weiss;
J.Chem.Soc., 245,(1942); 422,(1943).

6. Brackmann;
Rec.Trav.Chim, 68,147,(1949).

7. Mulliken;
J.Am.Chem.Soc., 72,600,(1950).

8. Mulliken;
J.Am.Chem.Soc., 74,811,(1952).

9. Mulliken;
J.Phys.Chem., 56,801,(1952).

10. Mulliken;
Rec.Trav.Chim., 75,845,(1956).

11. Mulliken;
J.Chim.Phys., 61,20,(1964).

12. Dewar and Thompson;
J.Phys.Chem., 56,801,(1952).

13. Briegleb;
Zwischen molekulare Krafte and Molekülstrutur,Stuttart (1937).

14. Weiss;
Phil.Mag., 91,1169,(1963).

15. McConnel,Ham and Platt;
J.Chem.Phys., 21,66,(1953).

16. Frankling,Hastings,Schiller and Matsen;
J.Am.Chem.Soc., 75,2900,(1953).

16. Frankling, Hastings, Schiller and Matsen;
J.Am.Chem.Soc., 75,2900,(1953).

17. Dewar and Lepley;
J.Am.Chem.Soc., 83,4560,(1961).

18. Dewar and Rogers;
J.Am.Chem.Soc., 84,395,(1962).

19. Lepley;
J.Am.Chem.Soc., 84,3577,(1962).

20. Briegleb;
Molelekulverbundugen and Ko-ordination svebindungen in Erazeldarstellungen Elecktronen-Donor-Acceptor Komplexe,Springer Verlag, Germany.

21. Benesi and Hildebrand;
J. Am.Chem.Soc., 71,2703,(1949).

22. Mulliken and Orgel;
J.Am.Chem.Soc., 79,4839,(1957).

23. Mulliken;
Rec.Trav.Chim., 75,845,(1956).

24. Carter,Murrel and Rosch;
J.Chem.Soc., 2048,(1965).

25. Merrifield and Phillips;
J.Am.Chem.Soc., 80,2779,(1958).

26. Corkill,Foster and Hammick;
J.Chem.Soc., 1202,(1955).

27. Tamres;
J.Phys.Chem., 65,654,(1961).

28. Emslie,Foster, Fyfe and Hormann;
Tetraheron, 21,2843,(1965).

29. Barb;
Trans.Far.Soc., 49,143,(1953).

30. Knorr and Schlenk;
Annalen, 368,287,(1909).

31. Torry;
J.Am.Chem.Soc., 34,708,(1912).

32. Benson;
J.Am.Chem.Soc., 82,6408,(1960).

33. Foster and Thomson;
Trans.Far.Soc., 59,296,(1963).

34. Foster and Thomson;
Trans.Far.Soc., 58,860,(1962).

35. Bijl, Kainer and Rose-Innes;
Naturwiss, 41,303,(1954).

36. Kainer and Uberle;
Ber., 80,1147,(1955).

37. Calvin,Eastmann and Engelsma;
J.Am.Chem.Soc., 84,1339,(1962).

38. Bijl,Kainer and Rose-Innes;
J.Chem.Phys., 30,765,(1959).

39. Eley,Inokuchi and Willis;
Disc.Far.Soc., 28,54,(1959)

40. Bose,Labes and Sehr;
J.Chem.Phys., 33,868,(1960); 32,1570,(1960).

41. Kommandeur and Singer;
J.Chem.Phys., 34,133,(1961).

42. Davis and Symons;
J.Chem.Soc., 2079,(1965).

43. Kuroda,Kinoshita, Kobayshi and Takemoto;
J.Chem.Phys., 36,457,(1962).

44. Haker;
J.Chim.Phys., 55,613,(1958); Z.phys.chem., 155,223,(1959).

45. Briegleb,Liptay and Schindler;
Z.Elektrochem., 66,311,(1962).

46. Lovelock;
Nature, 189,729,(1961).

47. Briegleb;
Angew.Chem.Intermat.Ed., 3,217,(1964).

48. Gaines, Kay and Page;
Trans.Far.Soc., 62,874,(1966).

49. Coppinger and Stevenson;
J.Am.Chem.Soc., 84,119,(1962).

50. Buttgereit and Dörr;
Ber.Bunsen Gesellschaft Phys.Chem., 67,867,(1963).

51. Anderson and Prausnitz;
J.Chem.Phys., 39,1225,(1963).

52. Prausnitz and Weiner;
J.Chem.Phys., 42,3643,(1965).

53. Davis and Farmer;
J.Chem.Soc.(B), 28,(1967).

54. Foster and Horman;
J.Chem.Soc.(B), 171,(1966).

55. Deshpande and Pandya;
Trans.Far.Soc., 61,1858,(1965).

56. Bayliss and Brackenridge;
J.Am.Chem.Soc., 77,3959,(1955).

57. Hooper;
J.Chem.Phys., 41,599,(1964).

58. Strieter and Templeton;
J.Chem.Phys., 37,161,(1962).

59. Bataafsche Petroleium Maatschappij;
Dutch 84,412,(1957).

60. McCartin;
J.Am.Chem.Soc., 85,2021,(1963).

Also Gouterman and Stevenson;
J.Chem.Phys., 37,2266,(1962).

61. Mulliken and Tsubomura;
J.Chem.Soc., 82,5966,(1960)

62. Murrell;
J.Am.Chem.Soc., 81,5037,(1959).

63. Boudart and Stevens;
Ann. New York Acad.Sci., 67,570,(1953).

64. Melhuish and Metcalf;
J.Chem.Soc.,480,(1958).

P A R T T W O

AN INVESTIGATION OF THE CATALYTIC PROPERTIES OF THE FIRST ROW TRANSITION METAL SALTS TO THE ORTHO-PARAHYDROGEN CONVERSION.

C H A P T E R F O U R

The ortho-parahydrogen conversion and experimental techniques used in following it.

4·1 Ortho and Para-Hydrogen

Quantum theory in 1927 led to the assertion[1,2] that the hydrogen molecule could exist in two distinct stable forms, para-hydrogen and ortho-hydrogen, which had differing physical properties. This development led to an explanation of the intensity distribution of the molecular spectrum[3] and the falling off of the rotational specific heat with temperature.[4] Dennison[5] stated that hydrogen cooled to low temperatures was not in thermodynamic equilibrium with respect to the two forms but that the equilibrium corresponding to higher temperatures was frozen.

The proton has a nuclear spin of $^1/_2$, the hydrogen molecule can thus have one combination anti-symmetrical in the nuclear spin and three combinations symmetrical, Para-hydrogen has its spins anti-parallel and has even rotational quantum numbers while ortho-hydrogen has its spins parallel and has odd rotational quantum numbers. Normal hydrogen consists of 25% para and 75% ortho. As the temperature of the hydrogen is lowered the energy content of the molecules decreases and the higher rotational levels become less common. Near absolute zero the majority of the gas molecules should occupy the lowest, which is the zero, rotational level. The zero rotational level is the para-state so the majority of the hydrogen molecules should be in the para-state at temperatures near absolute zero.

Owing to the difficulty of reversing nuclear spins the establishment of the low temperature equilibrium takes a considerable length of time. In 1929 Bonhoeffer and Harteck[6,7] discovered that the attainment of equilibrium could be accelerated by the use of charcoal as a catalyst, and they managed to isolate a sample of almost pure para-hydrogen.

Following the isolation of para-hydrogen various methods of analysing mixtures of ortho and para-hydrogen were developed[8,9,10], the catalytic chemist therefore had available a reaction of ideal simplicity - the conversion of para-hydrogen to ortho-hydrogen and vice versa. Later developments also showed that deuterium could exist in ortho and para forms thus making available two more catalytic reactions, deuterium-hydrogen exchange and the conversion of ortho-deuterium to normal-deuterium. Equilibration of the two forms of hydrogen has been achieved by a wide variety of catalysts. In particular charcoals, transition metals and salts, free radicals and paramagnetic gases.

The conversion

The conversion has been found to occur by two mechanisms, a paramagnetic conversion and a chemical conversion. The paramagnetic conversion involves a physical twisting of the spins of the hydrogen molecule without dissociation of the molecule. The spin reversal is catalysed by a paramagnetic centre, the inhomogenous magnetic

field of the centre mixing with the nuclear spins of the hydrogen molecule. It takes place at low temperatures and is characterised by a negative temperature coefficient[11] since the rate is dependent on the amount of molecularly adsorbed hydrogen and therefore should occur faster at lower temperatures where Van der Waals adsorption predominates. The chemical conversion involves actual rupture of the hydrogen-hydrogen bond with chemisorption of H atoms on the catalytic surface followed by recombination and subsequent desorption in the equilibrium condition. This type of conversion usually has a positive activation energy.

4·2 The chemical conversion

Several mechanisms have been postulated to describe the kinetics of the chemical conversion, these are summarised below.

(i) The Bonhoeffer-Farkas[12] mechanism :

$$pH_2 + M{\cdot}M \rightarrow MH{\cdot}MH \rightarrow M{\cdot}M + oH_2$$

here the chemisorbed atoms link up randomly in pairs and evaporate as molecules in the equilibrium condition.

(ii) The Rideal[13] mechanism. This mechanism was a development of (i) since it was shown[14] by statistical calculations that in an immobile layer of hydrogen atoms there are 8% vacant sites and that in certain cases chemisorbed films of hydrogen were too stable for the above mechanism to occur. The Rideal mechanism involves empty sites adjacent to chemisorbed H atoms

$$pH_2 + MH{\cdot}M \rightarrow MH{\cdot}MH \rightarrow M{\cdot}M + oH_2$$

(iii) The Eley[15] mechanism. Couper and Eley[16] showed that the existence of gaps as proposed in mechanism (ii) was unlikely and suggested that a more probable mechanism was the reaction between a chemisorbed hydrogen atom and a physically adsorbed hydrogen molecule.

$$pH_2 + MH \rightarrow MH_3 \rightarrow MH + oH_2$$

(iv) The Boreskov[17] mechanism. This is a variant of (ii) and (iii) and postulates migration of a H atom over adjacent chemisorbed H atoms until a H_2 molecule is formed on a site of low desorption energy, when it evaporates.

$$MH \cdot MH \cdot M \cdot H \rightarrow MH \cdot MH_2 \cdot M \rightarrow MH_2 \cdot MH \cdot M$$

4·3 The Physical conversion

A theoretical treatment of the paramagnetic conversion was developed by Wigner[18] to explain the homogenous conversion by paramagnetic gases such as oxygen and nitric oxide, this treatment was later refined by Kalckar and Teller.[19] Wigner obtained an expression for the overall collision efficiency ϕ of the para-hydrogen conversion by applying a time dependent perturbation theory to the interaction between a hydrogen molecule and a paramagnetic centre. The potential energy of interaction of the magnetic moments of the proton, μ_p, and of the magnetic dipole, μ_a, is introduced as a perturbation potential and from the resulting wave equation the probablity of transition W_{01}, between the zeroth and first rotational

levels of a hydrogen molecule in a time of interaction t_s can be calculated as

$$W_{01} = \frac{24\mu_a^2 \mu_p^2 I^2 \pi^2 t_s^2}{h^2 m^8 r_s} \qquad (4\cdot1)$$

where I is the moment of inertia of the hydrogen molecule, h is Planck's constant, m the mass of the hydrogen molecule and r_s the distance of the hydrogen molecule from the magnetic centre. To calculate the overall collision efficiency, ϕ, of all transitions W_{01} must be multiplied by a function G(T) which allows for the ortho-para equilibrium and the endothermicity of the transitions

$$\phi = W_{01}\, G(T) \qquad (4\cdot2)$$

$$\text{where } G(T) = \left(1 + \frac{n_p(T)}{n_o(T)}\right)\left(\frac{\sum_{J=0,1,2\cdots} J \exp(-E_J/kT)}{\sum_{J=0,2,4\cdots} (2J+1)\exp(-E_J/kT)}\right)$$

$n_p(T)/n_o(T)$ is the concentration ratio of para-hydrogen to ortho-hydrogen in equilibrium at temperature T and $E_J = J(J+1)h^2/8\pi^2 I$.

If the magnetic interaction causing catalysis of the conversion occurs during elastic collisions between hydrogen molecules and the paramagnetic surface, the same approximation used by Wigner for the corresponding homogenous reaction may be used. This assumes that the hydrogen molecule approaches the paramagnetic centre with infinite velocity, remains at the collision distance r_s for a time

$t_s = r_s/3c$ where c is the true velocity of the hydrogen molecule, and then leaves the centre at infinite velocity. c is given by the equation $Mc^2 = 3RT$

$$\text{Thus } t_s^2 = \frac{r_s^2 M}{27RT} = \frac{r_s^2 m}{27kT}$$

$$\therefore \phi = \frac{8\mu_a^2 \mu_p^2 I_\pi^2}{9r_s^6 h^2 kT} G(T) \qquad (4\cdot3)$$

ϕ is related to the absolute rate of the conversion, k_m, by

$$k_m = \phi\beta F_a$$

where F_a is the fraction of the surface which is catalytically active and β is the number of molecules desorbed from unit area of surface in one second. Since the conversion proceeds via pure collisions β can be replaced by Z, the number of collisions. Z at a pressure p of the experiment is given by,

$$Z = p/(2\pi mkT)^{1/2}$$

The absolute rate of the conversion is therefore given by

$$k_m = \phi\, ZF_a \qquad (4\cdot4)$$

From this expression the absolute rate of the conversion should vary directly with pressure and depend on the manner in which $G(T)/T^{3/2}$ varies with temperature. Equation (4·4) is based on the assumption that r_s is independent of temperature, any variation of r_s with temperature can be allowed for by using the Sutherland formula

$$r_s = r^2(1 + C/T)$$

where C is a constant and equal to 70·6 for hydrogen. Thus

$$k_m = \frac{8\mu_a^2\mu_p^2 I\pi^2}{9r_\infty^6 h^2 kT} G(T).Z.(1 + C/T)^{-3}.F_a \qquad (4\cdot5)$$

Using the Wigner treatment as described above Farkas and Sandler[33] found that the rate of conversion on the surface of copper sulphate and other paramagnetic crystals was 30 times faster than that predicted by the Wigner theory. This led them to conclude that the conversion was not occurring via simple collisions but instead the conversion was taking place in a physically adsorbed layer of hydrogen molecules. Turkevich and Selwood[43] also showed that absolute rate is greatly increased if the number of molecules held by Van der Waals forces in the neighbourhood of a paramagnetic site is increased. They showed that while the paramagnetic free radical αα-diphenyl-β-picryhydrazyl is a moderately good conversion agent at 85°K the efficiency is greatly increased on admixture with zinc oxide, a weak conversion agent but a strong Van der Waals adsorbent.

Determination of the absolute rate constant, k_m, where the conversion occurs in a physically adsorbed layer.

Two theoretical treatments have been developed from the Wigner theory to describe the mechanism of the conversion in a physically adsorbed layer of hydrogen. Harrison and McDowell[20] considered a mechanism where conversion takes place during the translational

motion of adsorbed hydrogen molecules across the paramagnetic surface, while Eley et al.[21] considered a mechanism where conversion occured while the molecule is vibrating over a "sunken" site.

Translational motion.

If the concentration of molecules corresponding to a complete monolayer is n_o molecules cm^{-2} and θ is the fraction of the surface covered, then the concentration of adsorbed molecules is $n_o\theta$. The rate of adsorption, α, is proportional to the fraction of surface not covered and the number of collisions between hydrogen molecules and the surface, thus assuming that adsorption does not require any activation energy

$$\alpha = \alpha_o (1-\theta)Z \qquad (4\cdot6)$$

If the hydrogen molecule in an adsorbed layer can move freely across the surface, then its motion perpendicular to the surface will be constrained by its Van der Waals interaction with the catalytic surface. The molecules will therefore vibrate in a direction perpendicular to the surface and the activation energy of desorption, q cal $mole^{-1}$, is the energy required to remove a molecule from the zero-point vibration in the adsorbed phase to a state with no translational energy in the gas phase. The rate of desorption β is given by :

$$\beta = \beta_o n_o \theta \exp(-q/kT) \qquad (4\cdot7)$$

where β_o is independent of temperature. At equilibrium $\alpha = \beta$ therefore from (4·6) and (4·7)

$$\theta = \frac{\alpha_o Z}{\alpha_o Z + \beta_o n_o} \exp\left(-q/kT\right) \qquad (4\cdot8)$$

and

$$\beta = \frac{\alpha_o Z}{1 + \alpha_o Z\left[\exp(q/kT)\right]} \cdot \frac{}{\beta_o n_o} \qquad (4\cdot9)$$

In calculating the mean time of sojourn of a molecule in an adsorbed layer, it is supposed that of the $n_o\theta$ molecules present at equilibrium, $n_o\theta_o$ have been introduced at time $t = 0$ and, $n_o\theta_t$ are assumed to remain in the adsorbed layer at time t. The rate of desorption at any subsequent time t_1 of the molecules introduced at time zero is $\beta n_o\theta_t/n_o\theta$ From which, on integration,

$\theta_t = \theta_o e^{-\beta t/n_o\theta}$

so $$d\theta_t = -\beta\theta_o e^{-\beta t/n_o\theta}\, dt/n_o\theta \qquad (4\cdot10)$$

The mean time of sojourn t_m of a molecule is given by

$$t_m = \int_o^\infty t\, d\theta_t \Big/ \int_o^\infty d\theta_t$$

On substituting for $d\theta_t$ as given in (4·10)

$$t_m = n_o\theta/\beta = \frac{\exp(q/kT)}{\beta_o}$$

There is no reason to assume that the actual time of interaction is identical to the period of sojourn. A catalytic surface is not uniformly paramagnetic but probably consists of paramagnetic centres

separated by extensive catalytic inactive areas. Harrison and McDowell assumed that these catalytic areas could be represented by circles of radius $\sim 2\text{Å}$ drawn in a plane parallel to the surface and $r_s\text{Å}$ therefrom. They further assumed that the magnetic interaction takes place with uniform intensity inside the circle and is inactive outside it. If the adsorbed layer is regarded as a two dimensional gas its velocity is given by

$$c = (2RT/M)^{1/2} = (2kT/m)^{1/2}$$

Thus the mean value of t_s, the time of interaction is given by

$$t_s^2 = \frac{1}{c^2}\frac{\sum l^2 n_l}{\sum n_l} \qquad (4\cdot11)$$

Where n_l is the number of paths of length l through a circle of interaction. Putting $\bar{l}^2 = \sum l^2 n_l / \sum n_l$ we get from equation (4·2) and (4·11)

$$\phi = K r_s^{-8} G(T) \bar{l}^2/c^2 \qquad (4\cdot12)$$

where $$K = \frac{24\mu_a^2 \mu_p^2 I\pi^2}{h^2 m}$$

To determine k_m from ϕ, equation (4·12) must be multiplied by n_m, the number of encounters between a molecule and the active centres during one period of sojourn in the adsorbed layer. If 1cm^2 of the surface contains ρ active centres each of area $a\ \text{cm}^2$ the total time of interaction is $t\rho a$. The mean time of interaction with one centre is l_m/c where $l_m = \frac{\sum l n_l}{\sum n_l}$ and the mean number of encounters is

$$n_m = t_m \rho ac/lm$$

$$n_m = t_m Fac/lm \quad \text{where } Fa = \rho a$$

Thus $$k_m = \phi \cdot Fa.t_m (C/l_m)\cdot\beta \qquad (4\cdot13)$$

$$\therefore k_m = \frac{k.r_s^{-8} G(T)\, \bar{l}^2\, Fa\, m^{1/2}}{(2kT)^{1/2} l_m\, \beta_o} \cdot \frac{e^{q/kT}\alpha_o Z}{1 + \alpha_o Z\left(\frac{e^{-q/kT}}{\beta_o n_o}\right)} \qquad (4\cdot14)$$

When the surface coverage is low (θ is small) $\beta_o n_o e^{-q/kT}$ in (4·8) is large compared with $\alpha_o Z$ and so $\beta \simeq \alpha_o Z$. Using $\alpha_o Z$ for β in (4·14) gives

$$k_m = \frac{K.r_s^{-8} G(T)\, \bar{l}^2.F_a\, m^{1/2}\, e^{q/kT}\alpha_o.Z}{(2kT)^{1/2} l_m \beta_o} \qquad (4\cdot15)$$

Where $Z = p/(2\pi mkT)^{1/2}$, $t_s^2 = \bar{l}^2/c^2 = 2r^2/c^2$ and $l_m = 4r/\pi$ [39]

Equation (4·15) requires the absolute rate constant to exhibit a "negative" activation energy equal to the heat of adsorption and be dependent on pressure.

When the surface coverage is high ($\theta \to 1$) $\beta_o n_o e^{-q/kT}$ in equation (4·8) is small compared with $\alpha_o Z$ so $\beta \simeq \beta_o n_o e^{-q/kT}$ then

$$k_m = \frac{Kr_s^{-8} G(T) \bar{l}^2\, F_a\, n_o\, m^{1/2}}{(2kT)^{1/2} l_m} \qquad (4\cdot16)$$

This equation requires the absolute rate constant to be independent of pressure and dependent on the way $(T)/T^{1/2}$ varies with temperature, i.e. it should exhibit a slight "positive" activation energy.

Vibrational motion

Sandler[22] considered the variation in transition probability of the conversion when an adsorbed hydrogen molecule vibrates perpendicularly to the plane of the surface on an adsorption site in a sunken position. Each vibration is then equated to a collision. Eley et al.[21] developing this idea showed that the number of vibrations was $\eta = \exp(q/RT)$, where q is the heat of adsorption. The collision probability from equation (4·3) must therefore be multiplied by this factor to give the "effective collision probability". The rate of desorption is given by

$$\beta = n_o \theta \nu \exp(-q/RT)$$

where ν is the frequency of vibration of the adsorbed molecule and is equivalent to β_o in equation (4·7) of the Harrison and McDowell treatment.

$$K_m = \phi \eta \beta$$

thus
$$K_m = \phi n_o \theta \nu \qquad (4·17)$$

for a surface which obeys a Langmuir isotherm

$$K_m = (\phi n_o \nu) bp/(1+bp) \qquad (4·18)$$

Thus for a surface where the fractional coverage of hydrogen is complete ($\theta = 1$) the Eley treatment predicts that the absolute rate should be independent of pressure and vary as $G(T)/T$ varies with

temperature. While when the fractional coverage of hydrogen approaches zero ($\theta \rightarrow 0$) and providing the surface obeys the Langmuir isotherm the absolute rate of the conversion should be dependent on pressure and again vary as $G(T)/T$ varies with temperature. Eley et al.[21,44] found that this mechanism fitted the absolute rates of conversion on the rare earth oxides in the region $T<135°K$

4·4 Diagnostic tests for the chemical and physical mechanisms

A chemical mechanism should show rates $pH_2 > H_2+D_2 > oD_2$, this being due to the effect of zero point energy on the activation energy.[40] If a paramagnetic mechanism is dominant on a given surface at low temperatures the order of rates will be $pH_2 > oD_2 >> H_2+D_2$, the hydrogen deuterium equilibration not occuring via a physical mechanism. In addition rate studies give reaction orders which in turn give information concerning surface coverage. Activation energy determinations are also useful since a paramagnetic conversion in a Van der Waals layer usually shows a negative apparent activation energy.[41]

4·5 The Kinetics of the conversion

(i) Rate of the conversion

The conversion is found to follow a first order law at constant pressure and temperature. The experimental first order constant k_e

may be expressed as

$$k_e = 1/t.\ln(x_o - x_{eq.})/(x_t - x_{eq.}) \quad min^{-1}$$

Where x_o, x_t, x_{eq} are the fractions of para-hydrogen present at zero time, time t, and at equilibrium respectively. If n is the number of molecules present the net velocity v in molecules sec^{-1} is

$$V = -n\,dx/dt = nk_e(x_t - x_e)$$

$$\text{or } V_m = nk_e\,(x_t - x_e)/60A \quad \text{molecules } cm^{-2}\ sec^{-1}$$

where A is the surface area in cm^2. Now $Vm = k_m\,(x_t - x_e)$

$$\therefore k_m = nk_e/60A \quad \text{molecules } cm^{-2}\ sec^{-1} \qquad (4\cdot19)$$

(ii) Variation of rate with temperature

The variation of k_m with temperature is given by the Arrhenius equation

$$k_m = B_m e^{-E_A/RT} \qquad \text{at constant pressure.}$$

B_m and E_A are the frequency factor and apparent activation energy respectively.

(iii) Variation of rate with pressure

If the conversion proceeds via adsorbed molecular hydrogen

$$k_m = k_1\theta \qquad \text{where } k_1 \text{ is a constant}$$

this expression can be substituted in equation (4·19) so that

$$k_e = k_2\,\theta/p \qquad \text{at constant temperature}$$

where k_2 is a constant. If adsorption obeys a Freundlich isotherm

$$\theta = ap^n$$

so $$k_e = k_2\,ap^{(n-1)}$$

Thus if the Freundlich isotherm is obeyed a plot of log k_e against log p should be linear with slope n-1. If,however, the adsorption obeys a Langmuir isotherm

$$\theta = bp/(1+bp)$$

then $k_e = k_2\,b/(1+bp)$ and a plot of $1/k_e$ against p is linear with slope $1/k_2$ and intercept $1/k_2b$. Where both isotherms are obeyed $d\ln\theta/dp$[23] derived for the two isotherms has the same value, this leads to the relationship

$$n = 1 - \theta$$

4·6 Experimental techniques used to follow the conversion

(i) Main vacuum system

The main vacuum system consisted of an electrically treated mercury diffusion pump backed by a single stage Genevac rotary oil pump connected to the vacuum line by wide bore pyrex tubing. The pressure in the system was measured by a Mcleod gauge. With a liquid nitrogentrap in front of the diffusion pump a vacuum of better than 10^{-6} mm.Hg.could be obtained. A backing line connected to a pulsometer pump was used for controlling the mercury levels in the Mcleod gauges and cut-offs.

(ii) Reaction system

The reaction system is shown in FIG. 4·1. The reaction vessel A was connected to the gas line and main vacuum line via a liquid nitrogen trap B, to prevent contamination by grease and mercury vapour, and a mercury cut off C which enabled the system to be isolated. The normal hydrogen,para-hydrogen and hydrogen-deuterium mixtures were stored in 3 litre bulbs attached to the gas line via small gas pipettes (see FIG. 5·1). In this way suitable quantities of gas could be admitted to the reaction vessel. The pressure of gas in the reaction system was measured by means of a Mcleod gauge for pressures up to 12 mm and a mercury manometer for higher pressures.

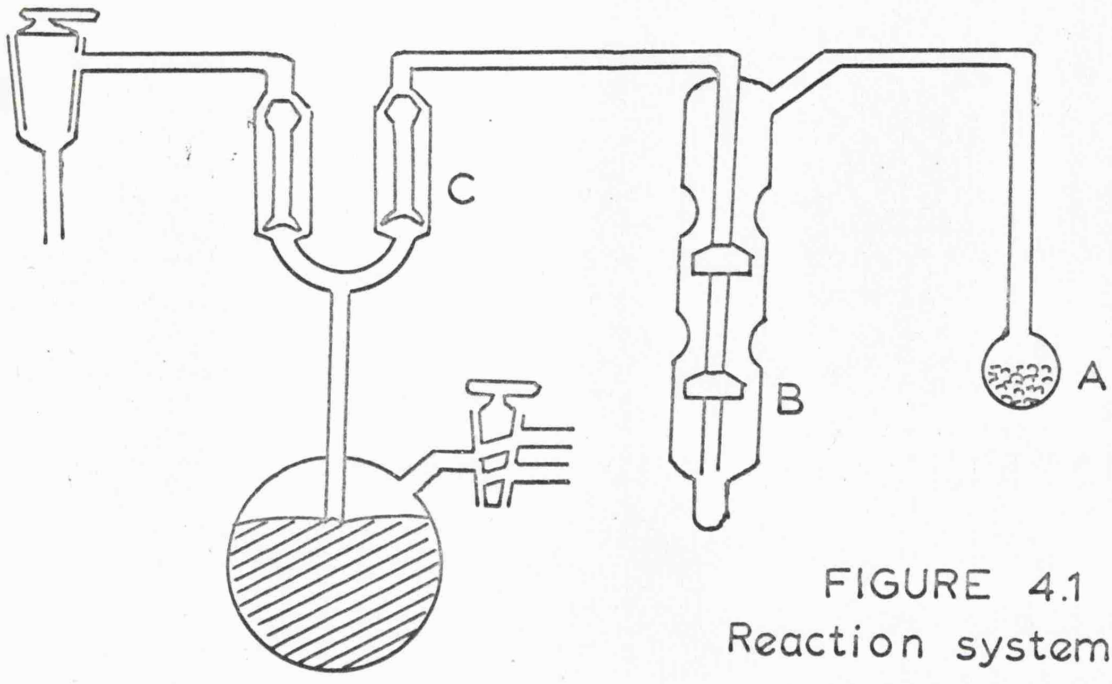

FIGURE 4.1
Reaction system

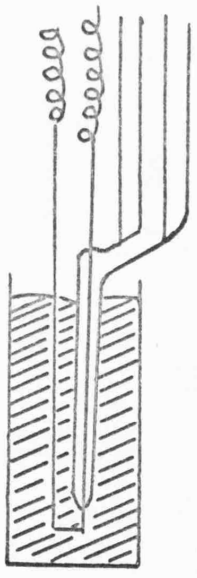

FIGURE 4.2
Micropirani gauge

(iii) Gas analysis

The method used was essentially that of Eley[24,25] and utilised the difference in thermal conductivity of the two forms of hydrogen. Analysis of the hydrogen mixtures was carried out using a micro-pirani gauge as described by Bolland and Melville.[26] The gauge consists of a fine tungsten spiral of resistance 70-100 ohms when stretched to $1\,1/2$ times its own length, spot welded at each end to a piece of platinum wire and sealed into a soda glass capillary (FIG. 4·2). The gauge was immersed in mercury in a small metal bucket for both protection and for greater thermal stability. While in operation the gauge was immersed in liquid nitrogen which maintained the walls at a constant temperature.

The gauge was sealed to the open end of a soda-glass Mcleod gauge which was connected to the rest of the system via soda-pyrex graded seals. All measurements of thermal conductivity were carried out using a standard pressure of 50 mm. Hg of hydrogen in the micro-pirani gauge, this pressure being obtained by raising or lowering the mercury level in the soda-glass Mcleod gauge.

The analysis depends on the thermal conductivity changes of the gas mixture and these were determined by measuring the change in resistance of the gauge at constant potential. To do this a type of Wheatstone Bridge was used with ratio arms of 100 ohms and 1 ohm (FIG. 4·3). It has been found[26] that in order to obtain maximum

FIGURE 4.3 Gauge circuit

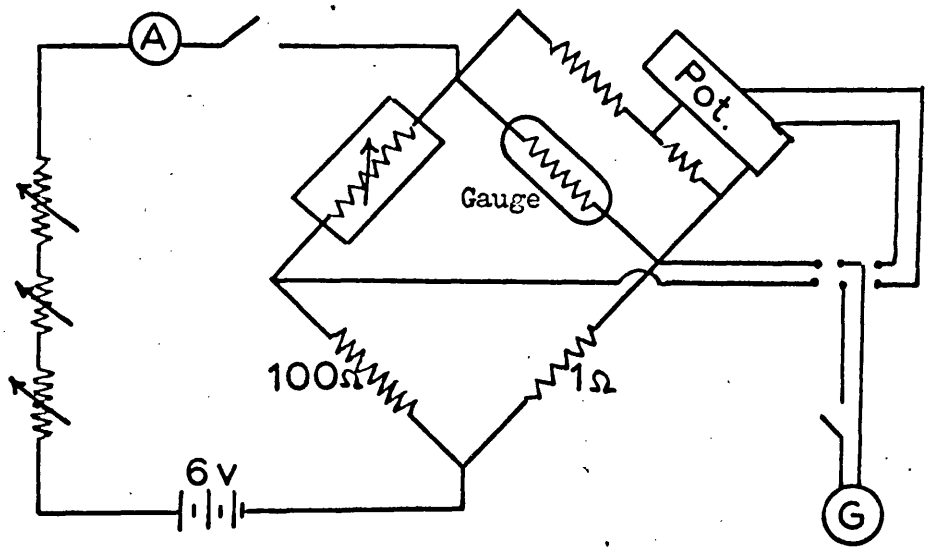

FIGURE 4.4

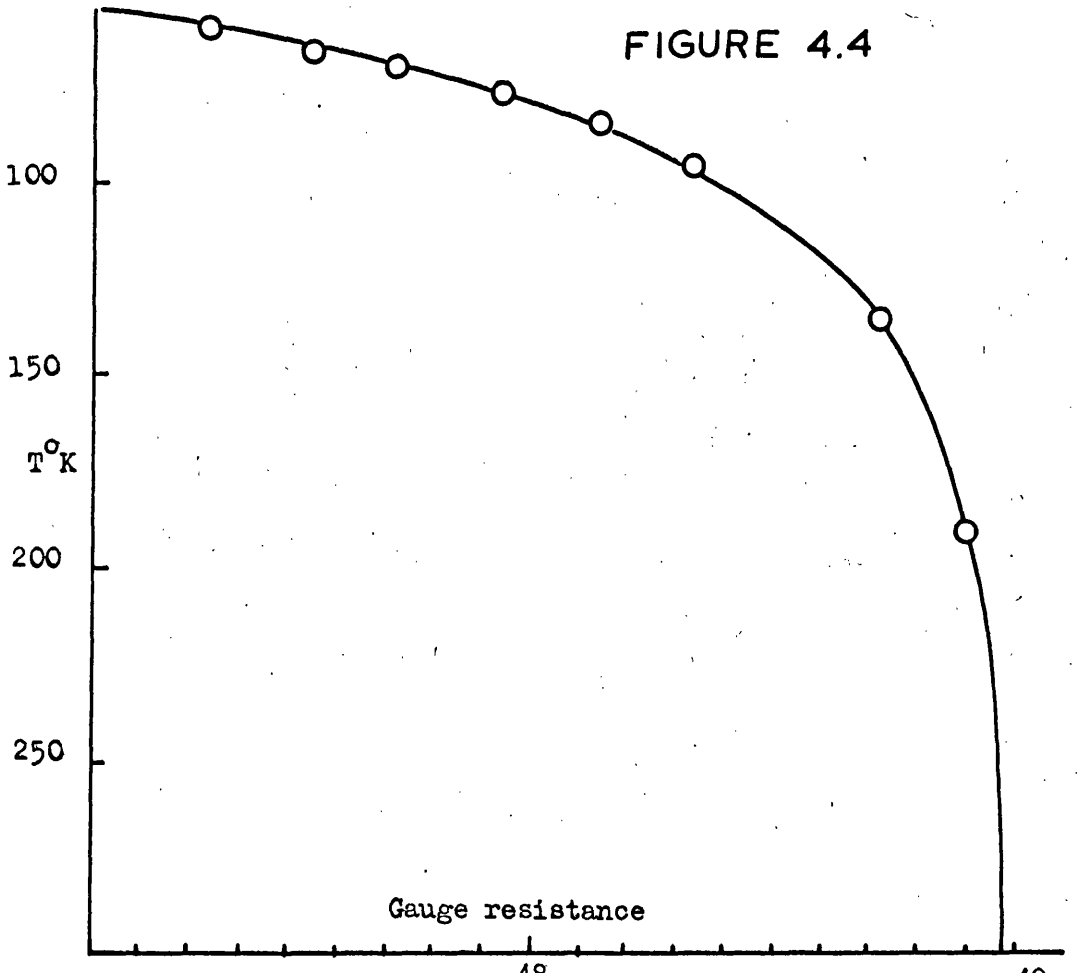

Calibration of gauge for equilibrium mixtures

sensitivity it is necessary to maintain the filament at 170°K. This was done by immersion of the gauge in liquid nitrogen and the application of a six volt potential across it. The potential across the gauge was measured by means of a Pye potentiometer.

To heat the gauge to 170°K it was necessary to know the resistance of the gauge at this temperature. The variation of resistance of the gauge with change in temperature, was, therefore, determined using a very low current to avoid heating the wire. Resistance measurements were made at 77°K, 90°K, 273°K and 298°K, and assuming a linear plot the value at 170°K was obtained by interpolation. The resistance box was set at this value and the gauge filled with normal hydrogen to a pressure of 50 mm. Hg. The current across the bridge was then adjusted to give a balance and the potential across the gauge measured. This value was taken as the standard working potential for the gauge and was only applied when the gauge was filled with 50 mm. of hydrogen and surrounded by liquid nitrogen. The normal hydrogen was then pumped away and replaced by 50 mm. of para-hydrogen. By successive adjustments of the resistance box and heating current, both the bridge and potentiometer circuits were balanced. The resistance box reading was then that characteristic of the sample of para-hydrogen used. The working potential was checked regularly during a catalytic experiment as it had a tendency to drift slightly.

(iv) Experimental procedure

The value of the resistance for an equilibrium mixture at different temperatures is required before a value for the rate constant can be determined. These values were determined in the following manner. The equilibrium resistances were known for room temperature, 90°K and 77°K thus a straight line plot of equilibrium resistance against percentage para-hydrogen could be plotted as the para-hydrogen percentage at different temperatures is known.[27] From this plot and the tables of para-hydrogen content against temperature, a plot of equilibrium resistance against temperature was obtained (FIG. 4·4).

The following procedure was adopted to obtain the rate constant for a conversion. About 1 g. of the sample to be examined was placed in the reaction vessel and outgassed as described in section 6·1. The whole of the reaction system up to the mercury cut-off was then flamed over to remove any adsorbed gases. The trap B (FIG. 4·1) was then surrounded by a bath at the required temperature. Normal or para-hydrogen, depending on the temperature, was admitted at a known pressure, usually about 5 mm. Hg. as the volume of the reaction system precluded using pressures of less than 5 mm. The mercury cut-off was run up and the hydrogen left in contact with the catalyst for the required time. After this time the gas was expanded into the gauge by pulling down the cut-off and the pressure adjusted to

50 mm by judicious use of the gas pipettes in the system. The resistance of the sample was measured and the rate constant was given by :

$$k_e = \frac{2 \cdot 303}{t} \log_{10} \frac{\Omega_o}{\Omega_x}$$

where $\Omega_o = R_e - R_o$

and $\Omega_x = R_e - R_t$

Where R_e, R_o and R_t are the resistances of the gauge for an equilibrium sample, the initial sample and a sample after time t.

(v) Temperature control

Obtaining stable temperatures is a major problem in the study of low temperature conversion. Two fixed points are available at low temperatures, liquid nitrogen (77°K) and liquid oxygen (90°K), and of these only the latter can be considered as a true fixed point since liquid nitrogen adsorbs oxygen thus increasing its boiling point. Higher temperatures (90°-350°K) were obtained by using cold baths which had a stability of ± 0·5° (measured by a copper-constantan thermocouple) over a period of 30 min., a demountable cryostat and furnace. The demountable cryostat was essentially the same as that of Ashmead and Rudham[28] and is shown in FIG. 4·5.

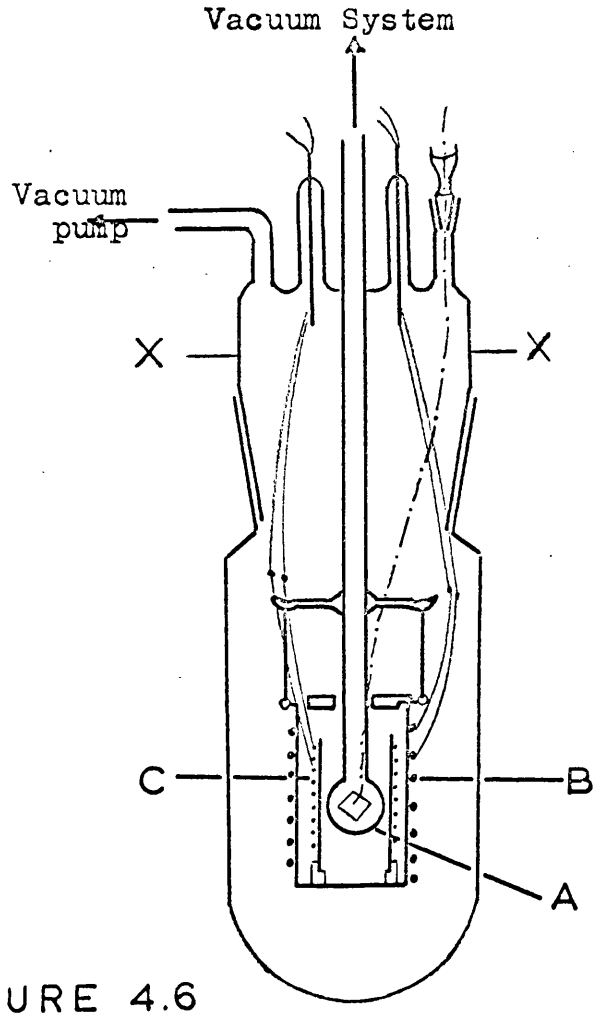

FIGURE 4.5

Cryostat

FIGURE 4.6

Temperature controller

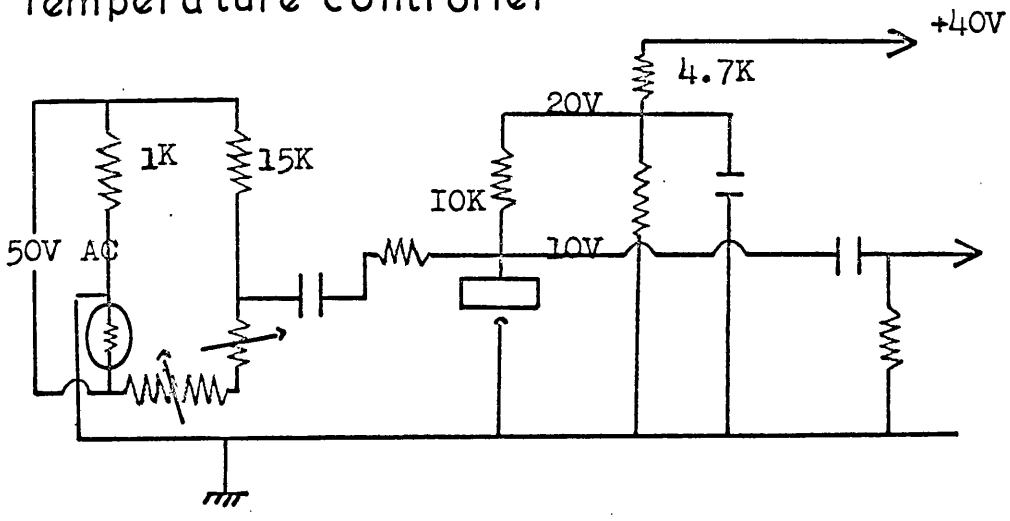

The cryostat is based upon a B·55 Quickfit cone and socket. The cone carries tubing connections to the reaction bulb(A) and vacuum jacket, two tungsten pinch seals for electrical circuits to the heater (B) and nickel resistance thermometer (C) and a B 7 socket. For temperature measurement a copper-constantan thermocouple, which enters the cryostat via a wax seal in the constricted B7 cone, is used. The apparatus is cooled by immersing in liquid nitrogen or solid C_{O_2}/acetone for temperatures above 195°K to level X-X with a little dry air in the vacuum jacket. When the desired temperature was reached the jacket was evacuated and the pre-adjusted control switched on.

Power for the heater is supplied by a Variac transformer, the voltage setting of which is increased as the required temperature increases. The current through the primary circuit of the variac is controlled by an electronic control unit developed by Mr. Brivati of this department, the main features of the circuit being shown in FIG. 4·6. Temperature stability was ± 0·2°.

(vi) Mass spectroscopy

To investigate hydrogen deuterium exchange an MS10 mass spectrometer was incorporated into the reaction system. A batch sampling system was used. Small "doses" of the sample gas at a known pressure were admitted to an expansion reservior volume and then

allowed into the spectrometer via a "metrosil" leak. Technical difficulties, however, prevented the use of this system in the examination of the catalytic properties of the series of compounds in this study so another sampling system using an MS9 mass spectrometer was used.

Samples of an almost 50:50 mixture of hydrogen and deuterium which had been exposed to the catalyst were collected in a 50 ml. bulb and then transferred to the sampling system of an MS9 spectrometer. The presence of any hydrogen deuteride in the sample and an approximate determination of its quantity could therefore be obtained. This method was also used to determine the purity of the hydrogen samples used.

4·7 Surface area determinations

The physical adsorption of a gas at a temperature near its boiling point can yield information concerning both the surface area and the porosity of the solid. Data of physical adsorption is normally expressed in the form of an isotherm - the amount of gas adsorbed at constant temperature against the relative pressure. Adsorption isotherms have been classified into five main types[29] (FIG. 4·7). Type I isotherms are usually associated with chemisorption, the adsorption slowly building up until it reaches P_o which is the saturation vapour pressure. Type II isotherms are associated with porous solids where monomolecular adsorption is

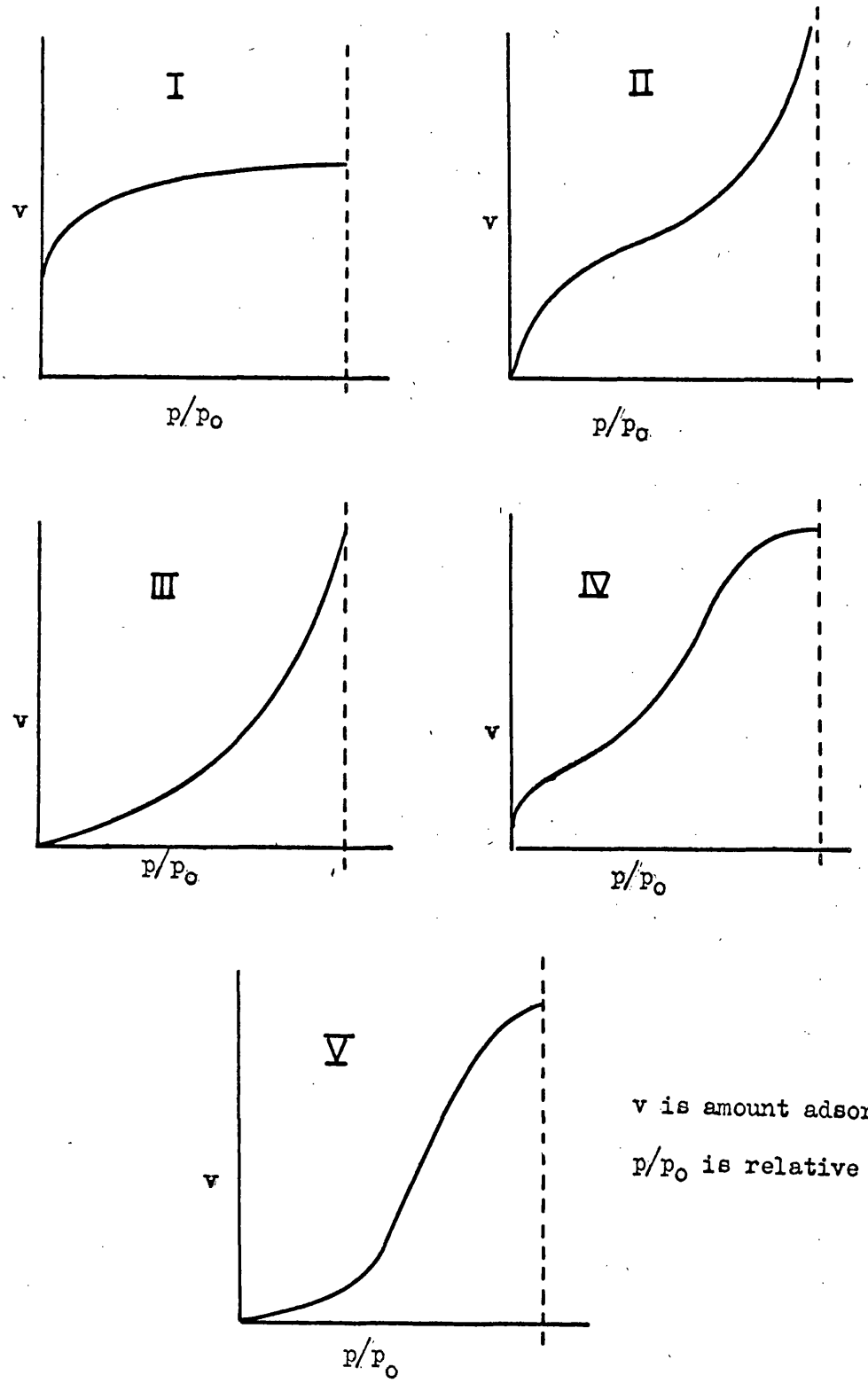

FIGURE 4.7

B.D.D.T Classification of adsorption isotherms

followed by multilayer formation and finally capillary condensation in infinite pores. Type III isotherms are rare and are only found where there is little affinity between gas and solid surface. Types IV and V isotherms are similar in form to types II and III respectively at low pressures but near p_o the adsorption becomes restricted and condensation occurs in pores of finite capacity.

The most common type of isotherm is II. Brunauer, Emmett and Teller[30] attempted to give a theoretical interpretation of this isotherm, and thus a means of determining the surface area of a sample. Since the behaviour of adsorbed molecules is even more difficult to describe in detail than that of molecules in the liquid state, the B.E.T equation contains some drastic assumptions.

1. The surface of the solid adsorbent is uniform.
2. Adsorbed molecules in the first layer are localised.
3. Each adsorbed molecule in the first layer provides a site for adsorption in the second layer, each one in the second layer provides a site for adsorption in the third, with no limitation on the number of the layers.
4. There is no interaction between molecules in a given layer.
5. All molecules in the second and higher layers are assumed to be like those in the bulk liquid. In particular the energy of these molecules is taken to be the same as the energy of a molecule in the liquid.

The original derivation of the B.E.T equation[30] was an extension and generalisation of Langmuirs treatment of monolayer adsorption. This derivation was based on kinetic considerations, in particular the fact that, at equilibrium the rate of condensation of gas molecules to form each adsorbed layer is equal to the rate of evaporation from that layer. From these considerations and applying the assumptions 1 to 5 the following equation was derived.

$$\frac{P}{v(p_o-p)} = \frac{1}{v_m c} + \frac{(c-1)p}{v_m c p_o} \qquad (4\cdot20)$$

Where v is the amount of gas adsorbed at p and v_m corresponds to monolayer coverage. c is given by

$$c = \exp.(E_1-E_L)/RT \qquad (4\cdot21)$$

where E_1 is the heat of adsorption in the first layer and E_L is the latent heat of condensation.

The main application of the B.E.T equation is in the determination of v_m. A plot of $p/v(p-p_o)$ against p/p_o should be a straight line; from which v_m can be determined. In practice, deviations from a linear plot are often observed below $p/p_o = 0\cdot05$ and above $p/p_o = 0\cdot3$. From a knowledge of v_m, the surface area of

the solid can be obtained

$$S = \frac{v_m N W_o}{vo} \qquad (4\cdot22)$$

Where S is the surface area, N is Avogadro's number, W_o is area of adsorbed molecule and v_o is the molar volume.

ΔH the heat of physical adsorption for a gas is always negative, since the process of adsorption results in a decrease in entropy. The isosteric heat of adsorption (the heat of adsorption at constant coverage) can be obtained by application of the Clausins-Clapeyron equation if isotherms are determined at several different temperatures; the thermodynamics of adsorption has been fully discussed by Hill.[31]

4·8 Experimental methods used in determining surface area.

(i) The adsorbate

The surface areas in this work were determined by observing the adsorption of N_2 gas on the solids at 77·4°K. The use of nitrogen in the determination of surface areas has been criticised[32] because at liquid nitrogen temperatures adsorption of nitrogen leads to a two-dimensional gas which shows super critical behaviour, this being particularly the case when the surface studied is homogeneous. In these cases krypton is usually used as the adsorbate as its

two-dimensional critical temperature is well below the temperature of the experiment. The solid surfaces studied here are considered to be sufficiently heterogenous to allow nitrogen to be used in determining their area.

(ii) The gas adsorption apparatus.

The gas adsorption apparatus used to determine adsorption isotherms at 77·4°K is shown in FIG. 4·8.

The apparatus incorporated a combined gas burette - manometer(1). One limb of the monometer consisted of part of a 50 ml. grade A burette, the range of which was extended by attachment to two precisely calibrated bulbs G and H, the other limb being a carefully selected length of pyrex tubing, such that capillary depression was negligible. The bulbs, manometer and sample tube were interconnected with 2 mm. capillary tubing to minimise the "dead space" volume. Pressures between 2 and 70 cm. registered on the manometer, were measured by means of a metre cathetometer. In order to obtain higher pressures it was necessary to pressurise the mercury in the reservoirs L and M.

A three stage diffusion pump backed by a single stage rotary pump, was connected to a high vacuum main and from this lines were taken to various parts of the apparatus. A pirani and Mcleod gauge (F) were attached to the vacuum main for continuous and more

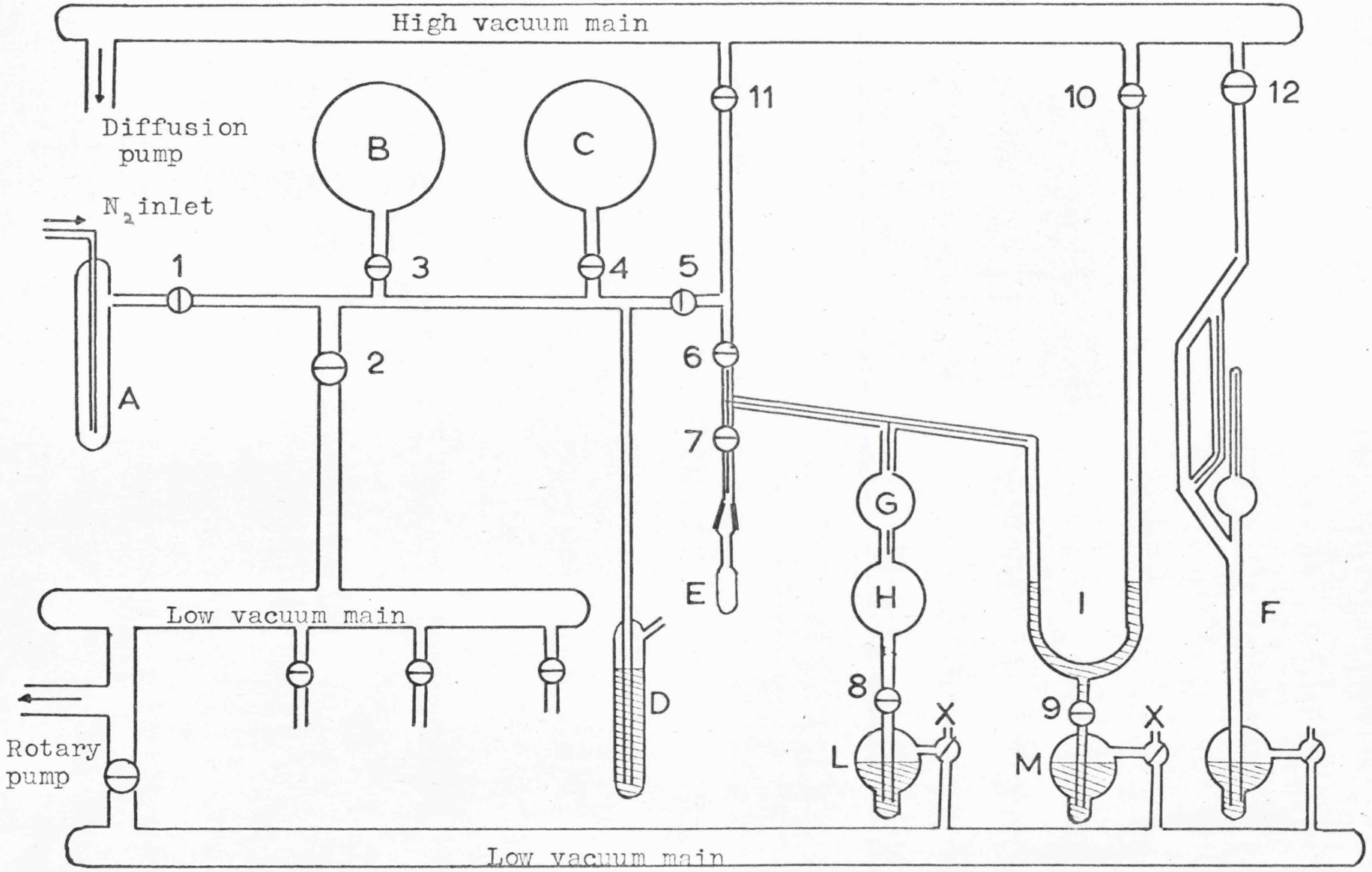

FIGURE 4.8 Gas adsorption apparatus

precise measurements of low pressures respectively. A separate pulsometer pump was connected to a low vacuum main. This was used for preliminary evacuation of samples and controlling the mercury levels in the Mcleod and other mercury resevoirs.

The two litre storage bulbs B and C were connected to the gas source via a three way tap (1) and a cold trap (A); an atmospheric manometer (D) was incorporated into the system and used as a safety valve during the filling process.

(iii) Calibration of the apparatus

The bulbs G and H were calibrated by weighing mercury which was collected after flowing through tap B. The volume of G was determined as 15·533 ± 0·004 ml. and the volume of H as 10·24 ± 0·004 ml The "dead space" volume V_1 which is the volume enclosed by the taps 6 and 7, the mark above bulb G and the zero mark on the gas burette was obtained by compression of a series of charges of gas in the system. The volume V_1 was determined as 4·06 ± 0·1 ml at N.T.P.

$(V_a + V_b)$ was the volume of the bulb and the capillary below tap 7 and including the tap bore. V_a was the part at room temperature and V_b that at liquid nitrogen temperature. $(V_a + V_b)$ was determined by allowing a charge of gas to expand into the empty bulb by opening tap 7. V_b was determined by performing the same operation as before but having the sample bulb immersed in liquid

nitrogen. V_b was calculated by assuming Boyles Law to hold for the gas at room temperature, and applying a correction factor, j, to that at 77·4°K. TABLE 4·1 gives the values for V_a and V_b for the various bulbs.

TABLE 4·1

bulb	x	y	z
V_a(ml)	0·308	0·308	0·308
Vb(ml)	4·592	4·282	4·692

(iv) Deviations from ideality

At room temperature the behaviour of the gas was assumed to be ideal, however at liquid nitrogen temperatures it is necessary to apply a deviation factor j, which is assumed to vary linearly with pressure and is taken to be 1·03 at 50 cm this means that the ideal pressure is given by the equation

$$\text{Ideal pressure} = p_1 (1 + 0.0006\ p_1)$$

where p_1 is the pressure reading in cm.of mercury.

(v) Measurement of the adsorption isotherm

The sample was weighed into a sample bulb and evacuated for a given time at the appropriate temperature. The sample weight

taken depended upon the anticipated area of the sample. Outgassing the sample as above continued until a pressure of 10^{-6} mm. Hg. was obtained on the Mcleod gauge. Tap 7 was then closed and the bulb immersed in liquid nitrogen up to a fixed mark. A charge of nitrogen was admitted to V_1, G and H which depended upon the area of the sample. This charge of nitrogen was admitted via taps 6, 5 and 4 or 3. The pressure of the charge of nitrogen was measured with the cathetometer. Tap 7 was opened and the system allowed to come to equilibrium. This time varied, depending upon the sample and equilibrium pressure between 5 and 10 minutes. The relative pressure p/p_o was obtained from the equilibrium pressure, p, and the atmospheric pressure p_o. Increased pressures were produced by raising the mercury in G and H to the calibrated fixed points. This gave three points on the adsorption isotherm, and in the case of a surface area determination these were sufficient if the points were in the relative pressure region $0{\cdot}05 \rightarrow 0{\cdot}35$. Further pressures of nitrogen were obtained by taking charges of nitrogen via taps 6, 5 and 4 or 3; their initial and equilibrium pressures being measured in each case. The amount of nitrogen adsorbed corresponding to each equilibrium pressure was calculated by difference after converting all volumes to N.T.P and making allowances for the volume occupied by the solid.

To determine the surface area of the solid, equation (4·20) is applied by plotting $p/v(p_o-p)$ against p/p_o, when according to theory a straight line should be obtained. A typical plot is given in FIG.6·1.

The slope, a, and the intercept at zero p/p_o, b, of the straight line is used to obtain v_m. Thus

$$a = \frac{c-1}{v_m c}$$

$$b = \frac{1}{v_m c}$$

$\therefore$ $v_m = 1/a+b$; by assuming the area of a nitrogen molecule to be $16{\cdot}2$ Å^2 the surface area of the solid is calculated from (4·22)

$$S_{B.E.T} = \frac{V_m x 6{\cdot}023 \times 10^{23} \times 16{\cdot}2 \times 10^{-20}}{22{,}414}$$

$$= 4{\cdot}35\ v_m\ m^2\ g^{-1} \qquad (4{\cdot}23)$$

C H A P T E R F I V E

Preparation of Materials.

5·1 Normal Hydrogen

Pure normal hydrogen was prepared by the diffusion of cylinder hydrogen through a heated palladium thimble A (FIG. 5·1). The thimble was tested for leaks by holding a vacuum one side against air the other side at atmospheric pressure. Before use the thimble was outgassed by heating the surrounding coil to a dull red heat and pumping to a vacuum of better than 10^{-6} mm. Hg. When outgassed the thimble was isolated from the gas inlet by closing tap (1). The hydrogen cylinder was connected at B by means of a rubber tube which was evacuated. Hydrogen was admitted to a pressure of one atmosphere and subsequently pumped away. This flushing process was repeated six times, after which the reservoir C was filled to a pressure of one atmosphere with hydrogen. The hydrogen was then admitted to the treated palladium thimble and allowed to diffuse through into the storage bulbs. Care was taken throughout to avoid heating the palladium thimble above 300°C, as above this temperature the life time of the thimble is shortened due to coarsening of the crystalline structure of the palladium. As the diffusion rate fell due to the fall in the pressure difference across the thimble, the pressure of the input side was restored to one atmosphere. The liquid nitrogen trap, F, was incorporated to remove condensible impurities. Nine litres of normal hydrogen at a pressure of 35 cm. Hg were obtained.

FIGURE 5.1

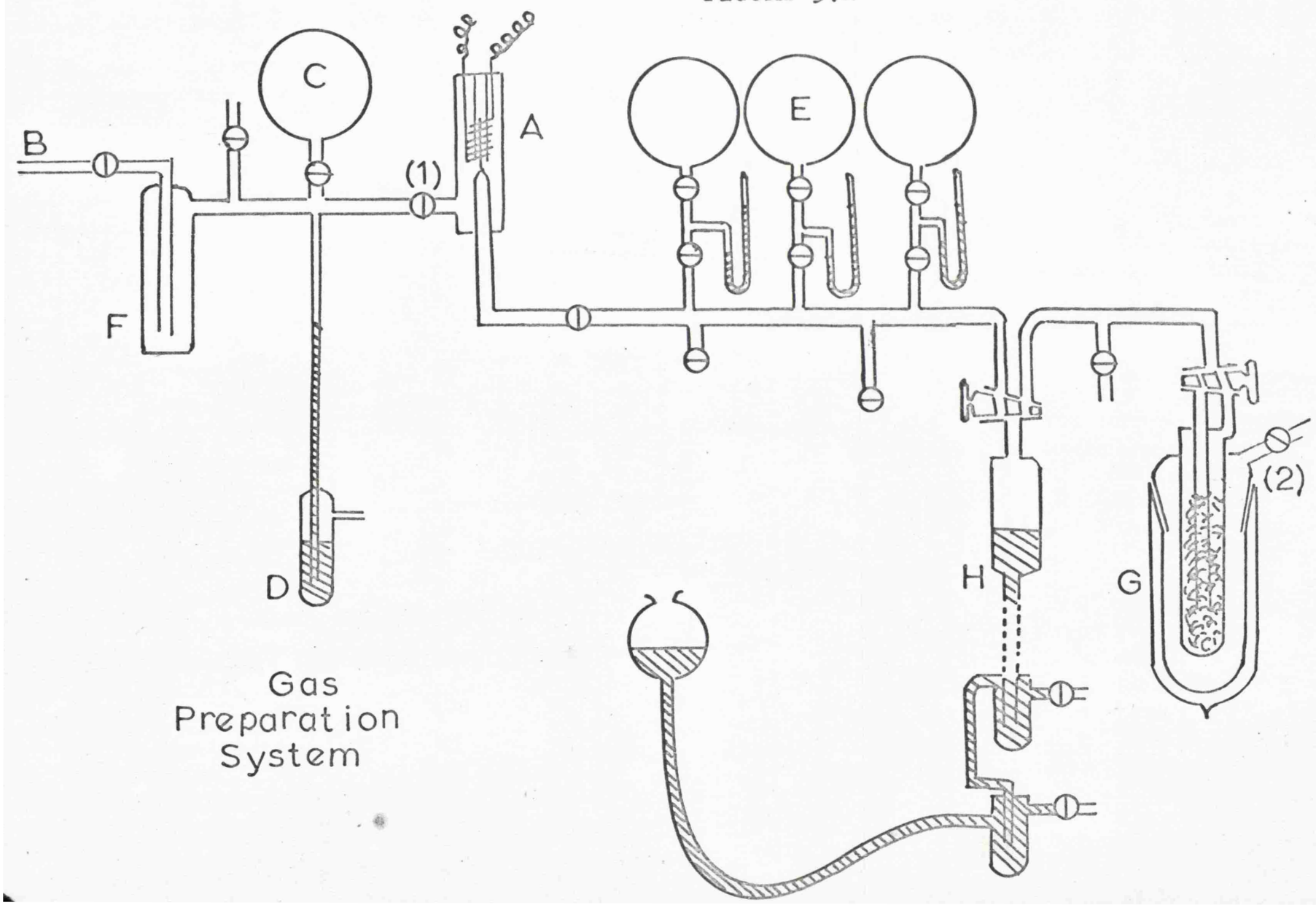

5·2 Para-hydrogen

Para-hydrogen was prepared by adsorbing normal hydrogen onto charcoal at 65°K. The charcoal trap, G, was outgassed at 400°C until a pressure of 10^{-6} mm. Hg was obtainable. The trap was then immersed in a liquid nitrogen bath contained in a dewar flask which could be attached to the charcoal trap by means of a B34 cone and socket joint. By pumping through tap (2) the nitrogen solidified and reached its triple point. Normal hydrogen was pumped onto the charcoal from the storage bulbs via the Toepler pump, H, until the pressure of hydrogen in the trap was almost one atmosphere. The hydrogen was circulated for half an hour over the trap. After this time the para-hydrogen was pumped off by means of the Toepler pump into an evacuated storage bulb. The resistance characteristic for the sample was measured.

5·3 Deuterium

Deuterium was prepared from commercially available heavy water (99·9%) by chemical reaction with sodium. The apparatus used in the preparation of deuterium is shown in FIG. 5·2. The apparatus is prepared as shown with sodium in D, D_2O is then run into A where it is frozen in liquid nitrogen and then repeatedly outgassed. The sodium is distilled past the constrictions into the trap B, the pumps being on continuously. D_2O was slowly decanted into B by warming A or by dry nitrogen as indicated. The deuterium

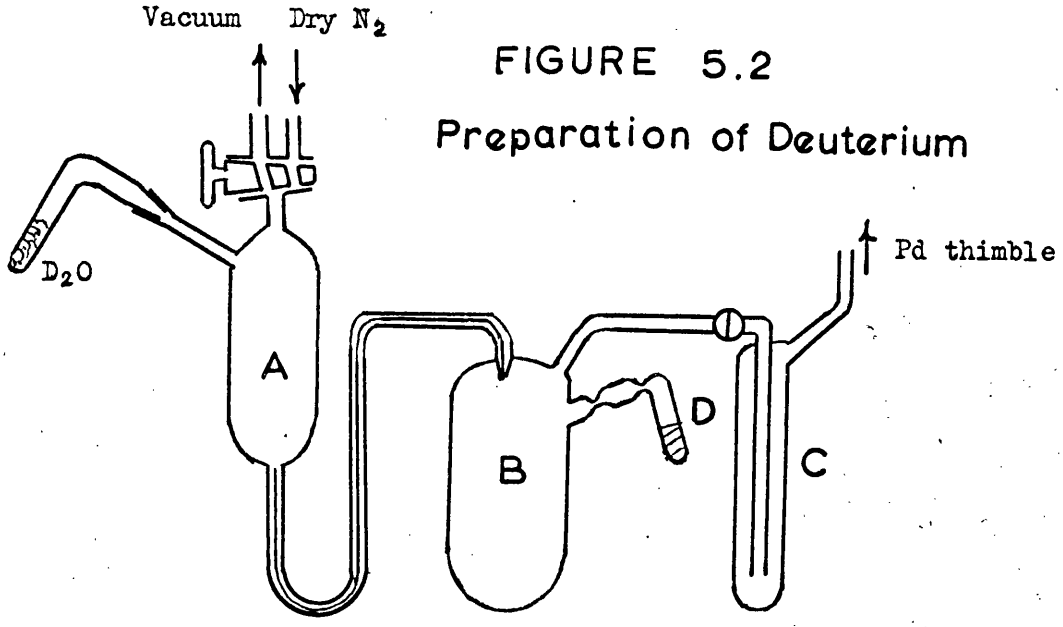

FIGURE 5.2

Preparation of Deuterium

FIGURE 5.3

Reaction vessel

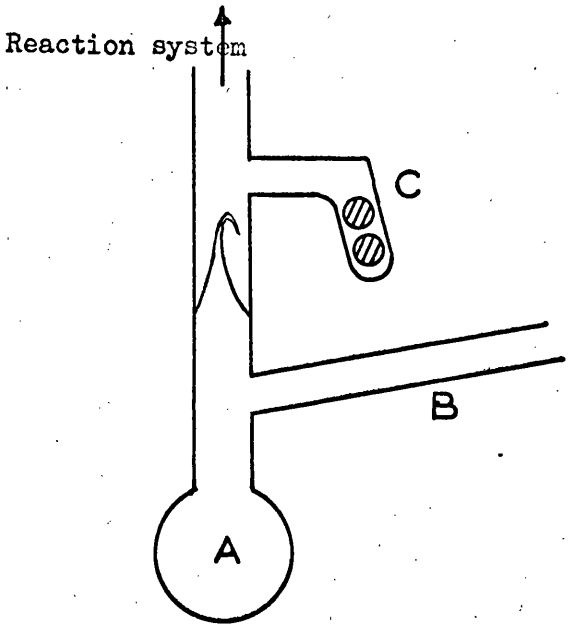

evolved is passed through the cold trap C and into the low vacuum side of the gas preparation apparatus (FIG. 5·1) where it is further purified by passing through the palladium thimble.

Purity of the hydrogen samples

Checks on the impurity level of the hydrogen samples were made using the sampling technique described in section 4.6. The traces obtained for the samples using the MS9 mass spectrometer were compared with that of the background trace and it was found that for all the samples examined there was no measurable impurity of H_2O, O_2 or N_2.

5·4 The anhydrous transition metal sulphates

The anhydrous sulphates were all prepared by very careful dehydration of the hydrated salts, as described in TABLE 5·1.[47] The anhydrous salts were ground in a vibration mill and transferred to the reaction vessel in a dry nitrogen atmosphere. The reaction vessel was attached to the reaction system as shown in FIG. 4·1. For very deliquescent samples a special reaction vessel was employed, FIG. 5·3. The sample is transferred to the reaction bulb A via a side arm B under a dry nitrogen atmosphere. The side arm is then sealed off and removed. The vessel is attached to the reaction system and under vacuum the break-seal is broken by a glass sealed metal slug which is returned to C and removed.

TABLE 5·1

Compound	Preparation	Source
$MnSO_4$	$MnSO_4.4H_2O$. 8 hrs at 500°C in N_2	Analar.
$CoSO_4$	$CoSO_4.7H_2O$. 4 hrs at 270°C in N_2	Analar.
$NiSO_4$	$NiSO_4.6H_2O$. 4 hrs at 370°C in N_2	K & K ultra pure.
$CuSO_4$	$CuSO_4.5H_2O$. 5 hrs at 260°C in N_2	Analar.

5·5 Transition metal oxides

Cobalt and nickel oxides were obtained as specpure samples from Johnson and Mathey, and were used without further treatment. The copper oxide, CuO, used was Analar grade. This sample was pretreated before use by heating in an atmosphere of oxygen to 400°C for 12 hrs. This removed any reduction products which might be present and also surface hydroxyl radicals.

5·6 Anhydrous chlorides

Manganous chloride was obtained in the anhydrous state from K & K.

Cobaltous chloride was prepared from cobaltous acetate and acetyl chloride.

$$Co(CH_3COO)_2 4\,H_2O + 6CH_3COCl \rightarrow CoCl_2 + 2(CH_3CO)_2O + 4CH_3COOH + 4HCl$$

A 100 ml. conical flask was charged with 4g of fine cobaltous acetate powder. It was closed with an adaptor which carried a dropping funnel and filtering finger and 15 ml. of benzene was added with agitation (magnetic stirrer) followed by 10 ml. of CH_3COCl. The mixture was stirred for 30 minutes, the $CoCl_2$ ppt. allowed to settle and the mother liquor siphoned off via the filtering finger. The residue was treated with benzene and acetyl chloride to complete the reaction.

The supernatant liquid was removed by filtration in a dry box and the $CoCl_2$ washed thoroughly with benzene. It was transferred to a drying tube and dried for two hours at 150°C under nitrogen. The anhydrous salt was then transferred to a reaction vessel.

C H A P T E R S I X

Results and Discussion

6·1 Introduction

The effect of the d-orbital electrons on the catalytic properties of transition metal oxides has been thoroughly examined, for a large number of catalytic systems.[45,44,38,34,35] Little work has, however, been done on the catalytic properties of the transition metal salts, in particular using the ortho-para-hydrogen conversion. Farkas and Sandler[33] examined the conversion on $CuSO_4$ and $NiCl_2$ but their results were only of a qualitative nature. The present work examines the catalytic properties of the compounds in TABLE 6·1.towards the ortho-parahydrogen conversion and attempts to determine the mechanism of the reaction and any correlation between the catalytic activity and 3d electronic structure of the salts.

Of the transition metal series Mn, Fe, Co, Ni and Cu only the divalent sulphate of Fe was not examined. This was due to the difficulty of preparing it in the pure state without oxidation products being present. The remaining sulphates were all prepared as given in section 5·4. The study of the catalytic activity of the oxides was initiated to determine whether the conversion observed on the corresponding salts could be attributed to oxide impurities as has been suggested by other workers.[46] The effect of changing the anion on the catalytic properties of the cations

Mn^{2+} and Co^{2+} has also been studied by examining the catalytic activity of two chlorides $MnCl_2$ and $CoCl_2$.

6.2 Results

The ortho-para hydrogen conversion has been examined on the compounds listed in TABLE 6.1

TABLE 6.1

$CuSO_4$	CuO	
$NiSO_4$	NiO	
$CoSO_4$	CoO	$CoCl_2$
$MnSO_4$		$MnCl_2$

The conversion was followed over the temperature range 77° to $300^{\circ}K$ and the data obtained for each compound is presented in tabular form in the following order

(i) Surface area determination; For $CuSO_4$ a typical B.E.T. plot of $p/v'(p_o-p)$ against p/p_o is shown in FIG 6.1

(ii) the rate of conversion with increasing and decreasing temperature. The values of k_e, the experimental rate constant, were determined by taking runs at different times for each temperature and plotting $\log_{10}\Omega_o/\Omega_t$ against t, when k_e is equal to 2.303 times the slope of the graph. This eliminates individual errors in the measurement of k_e for any one time. For $CuSO_4$ a typical $\log_{10}\Omega_o/\Omega_t$ against t plot is shown in FIG. 6.2, also values for Ω_o, Ω_t, and $\log \Omega_o/\Omega_t$ are quoted as well as values for time, temperature, pressure, k_e, $\log_{10}k_e$ and k_m.

For subsequent compounds only values for the average pressure, temperature, k_e, $\log_{10} k_e$ and k_m are quoted.

(iii) Arrhenius plots and the apparent activation energy and frequency factors obtained from them;

(iv) pressure dependence of the conversion, and the Freundlich and Langmuir isotherm plots obtained from the data;

(v) the adsorption of hydrogen at various temperatures. This data was only obtained for $MnSO_4$;

(vi) hydrogen deuterium equilibration.

The gradient and intercept of all straight line graphs i.e. the rate plots, surface area determinations, Langmuir and Freundlich isotherm plots, were obtained using a root mean square analysis carried out on an Elliot 803 computer.

(i) Kinetic data obtained from the divalent anhydrous sulphates of the first row transition metals.

Anhydrous Copper Sulphate, $CuSO_4$

The sample of anhydrous copper sulphate used in the catalytic experiments was heated to 373°K in a dynamic vacuum of 10^{-6} mm Hg for 10 hrs., and then repeatedly heated at this temperature until constant activity to the conversion was attained. The sample used in the surface area determinations was from the same source as that used in the catalytic work and was pretreated in an identical manner.

Determination of the surface area of $CuSO_4$

The mean of two surface area determinations is taken. A typical plot of p/p_o against $p/(p_o-p)v'$ is shown in FIG. 6.1.

Detn	p_o (mm)	p (mm)	v_{ads} (cc)	v_{ads}/g (v')	$p/(p_o-p)v'$	p/p_o
A	765.3	112.5	11.58	2.71	0.064	0.15
	765.3	143.2	11.94	2.80	0.082	0.19
	765.3	173.8	12.44	2.92	0.101	0.23
B	765.3	98.8	11.10	2.60	0.057	0.13
	765.3	126.0	12.00	2.82	0.070	0.16
	765.3	153.4	12.42	2.91	0.086	0.20

If intercept = a and gradient = b then $S.A._{B.E.T} = (1/a+b) \times 4.35\ m^2 g^{-1}$

$S.A._{B.E.T}$ (A) = $9.44\ m^2 g^{-1}$ $S.A._{B.E.T}$ (B) = $9.56\ m^2 g^{-1}$

The mean surface area is therefore determined as

$$\underline{9.50\ m^2 g^{-1}}$$

FIGURE 6.1

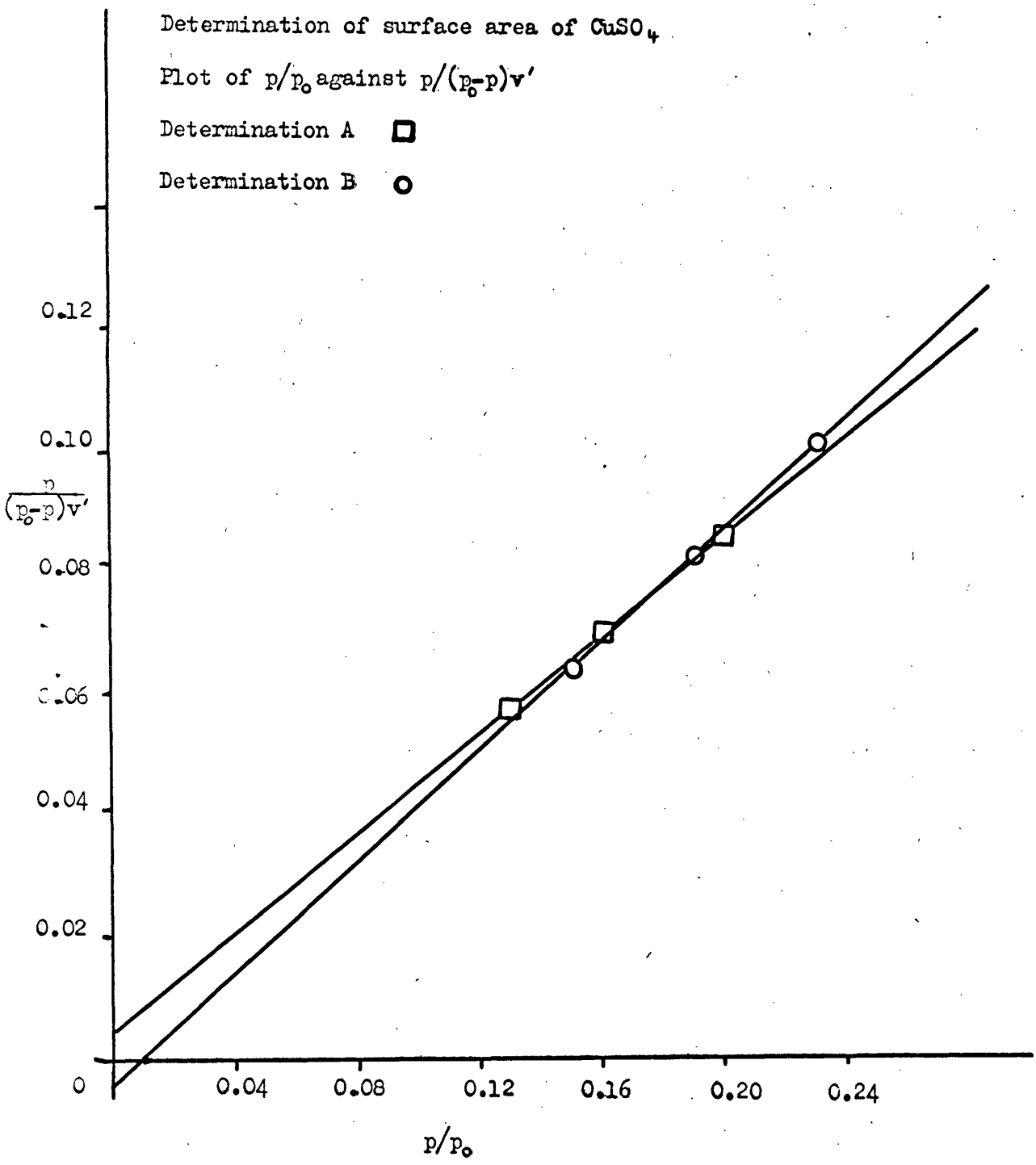
Determination of surface area of $CuSO_4$
Plot of p/p_o against $p/(p_o-p)v'$
Determination A
Determination B
0.12
0.10
$\frac{p}{(p_o-p)v'}$
0.08
0.06
0.04
0.02
0
0.04
0.08
0.12
0.16
0.20
0.24
p/p_o

Table 6.2 The Kinetics of the conversion at ~ 6mm pressure of hydrogen

Time (mins)	Temp (°K)	Press (mm)	Ω_o	Ωt	$\log\Omega_o/\Omega t$	$k_e \times 10^2$ (min^{-1})	$10^2/T$
			With increasing temperature				
15	77	5.9	0.60	0.06	1.08	16.03	1.3
10	77	5.6	0.60	0.13	0.65		
5	77	5.6	0.60	0.29	0.30		
5	90	5.9	0.42	0.23	0.27	13.83	1.1
10	90	5.9	0.42	0.12	0.53		
15	90	5.9	0.42	0.07	0.81		
6	112.5	5.9	0.23	0.14	0.21	8.35	0.89
10	112.5	5.9	0.23	0.10	0.37		
15	112.5	5.8	0.23	0.07	0.54		
5	135	6.0	0.12	0.09	0.11	5.13	0.74
10	135	5.8	0.12	0.07	0.22		
15	135	5.9	0.12	0.06	0.33		
10	146	5.9	0.41	0.29	0.15	3.45	0.69
15	146	5.9	0.41	0.25	0.22		
5	146	5.9	0.41	0.35	0.07		
10	209.5	5.9	0.48	0.470	0.01	0.26	0.48
15	209.5	5.7	0.48	0.465	0.02		
20	209.5	5.9	0.48	0.460	0.02		

A typical plot of $\log_{10}(\Omega_o/\Omega t)$ against time at different temperatures is shown in FIG. 6.2

FIGURE 6.2

Plots of $\log(\Omega_\infty/\Omega_t)$ against time at different temperatures.

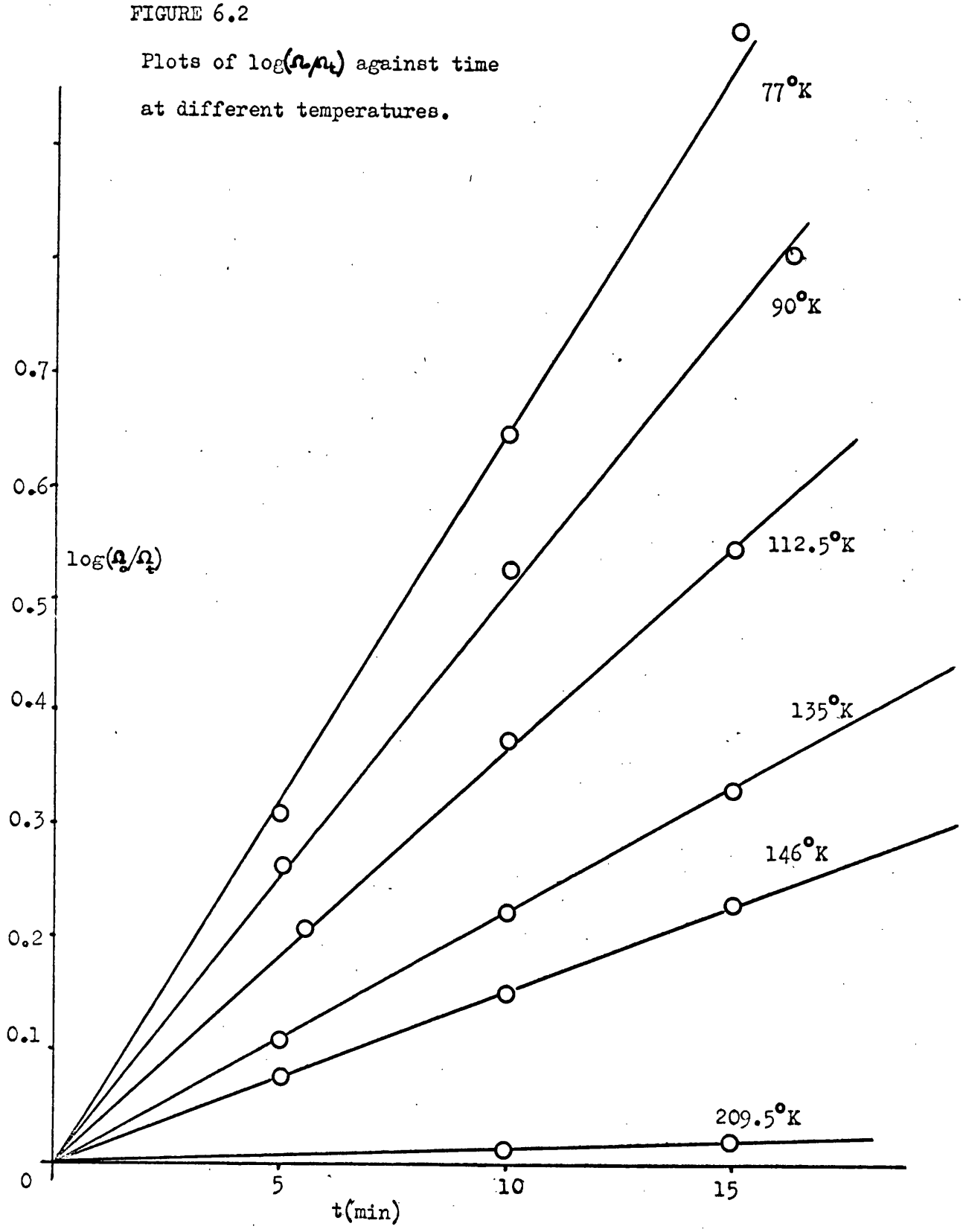

Table 6.3* The Kinetics of the conversion

k_m, the absolute rate constant is given by,

$$k_m = k_e/60A.pv/kT$$

Surface area of sample = 10.71 m^2, Reaction volume (v) = 322 cc.

Temp. (°K)	Av.Press (mm)	k_e X 10^2 (min^{-1})	$\log_{10}k_e$	k_m (molecules) ($cm^{-2}sec^{-1}$)	$\log_{10}k_m$	$10^2/T$
			increasing temperature			
77	12.0	7.46	$\bar{2}.87$	5.62×10^{12}	12.75	1.30
90	12.2	5.66	$\bar{2}.75$	3.71×10^{12}	12.57	1.11
112.5	12.4	4.06	$\bar{2}.61$	2.16×10^{12}	12.34	0.89
135	12.5	3.26	$\bar{2}.51$	1.46×10^{12}	12.16	0.74
146	12.5	1.98	$\bar{2}.30$	8.19×10^{11}	11.91	0.69
160.5	12.5	0.82	$\bar{3}.91$	3.08×10^{11}	11.49	0.62
209.5	12.4	0.13	$\bar{3}.13$	3.72×10^{10}	10.57	0.48
273	12.5	0.06	$\bar{4}.78$	1.33×10^{10}	10.12	0.37
296	12.4	0.04	$\bar{4}.60$	8.09×10^{9}	9.91	0.34
77	5.7	16.03	$\bar{1}.21$	5.73×10^{12}	12.76	1.30
90	5.9	13.83	$\bar{1}.14$	4.38×10^{12}	12.64	1.11
112.5	5.8	8.35	$\bar{2}.92$	2.08×10^{12}	12.32	0.89
135	5.9	5.13	$\bar{2}.71$	1.08×10^{12}	12.03	0.74
146	5.9	3.45	$\bar{2}.54$	6.73×10^{11}	11.83	0.69
209.5	5.8	0.26	$\bar{3}.42$	3.48×10^{10}	10.54	0.48

The Arrhenius plots of $\log_{10}k_e$ and $\log_{10}k_m$ against $1/T°K$ are shown in FIG. 6.3 and 6.4 respectively.

* This table in addition to giving further data on the kinetics of the conversion at a pressure of ~ 12 mm, summarises the results given in TABLE 6.2. In addition the table also gives calculated values for the absolute rate constant at each temperature. For subsequent compounds the kinetic data is presented only in tables of this form.

FIGURE 6.3

Arrhenius plot of
log k_e against $1/T^oK$

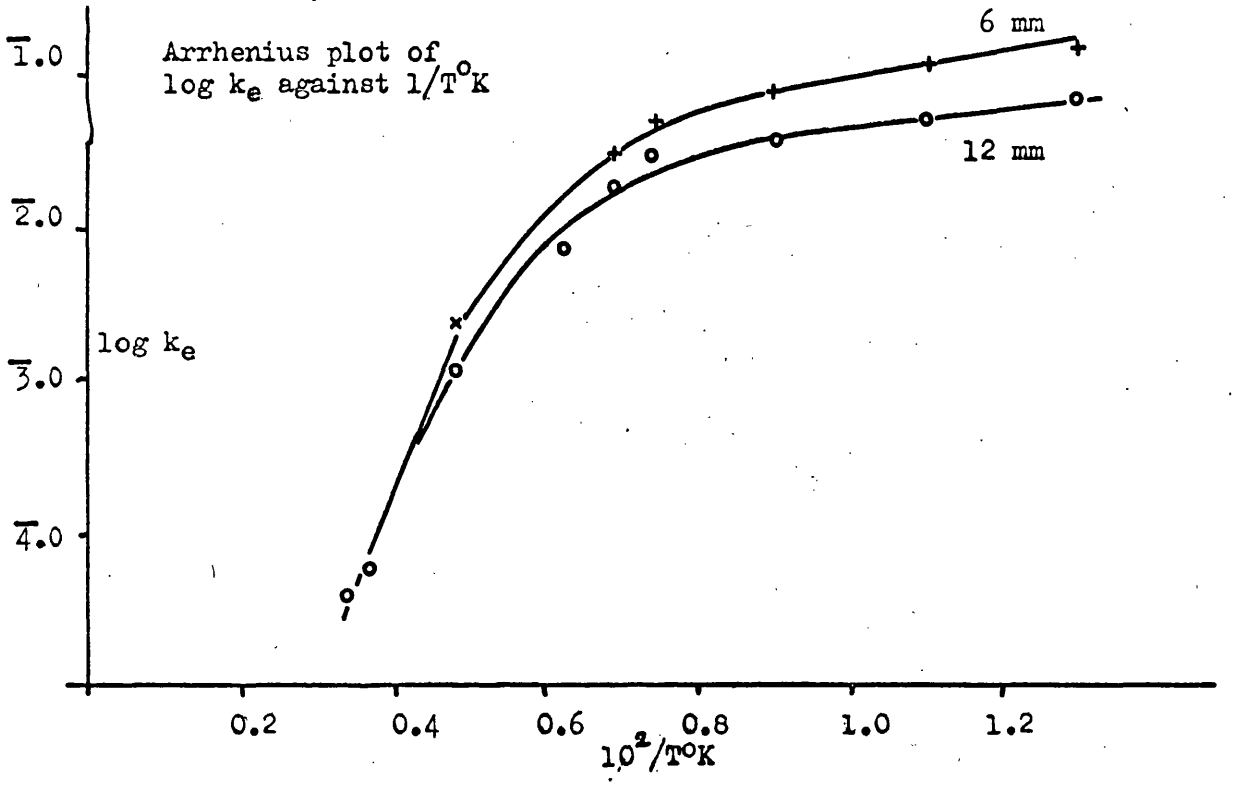

FIGURE 6.4

Arrhenius plot of
log k_m against $1/T^oK$

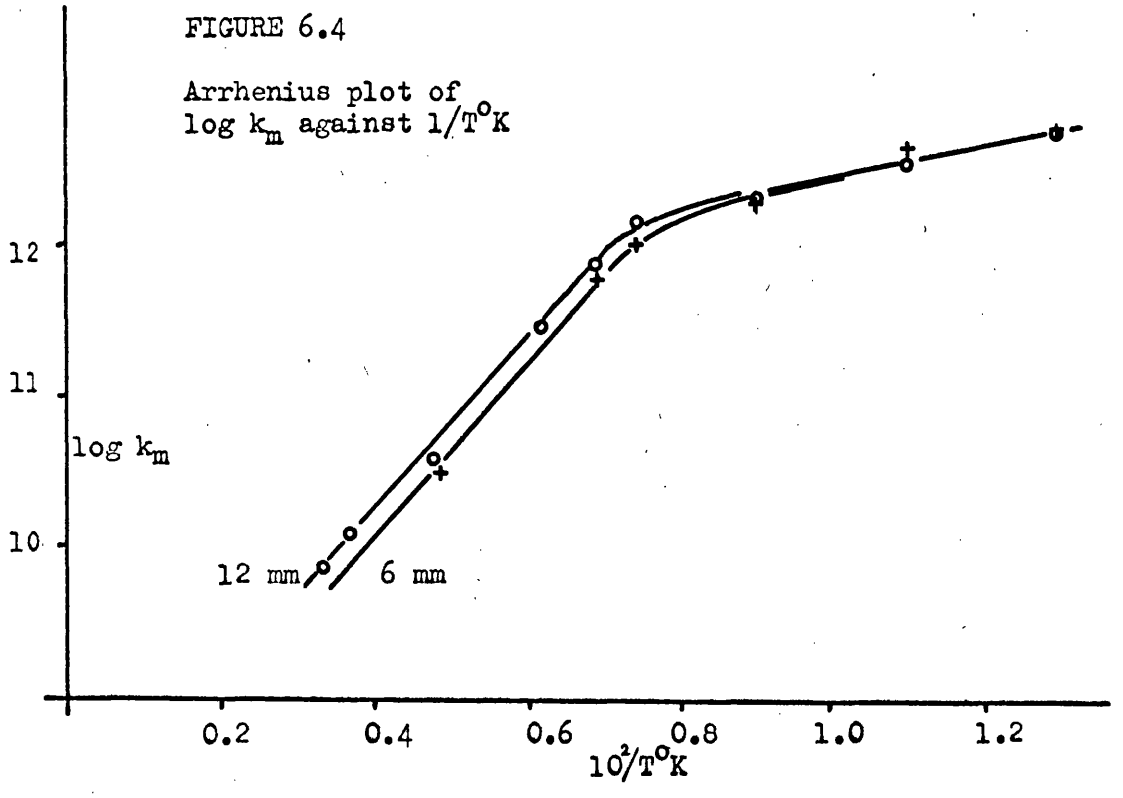

From the slope and intercept of the Arrhenius plot of $\log_{10}k_m$ against $1/T^{\circ}K$ the apparent activation energy (E_a) and frequency factors (B_m) were determined.

$$\text{i.e. } 2.303 \log_{10}k_m = \log B_m - E/RT$$

For temperature range 77°-$150^{\circ}K$

$E_a = -0.47$ k cals/mol $\quad \log_{10}B_m = 11.42 \quad B_m = 2.63 \times 10^{11}$

For temperature range 150°-$300^{\circ}K$

$E_a = -2.56$ k cals/mol $\quad \log_{10}B_m = 8.00 \quad B_m = 1.0 \times 10^{8}$

TABLE 6.4 Pressure dependence of the conversion

Temp (°K)	Press (mm)	$\log_{10} p$	time (min)	$\log \Omega_o/\Omega_t$	$k_e \times 10^2$ (min^{-1})	$1/k_e$	$\log_{10} k_e$
77	6.07	0.78	10	0.60	13.50	7.41	$\bar{1}.13$
77	9.00	0.95	10	0.40	9.10	10.99	$\bar{2}.96$
77	11.62	1.07	10	0.30	7.10	14.20	$\bar{2}.85$
77	7.03	0.85	10	0.52	11.91	8.40	$\bar{1}.07$
90	5.76	0.76	15	0.88	13.51	7.42	$\bar{1}.13$
90	8.40	0.93	15	0.64	9.84	10.25	$\bar{2}.99$
90	11.03	1.04	15	0.49	7.42	13.45	$\bar{2}.87$
112.5	5.70	0.76	10	0.54	8.28	12.08	$\bar{2}.92$
112.5	8.33	0.93	10	0.39	6.00	16.80	$\bar{2}.78$
112.5	12.15	1.09	10	0.27	4.11	24.61	$\bar{2}.61$
135	5.76	0.76	10	0.22	5.09	19.57	$\bar{2}.71$
135	10.02	1.00	10	0.15	3.32	30.00	$\bar{2}.52$
135	12.43	1.09	5	0.06	2.71	37.44	$\bar{2}.43$
146	5.89	0.77	5	0.07	3.41	29.62	$\bar{2}.53$
146	9.31	0.97	10	0.10	2.40	42.24	$\bar{2}.37$
146	12.43	1.09	10	0.09	1.93	52.33	$\bar{2}.28$
209.5	5.78	0.76	20	0.023	0.20	477.1	$\bar{3}.32$
209.5	7.45	0.87	20	0.017	0.20	340.5	$\bar{3}.29$
209.5	9.27	0.97	20	0.023	0.20	477.1	$\bar{3}.32$
209.5	13.56	1.13	20	0.023	0.20	477.1	$\bar{3}.32$
273	7.68	0.89	30	0.008	0.06	1650	$\bar{4}.78$
273	11.45	1.06	30	0.009	0.07	1479	$\bar{4}.83$
273	6.46	0.81	30	0.008	0.06	1650	$\bar{4}.78$
273	12.80	1.11	30	0.008	0.07	1650	$\bar{4}.78$

The Freundlich and Langmuir isotherm plots are shown in FIG. 6.5 and 6.6 respectively. Since both the Langmuir and Freundlich isotherms hold $n = (1 - \theta)$

Therefore θ, the coverage of adsorbed hydrogen can be determined.

FIGURE 6.5

Pressure dependencies of the conversion at different temperatures, expressed as Freundlich plots.

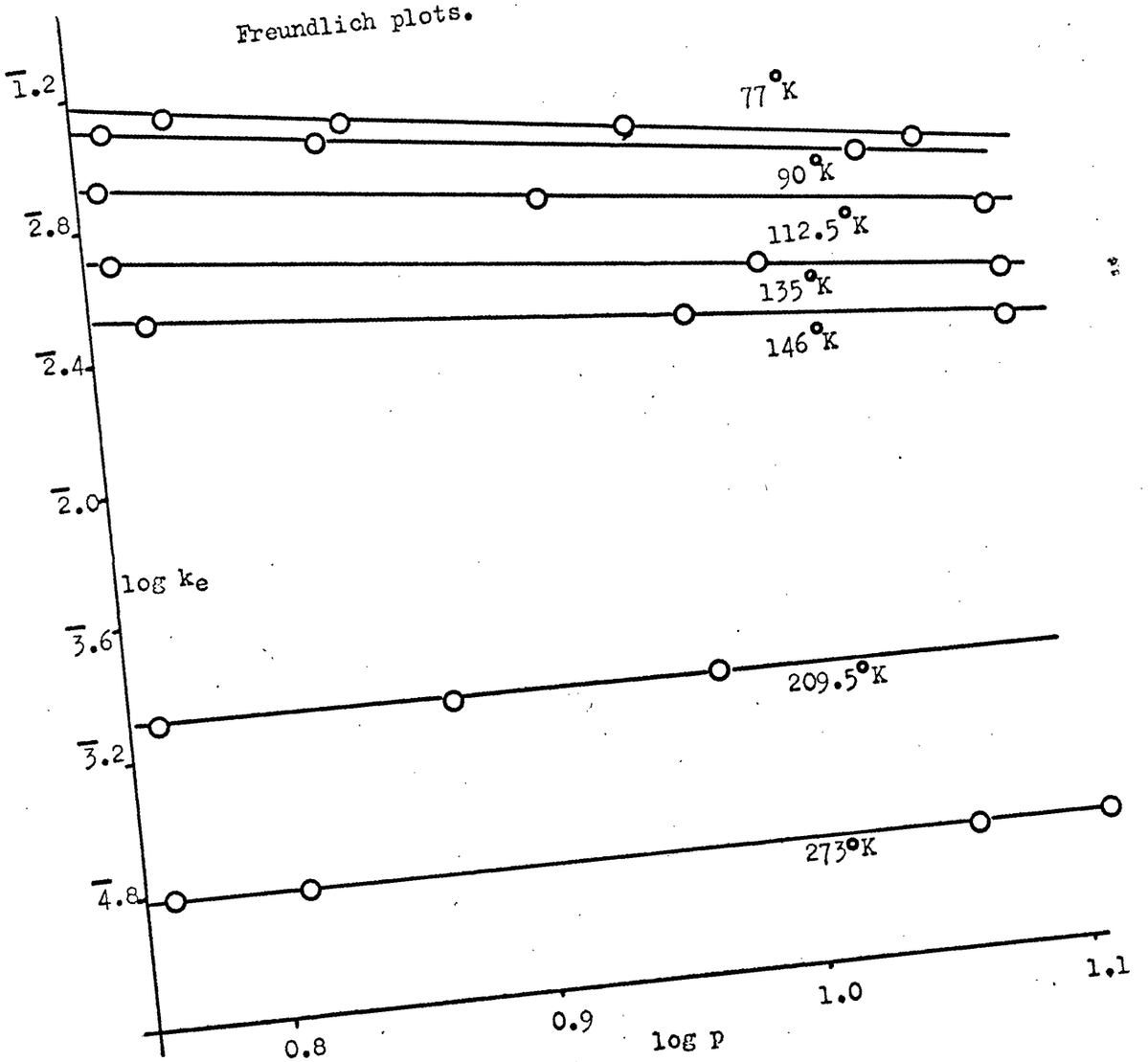

FIGURE 6.6

Pressure dependencies of the conversion at different temperatures, expressed as Langmuir plots.

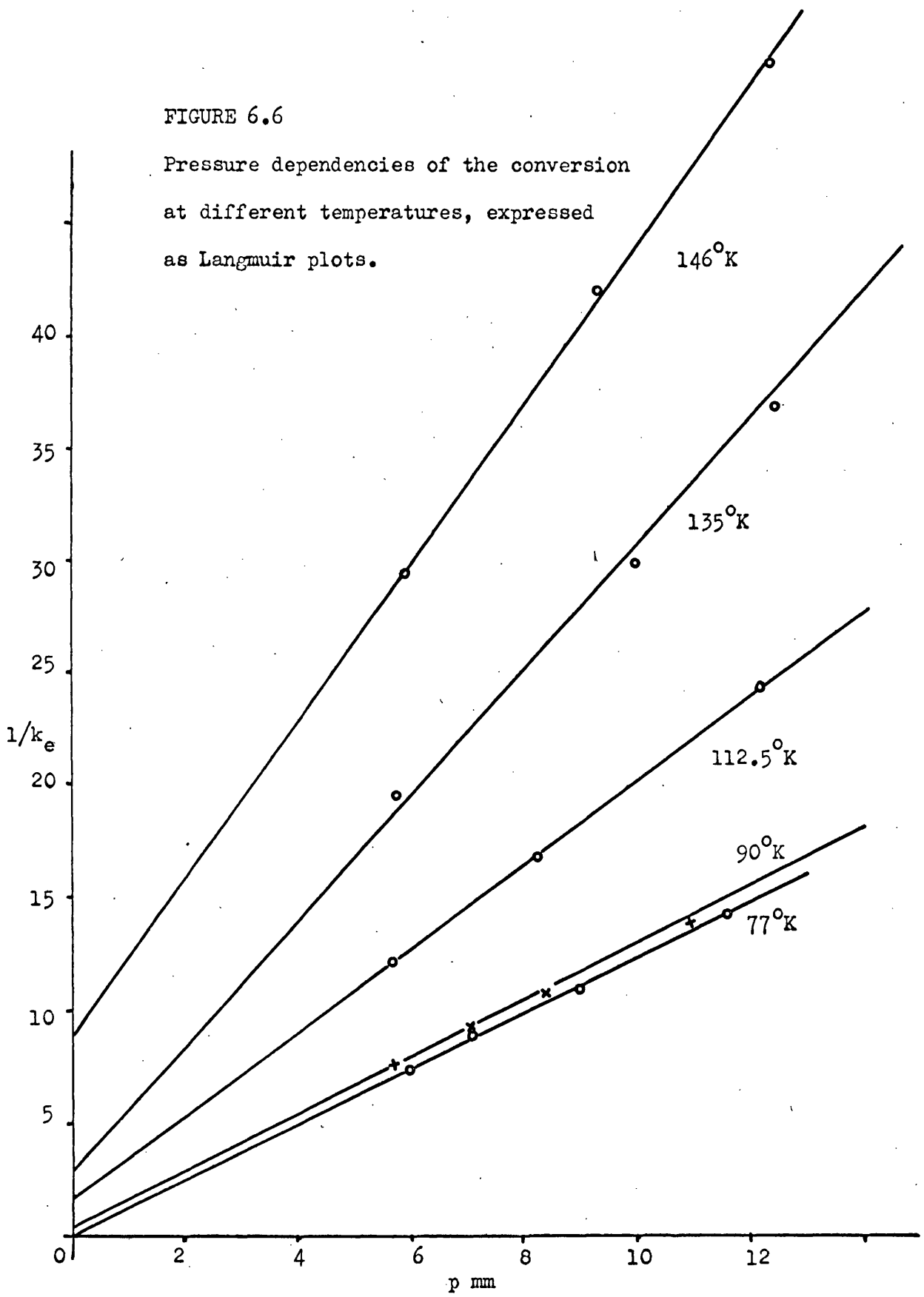

TABLE 6.6 Variation of Freundlich pressure exponent (n) with temperature.

$T^{o}K$	77	90	112.5	135	146	209.5	273
n	0.00	0.08	0.095	0.17	0.24	1	1
θ	1.00	0.92	0.905	0.83	0.76	0	0

Anhydrous Nickel Sulphate, $NiSO_4$

The sample of anhydrous nickel sulphate was heated to 420°K in a dynamic vacuum of 10^{-6} mm of Hg for 12 hours, and then repeatedly heated at this temperature until constant activity to the conversion was attained. The sample used for surface area determinations was from the same source as that used in the catalytic work, and was pretreated in an identical manner.

Determination of surface area

Detn	p_o (mm)	p (mm)	v_{ads} (cc)	v_{ads}/g v'	$p/v(p_o-p)$	p/p_o
A	746.8	65.35	21.43	3.09	0.031	0.088
	746.8	82.34	22.19	3.20	0.034	0.110
	746.8	99.73	22.85	3.30	0.040	0.134
B	742.7	93.82	22.96	3.32	0.044	0.126
	742.7	117.70	23.91	3.45	0.054	0.159
	742.7	141.59	24.83	3.52	0.066	0.191

$S.A_{B.E.T}(A) = 14.31\ m^2\ g^{-1}$ $S.A_{B.E.T}(B) = 12.83\ m^2\ g^{-1}$

Mean surface area of sample $13.57\ m^2\ g^{-1}$

TABLE 6.5 The Kinetics of the conversion

Surface area of sample 36.36 $m^2 g^{-1}$ Reaction volume 322cc

Temp (°K)	Av.Press. (mm)	$k_e \times 10^2$ (min^{-1})	$\log_{10} k_e$	k_m (molecules) ($cm^{-2} sec^{-1}$)	$\log_{10} k_m$	$10^2/T$
			increasing temperature			
70	5.4	16.81	$\bar{1}.23$	1.68×10^{12}	12.23	1.30
90	5.6	18.20	$\bar{1}.26$	1.61×10^{12}	12.21	1.11
112.5	5.3	19.72	$\bar{1}.30$	1.32×10^{11}	12.12	0.89
135	5.5	16.45	$\bar{1}.22$	9.55×10^{11}	11.98	0.75
146	5.6	17.56	$\bar{1}.25$	9.58×10^{11}	11.98	0.69
178	5.7	17.30	$\bar{1}.24$	7.88×10^{11}	11.90	0.56
209.5	5.4	21.36	$\bar{1}.33$	7.83×10^{11}	11.89	0.48
273	5.5	10.80	$\bar{1}.03$	3.10×10^{11}	11.49	0.37
350	5.4	2.90	$\bar{2}.46$	6.36×10^{10}	10.80	0.29
			decreasing temperature			
273	5.9	10.10	$\bar{1}.00$	3.10×10^{11}	11.49	0.37
209.5	5.7	20.60	$\bar{1}.31$	7.97×10^{11}	11.90	0.48
178	5.7	19.91	$\bar{1}.30$	9.06×10^{11}	11.96	0.56
146	5.4	19.00	$\bar{1}.28$	1.00×10^{12}	12.00	0.69
90	5.5	16.82	$\bar{1}.25$	1.46×10^{12}	12.16	1.11
77	5.7	14.41	$\bar{1}.16$	1.52×10^{12}	12.18	1.30

The Arrhenius plots of $\log_{10} k_e$ and $\log_{10} k_m$ against $1/T°K$ are shown in FIGS. 6.7 and 6.8 respectively. From the slopes and intercepts of plot 6.8 the apparent activation energy, and frequency factors were determined.

For temperature range 77°-200°K

$E_a = -0.18$ k cal/mol. $\log_{10} B_m = 11.73$ $B_m = 5.37 \times 10^{11}$

For temperature range 200°-300°K

$E_a = -3.21$ k cal/mol. $\log_{10} B_m = 8.85$ $B_m = 7.08 \times 10^{8}$

FIGURE 6.7

Arrhenius plot of log k_e against $1/T^{o}K$.

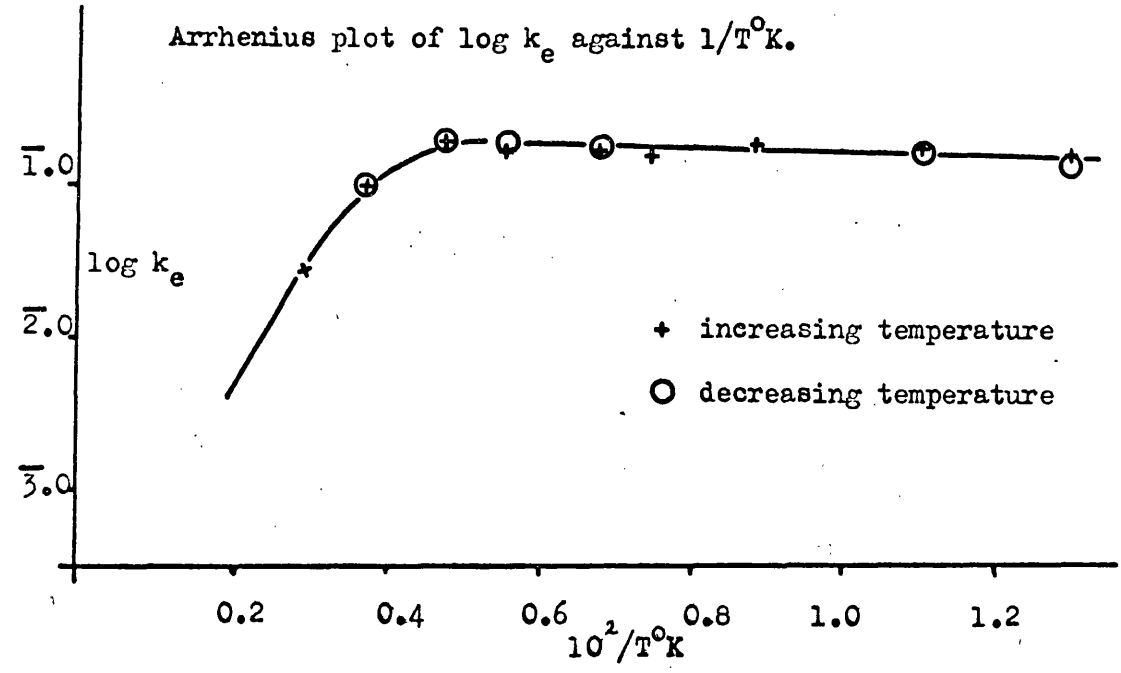

FIGURE 6.8

Arrhenius plot of log k_m against $1/T^{o}K$.

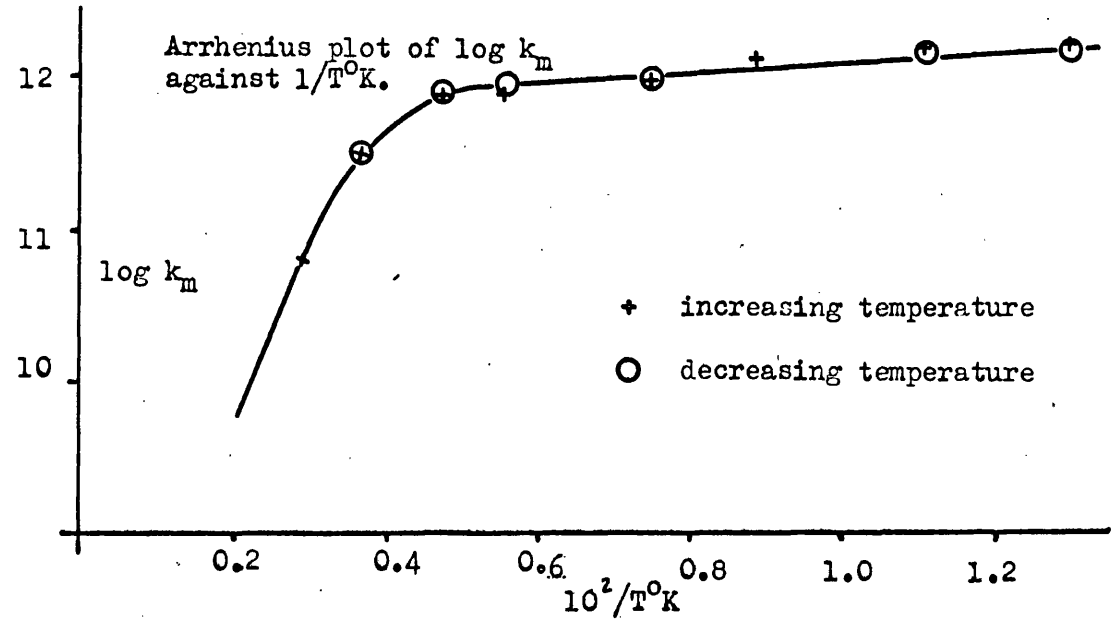

TABLE 6.6 Pressure dependence of the conversion.

Temp (°K)	Press (mm)	$\log_{10}p$	time (min)	$\log\Omega_o/\Omega t$	$k_e \times 10^2$	$1/k_e$	$\log_{10}k_e$
77	5.95	0.774	6	0.39	14.9	6.71	$\bar{1}.17$
77	5.22	0.718	9	0.68	17.4	5.75	$\bar{1}.24$
77	9.08	0.958	10	0.41	9.5	10.53	$\bar{2}.98$
77	7.05	0.848	10	0.55	12.6	7.94	$\bar{1}.10$
178	5.77	0.761	10	0.76	17.6	5.68	$\bar{1}.25$
178	8.40	0.924	5	0.27	12.4	8.06	$\bar{1}.09$
178	11.19	1.049	5	0.19	8.8	11.36	$\bar{2}.95$
178	7.50	0.875	5	0.38	13.9	7.19	$\bar{1}.14$
350	5.46	0.737	7	0.089	2.9	34.48	$\bar{2}.47$
350	10.28	1.012	8	0.088	2.5	40.00	$\bar{2}.41$
350	7.10	0.851	10	0.118	2.7	37.04	$\bar{2}.44$

The Freundlich and Langmuir isotherm plots are shown in FIG 6.9 and 6.10 respectively. Since both the Langmuir and Freundlich plots hold $n = (1 - \theta)$

TABLE 6.7 Variation of Freundlich pressure exponent with temperature

Temp°K	77	178	350
n	0.00	0.00	0.77
θ	1.00	1.00	0.23

FIGURE 6.9

Pressure dependencies of the conversion at different temperatures expressed as Freundlich plots.

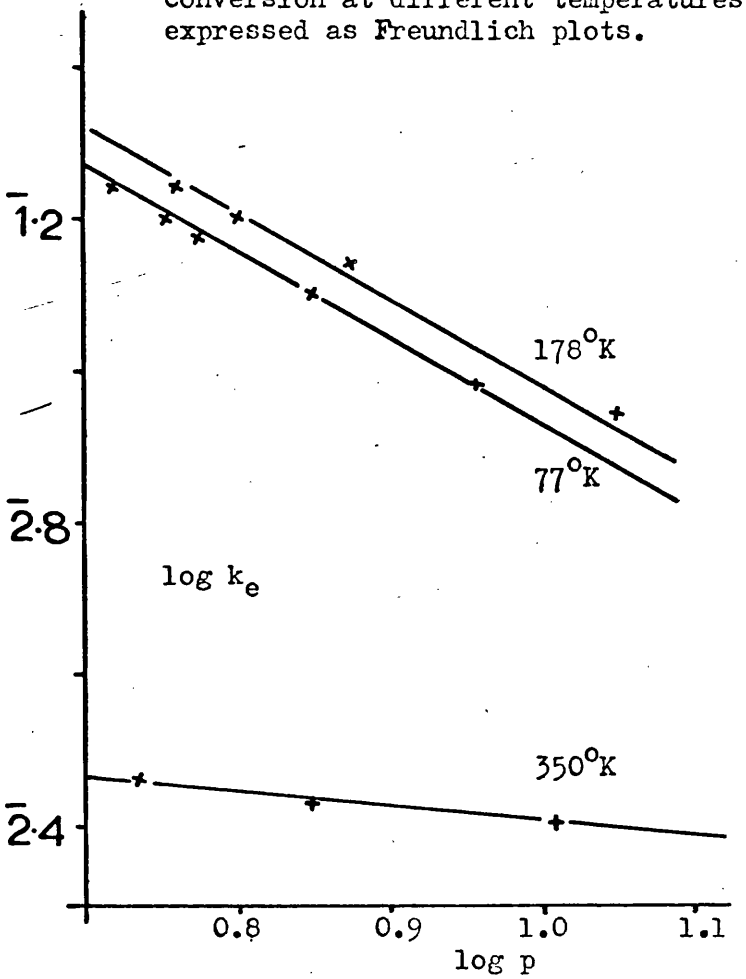

FIGURE 6.10

Pressure dependencies of the conversion at different temperatures expressed as Langmuir plots

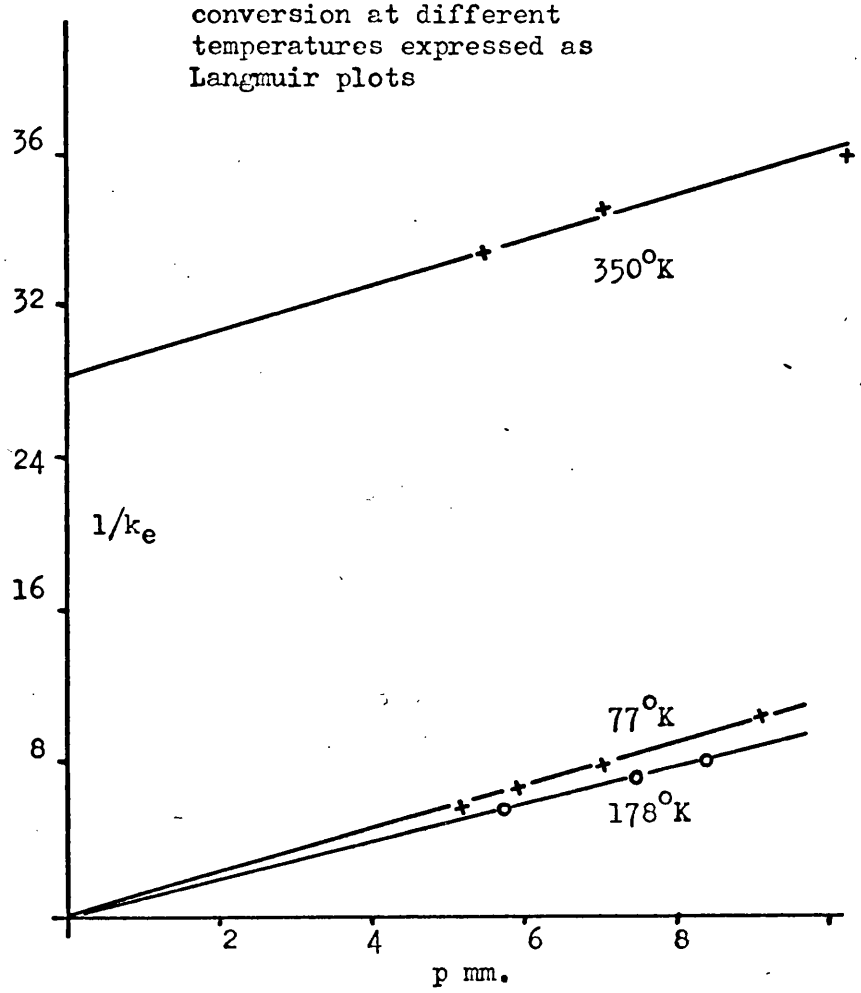

Hydrogen Deuterium Equilibration Reaction

Some hydrogen deuteride was found to be present in the hydrogen deuterium mixture which was exposed to the catalyst. This hydrogen deuteride was probably formed during the preparation of the deuterium and subsequent purification by passage through a hydrogen contaminated palladium thimble. The presence of the hydrogen deuteride proves to be a useful reference, for if no more hydrogen deuteride is formed during the exposure of the mixture to the catalyst the ratio of HD to D_2 should be the same as that of the original mixture.

Temp (°K)	t (min)	p (mm)	ratio HD/D_2
77	15	7.2	1:7.4
90	15	7.1	1:7.3
273	30	7.3	1:7.4
298	60	7.2	1:7.5
Blank		7.3	1:7.4

Anhydrous Cobalt Sulphate, $CoSO_4$

The sample of anhydrous cobalt sulphate was heated to 380°K in a dynamic vacuum of 10^{-6} mm Hg for 9 hrs., and then repeatedly heated at this temperature until constant activity was attained. The sample used for surface area determinations was from the same source as that used in the catalytic work and was pretreated in an identical manner.

Surface area determination

Determination	p_o (mm)	p (mm)	v_{ads} (cc)	$v_{ads}./g$ v'	$p/v'(p_o-p)$	p/p_o
A	756.4	100.7	11.76	2.648	0.058	0.133
	756.4	128.0	12.39	2.790	0.073	0.169
	756.4	155.8	12.95	2.915	0.089	0.206
B	756.4	123.7	12.90	2.905	0.067	0.164
	756.4	156.7	13.80	3.107	0.084	0.207
	756.4	189.5	14.68	3.305	0.101	0.251

$S.A_{B.E.T}(A) = 10.4\ m^2\ g^{-1}$ $S.A_{B.E.T}(B) = 10.9\ m^2\ g^{-1}$

Mean surface area of sample = $10.65\ m^2\ g^{-1}$

TABLE 6.8 The Kinetics of the conversion

Surface area of sample = 22.8 m^2 Reaction volume = 325cc.

Temp (°K)	Av.Press (mm)	k_e X 10^2 (min^{-1})	$\log_{10} k_e$	k_m (molecules $cm^{-2} sec^{-1}$)	$\text{Log}_{10} k_m$	$10^2/T$
		increasing temperature				
77	5.1	18.05	$\bar{1}.23$	2.74×10^{12}	12.44	1.30
90	5.3	16.10	$\bar{1}.21$	2.17×10^{12}	12.34	1.11
112.5	5.3	19.86	$\bar{1}.30$	2.14×10^{12}	12.33	0.89
135	5.4	22.41	$\bar{1}.35$	2.05×10^{12}	12.31	0.74
146	5.3	19.27	$\bar{1}.30$	1.60×10^{11}	12.20	0.69
178	5.4	12.90	$\bar{1}.11$	8.96×10^{11}	11.95	0.56
209.5	5.2	7.24	$\bar{2}.86$	4.04×10^{11}	11.61	0.48
273	5.6	2.07	$\bar{2}.32$	9.72×10^{11}	10.99	0.37
368	5.1	0.81	$\bar{3}.91$	2.57×10^{10}	10.41	0.27
		decreasing temperature				
273	5.2	2.07	$\bar{2}.32$	9.47×10^{10}	10.98	0.37
146	5.4	19.30	$\bar{1}.29$	1.63×10^{12}	12.21	0.69
90	5.3	18.10	$\bar{1}.26$	2.44×10^{12}	12.39	1.11
77	5.2	17.85	1.25	2.76×10^{12}	12.44	1.30

The Arrhenius plots of $\log_{10} k_e$ and $\log_{10} k_m$ against $1/T°K$ are shown in FIGS. 6.11 and 6.12 respectively. From the slopes and intercepts of plot 6.12 the apparent activation energies (E_a) and frequency factors (B_m) were determined.

Temperature region 77°-150°K

E_a = -0.084 k cals/mol $\log_{10} B_m = 12.137$ $B_m = 1.37 \times 10^{12}$

Temperature region 150°-350°K

E_a = -2.5 k cals/mol $\log_{10} B_m = 8.920$ $B_m = 8.38 \times 10^{8}$

FIGURE 6.11

Arrhenius plot of log k_e against $1/T^{o}K$.

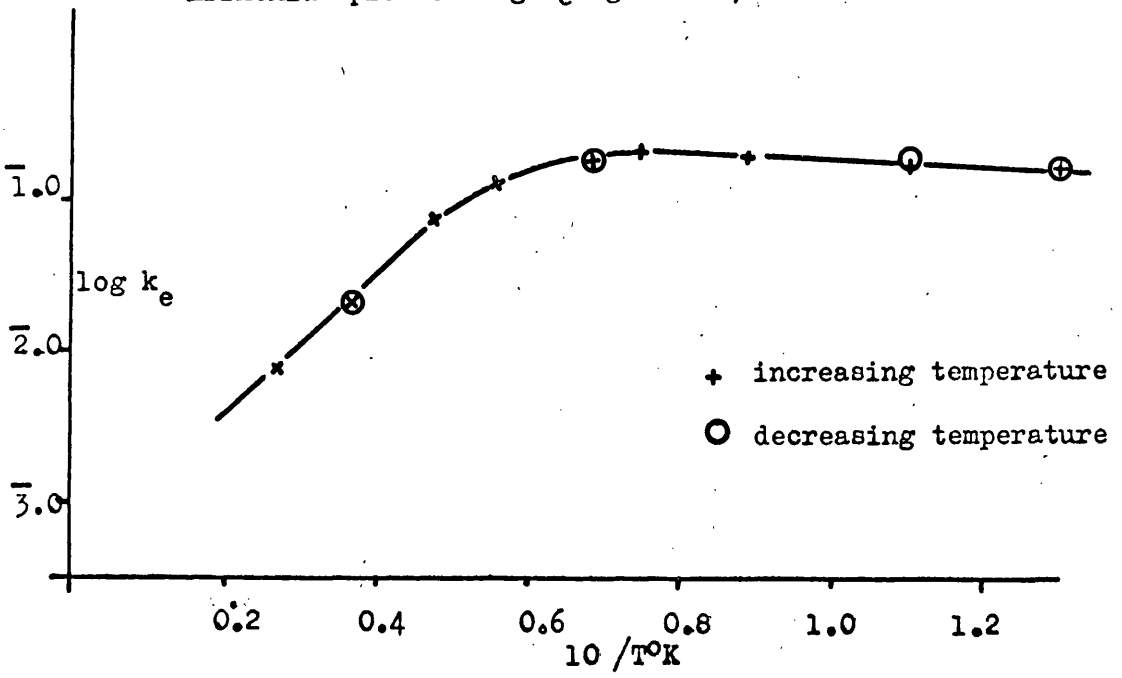

FIGURE 6.12

Arrhenius plot of log k_m against $1/T^{o}K$.

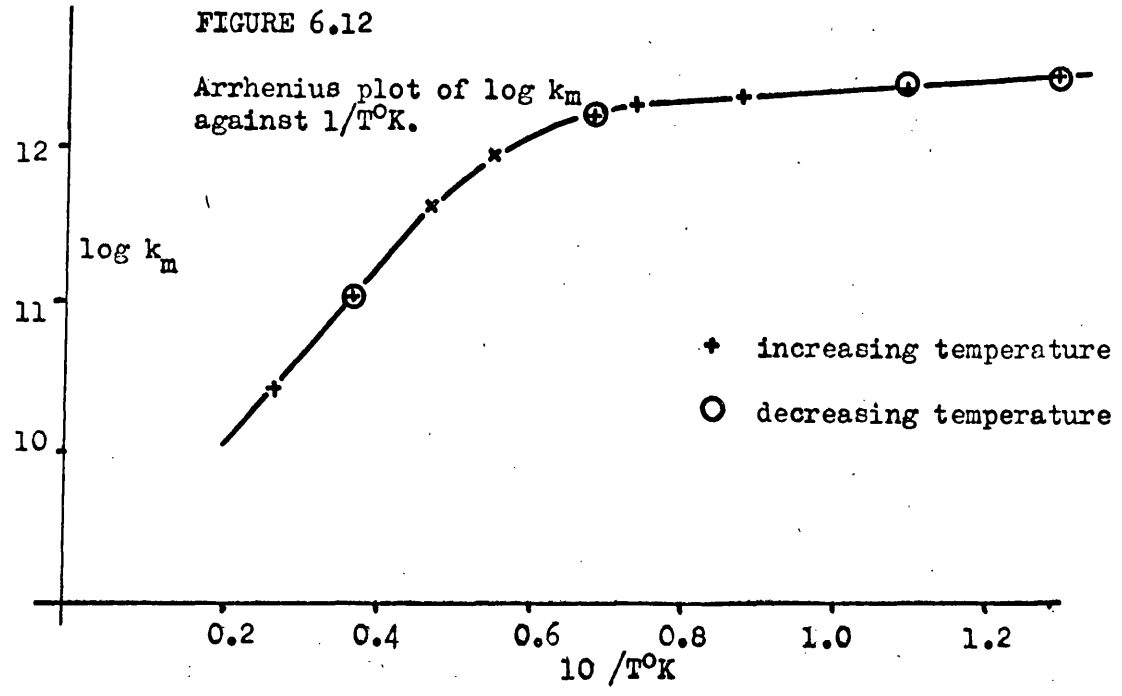

TABLE 6.9 Pressure dependence of the conversion

Temp (°K)	Press (mm)	$\log_{10}p$	time (min)	$\log \Omega_o/\Omega_t$	k_e (min^{-1})	$1/k_e$	$\log_{10}k_e$
77	6.41	0.81	10	0.59	0.14	7.35	$\bar{1}.13$
77	8.92	0.95	10	0.44	0.10	10.00	$\bar{1}.00$
77	9.43	0.97	10	0.43	0.09	10.10	$\bar{2}.95$
77	12.24	1.09	10	0.35	0.08	12.50	$\bar{2}.90$
146	5.28	0.72	5	0.40	0.19	5.41	$\bar{1}.27$
146	8.17	0.91	5	0.27	0.12	8.07	$\bar{1}.09$
146	9.63	0.98	6	0.28	0.11	9.09	$\bar{1}.04$
273	5.82	0.76	10	0.085	0.020	50.76	$\bar{2}.29$
273	7.28	0.86	10	0.81	0.019	51.48	$\bar{2}.28$
273	12.80	1.08	10	0.80	0.018	54.35	2.26
368	5.11	0.71	9	0.032	0.008	122.0	$\bar{3}.91$
368	7.10	0.85	9	0.032	0.008	122.0	$\bar{3}.91$
368	10.00	1.00	9	0.032	0.008	122.0	$\bar{3}.91$

The Freundlich and Langmuir isotherm plots are shown in FIGS. 6.13 and 6.14 respectively. Since both isotherms are shown to hold over the pressure region investigated $n = (1-\theta)$

TABLE 6.10 Variation of Freundlich pressure exponent with temperature

Temp(°K)	77	146	273	368
n	0.00	0.00	0.83	-
θ	1.00	1.00	0.17	-

FIGURE 6.13

Pressure dependencies of the conversion at different temperatures expressed as Freundlich plots.

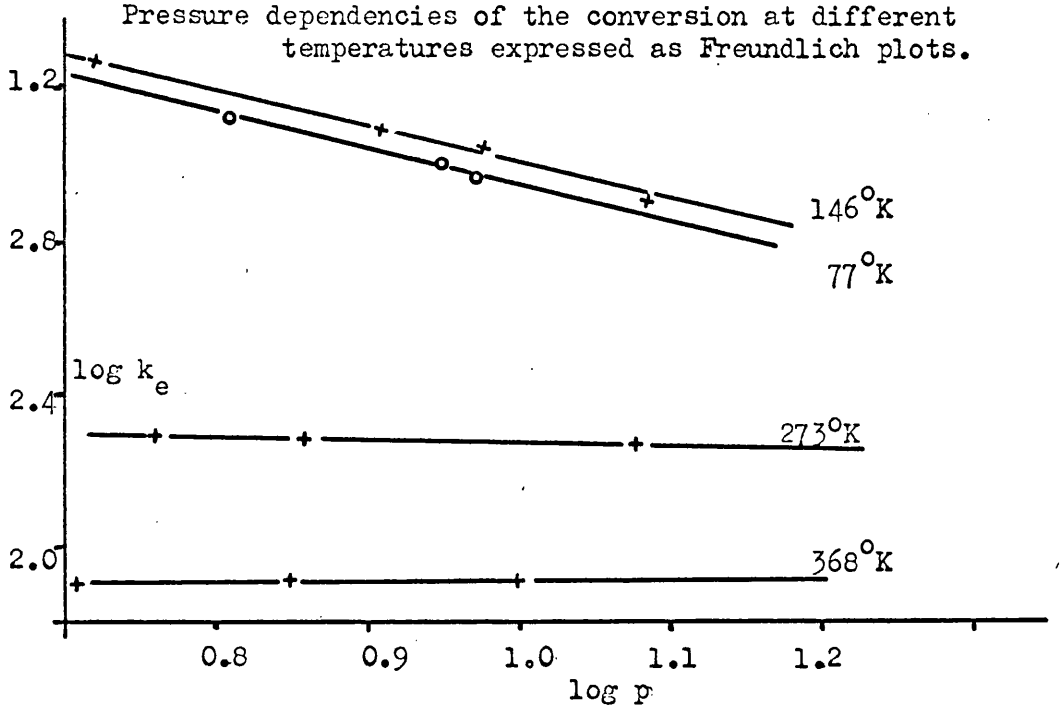

FIGURE 6.14

Pressure dependencies of the conversion at different temperatures expressed as Langmuir plots.

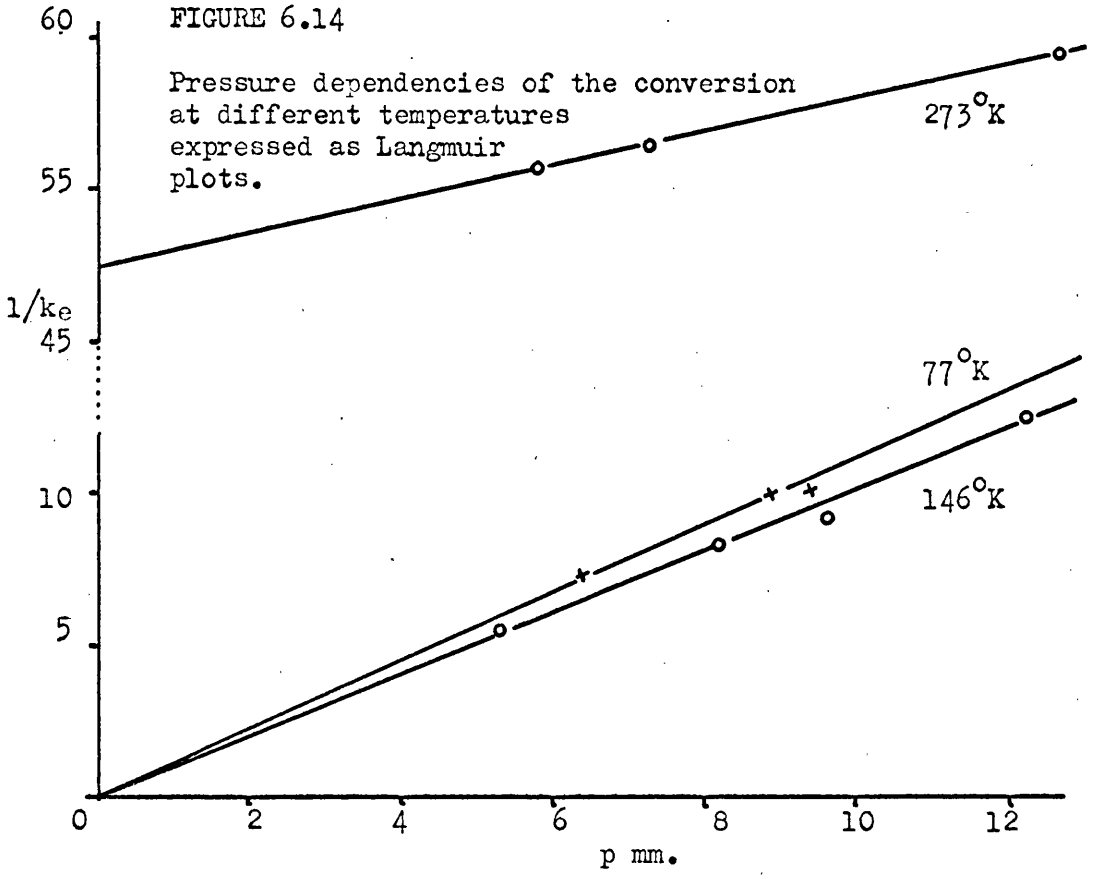

Anhydrous Manganese Sulphate, $MnSO_4$

Two samples of anhydrous manganese sulphate were studied, to determine whether the activity of the catalysts was reproducible. The samples are denoted by $MnSO_4$ (I) and $MnSO_4$ (II). Heat pretreatment of both samples involved heating to 420°K in a dynamic vacuum of 10^{-6} mm Hg. until constant activity was obtained.

Determination of surface area of $MnSO_4$ (I)

Determination	p_o (mm)	p (mm)	vads (cc)	vads/g v'	$p/v'(p_o-p)$	p/p_o
A	763.8	91.48	3.96	0.46	0.29	0.12
	763.8	118.26	3.21	0.50	0.37	0.16
	763.8	146.04	4.47	0.53	0.45	0.19
B	766.6	112.07	4.211	0.49	0.35	0.15
	766.6	143.85	4.66	0.55	0.42	0.19
	766.6	176.51	5.02	0.60	0.51	0.23

$S.A_{B.E.T}$ (A) = 1.98 $m^2 g^{-1}$ $\quad$ $S.A_{B.E.T}$ (B) = 2.22 $m^2 g^{-1}$

Mean surface area = 2.099 $m^2 g^{-1}$

Determination of surface area of $MnSO_4$ (II)

Determination	p_o (mm)	p (mm)	v_{ads} (cc)	v_{ads}/g v'	$p/v'(p_o-p)$	p/p_o
A	762.6	99.14	4.89	0.52	0.28	0.13
	762.6	128.03	5.16	0.55	0.37	0.17
	762.6	157.87	5.46	0.58	0.45	0.21
B	766.0	117.68	5.07	0.54	0.18	0.15
	766.0	151.21	5.48	0.59	0.42	0.19
	766.0	185.87	5.66	0.61	0.53	0.24

$S.A_{B.E.T}$ (A) = 2.041 $m^2 g^{-1}$ $S.A_{B.E.T}$ (B) = 2.041 $m^2 g^{-1}$

Mean surface area = 2.041 $m^2 g^{-1}$

TABLE 6.11 The Kinetics of the conversion on $MnSO_4$(I)

Reaction volume = 322cc Surface area of sample = 3.28 m^2

Temp (^oK)	Av.press (mm)	$k_e \times 10^2$ (min^{-1})	$\log_{10} k_e$	k_m (molecules) ($cm^{-2} sec^{-1}$)	$\log_{10} k_m$	$10^2/T$
			increasing temperature			
77	5.5	15.59	$\bar{1}.19$	1.78×10^{13}	13.25	1.30
90	5.5	17.28	$\bar{1}.24$	1.69×10^{13}	13.23	1.11
112.5	5.4	17.91	$\bar{1}.25$	1.38×10^{13}	13.14	0.89
135	5.5	9.40	$\bar{2}.97$	6.13×10^{12}	12.79	0.74
146	5.5	7.60	$\bar{2}.88$	4.58×10^{12}	12.66	0.69
178	5.6	2.30	$\bar{2}.36$	1.16×10^{12}	12.06	0.56
273	5.6	0.27	$\bar{3}.44$	8.87×10^{10}	10.95	0.37
			decreasing temperature			
209.5	5.5	0.89	$\bar{3}.95$	3.74×10^{11}	11.57	0.48
146	5.5	7.23	$\bar{2}.86$	4.36×10^{12}	12.64	0.69
112.5	5.5	17.29	$\bar{1}.24$	1.35×10^{13}	13.13	0.89
77	5.5	15.81	1.20	1.81×10^{13}	13.26	1.30

The Arrhenius plots of $\log k_e$ and $\log k_m$ against $1/T^oK$ are shown in FIGS. 6.15 and 6.16. From the slopes and intercepts of FIG. 6.16 the apparent activation energies (E_a) and frequency factors (B_m) can be found.

Temperature range 77-110^oK

E_a = -0.094 k cal/mole $\log B_m$ = 12.98 $B_m = 9.5 \times 10^{12}$

Temperature range 110^o-300^oK

E_a = -2.64 k cal/mol $\log B_m$ = 7.78 $B_m = 6.03 \times 10^7$

FIGURE 6.15

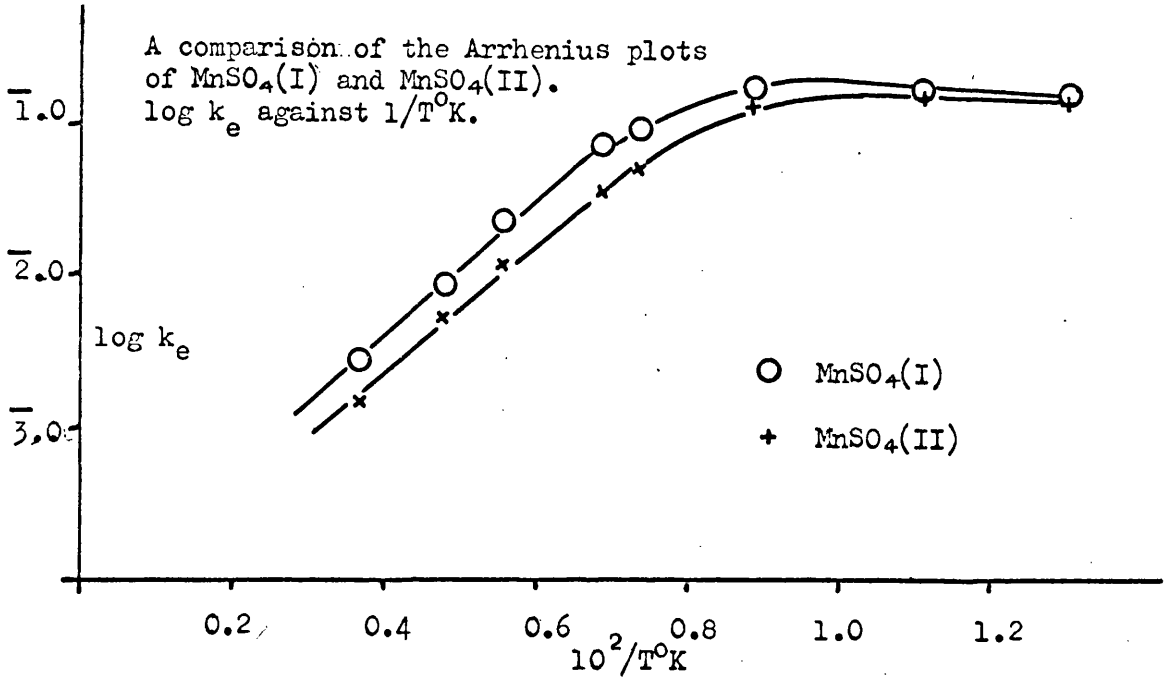

FIGURE 6.16

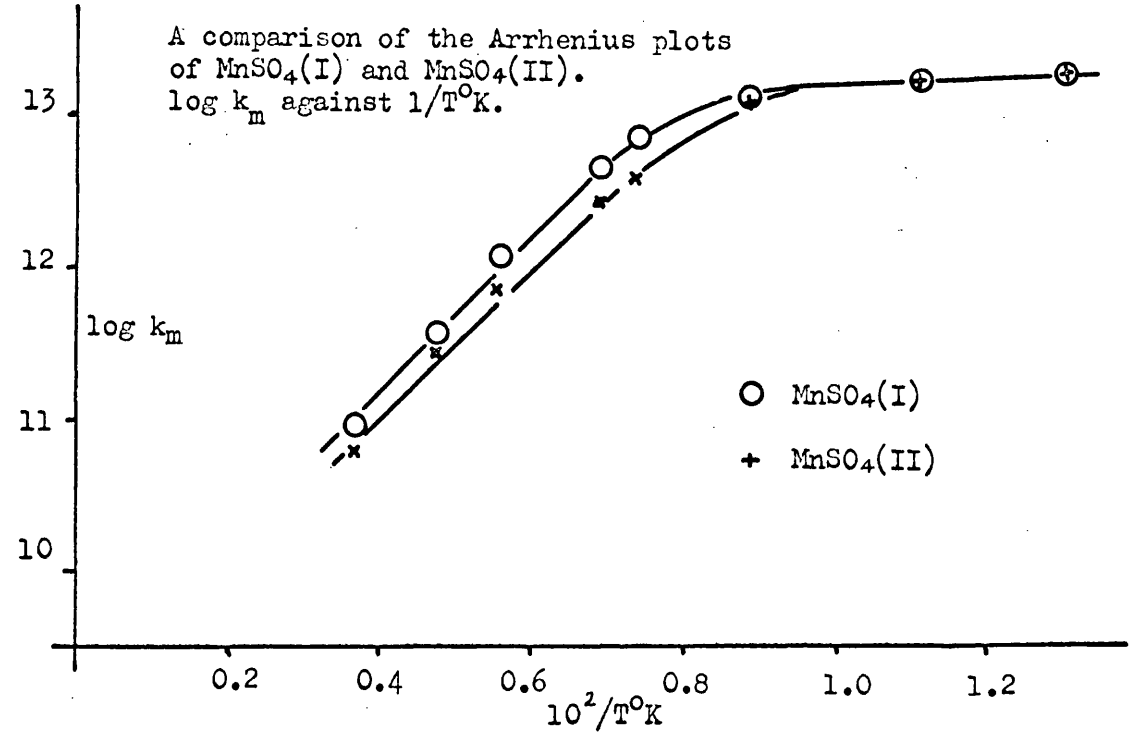

TABLE 6.12 The Kinetics of the conversion on $MnSO_4$ (II)

Reaction volume = 322cc Surface area of sample = 2.7 m^2

Temp (^oK)	Av.press. (mm)	k_e X 10 (min^{-1})	$\log_{10} k_e$	k_m (molecules $cm^{-2} sec^{-1}$)	$\log_{10} k_m$	$10^2/T$
			increasing temperature			
77	5.5	14.17	$\bar{1}.15$	1.94×10^{13}	13.29	1.30
90	5.6	17.06	$\bar{1}.23$	2.03×10^{13}	13.31	1.11
112.5	5.4	13.12	$\bar{1}.12$	1.21×10^{13}	13.08	0.89
135	5.3	5.30	$\bar{2}.72$	4.00×10^{12}	12.60	0.74
146	5.5	3.91	$\bar{2}.59$	2.83×10^{12}	12.45	0.69
178	5.4	1.20	$\bar{2}.08$	6.96×10^{11}	11.84	0.56
209.5	5.5	0.55	$\bar{3}.74$	2.77×10^{11}	11.44	0.48
273	5.6	0.16	$\bar{3}.21$	6.29×10^{10}	10.80	0.37
			decreasing temperature			
178	5.6	1.20	$\bar{2}.08$	7.23×10^{11}	11.86	0.56
146	5.5	3.92	$\bar{2}.59$	2.83×10^{12}	12.45	0.69
90	5.3	15.09	$\bar{1}.18$	1.70×10^{13}	13.23	1.11
77	5.4	13.87	$\bar{1}.14$	1.86×10^{13}	13.27	1.30

The Arrhenius plots of $\log_{10} k_e$ and $\log_{10} k_m$ against $1/T^oK$ are shown in FIGS. 6.15 and 6.16. From the slopes and intercepts of FIG 6.16 the apparent activation energies (E_a) and frequency factors (B_m) can be found.

Temperature region 77^o-110^oK

E_a = -0.094 k cal/mol $\log B_m$ = 12.98 $B_m = 9.5 \times 10^{12}$

Temperature region 110^o-300^oK

E_a = -2.46 k cal/mol $\log B_m$ = 8.82 $B_m = 6.6 \times 10^{8}$

TABLE 6.13 Pressure dependence of the conversion for $MnSO_4$ (I)

Temp. (^oK)	Press. (mm)	$\log_{10}p$	time (min)	$\log \Omega_o/\Omega_t$	$k_e \times 10^2$ (min^{-1})	$1/k_e$	$\log_{10}k_e$
112.5	5.46	0.74	10	0.75	17.2	5.81	$\bar{1}.24$
112.5	9.12	0.96	5	0.25	10.5	9.52	$\bar{1}.02$
112.5	10.23	1.01	5	0.22	9.3	10.75	$\bar{2}.97$
112.5	7.24	0.86	5	0.30	13.2	7.58	$\bar{1}.12$
146	5.46	0.74	10	0.31	7.2	13.89	$\bar{2}.86$
146	9.08	0.96	10	0.24	5.6	17.86	$\bar{2}.75$
146	10.76	1.03	10	0.22	5.0	20.00	$\bar{2}.70$
146	13.06	1.12	10	0.19	4.4	22.73	$\bar{2}.65$
209.5	8.38	0.92	10	0.04	0.9	111.1	$\bar{3}.95$
209.5	10.47	1.02	10	0.04	0.9	111.1	$\bar{3}.95$
209.5	14.79	1.17	10	0.04	0.9	111.1	$\bar{3}.95$
209.5	5.46	0.74	10	0.04	0.9	111.1	$\bar{3}.95$

TABLE 6.14 Pressure dependence of the conversion for $MnSO_4$ (II)

Temp. (^oK)	Press. (mm)	$\log_{10}p$	time (min)	$\log \Omega_o/\Omega_t$	$k_e \times 10^2$ (min^{-1})	$1/k_e$	$\log_{10}k_e$
77	5.46	0.74	5	0.30	14.0	7.14	$\bar{1}.14$
77	8.70	0.94	6	0.24	9.0	11.11	$\bar{2}.96$
77	9.95	0.99	5	0.17	7.7	12.99	$\bar{2}.89$
77	12.24	1.09	15	0.43	6.6	15.15	$\bar{2}.82$
112.5	5.40	0.73	5	0.29	13.5	7.41	$\bar{1}.13$
112.5	7.47	0.87	5	0.23	10.0	10.00	$\bar{1}.00$
112.5	10.76	1.03	6	0.25	7.1	14.08	$\bar{2}.85$
112.5	14.29	1.15	7	0.25	5.9	16.95	$\bar{2}.77$
146	5.46	0.73	6	0.10	3.7	27.03	$\bar{2}.57$
146	7.19	0.86	10	0.16	3.6	27.78	$\bar{2}.56$
146	10.52	1.02	10	0.13	3.0	33.33	$\bar{2}.47$
146	14.29	1.15	10	0.13	2.9	34.48	$\bar{2}.46$
273	5.70	0.76	30	0.02	0.15	666.7	$\bar{3}.19$
273	8.13	0.91	30	0.02	0.15	666.7	$\bar{3}.19$
273	6.31	0.80	30	0.02	0.15	666.7	$\bar{3}.19$
273	9.12	0.96	30	0.02	0.15	666.7	$\bar{3}.19$

FIGURE 6.17

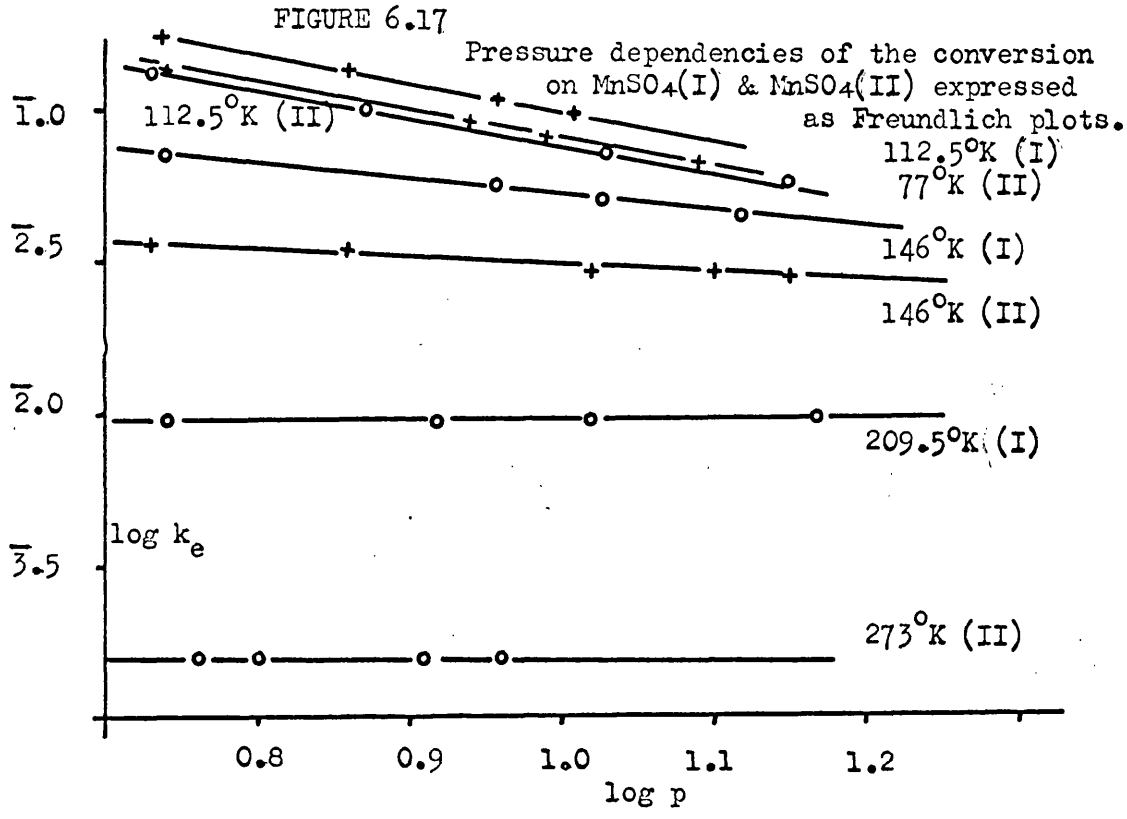

FIGURE 6.18

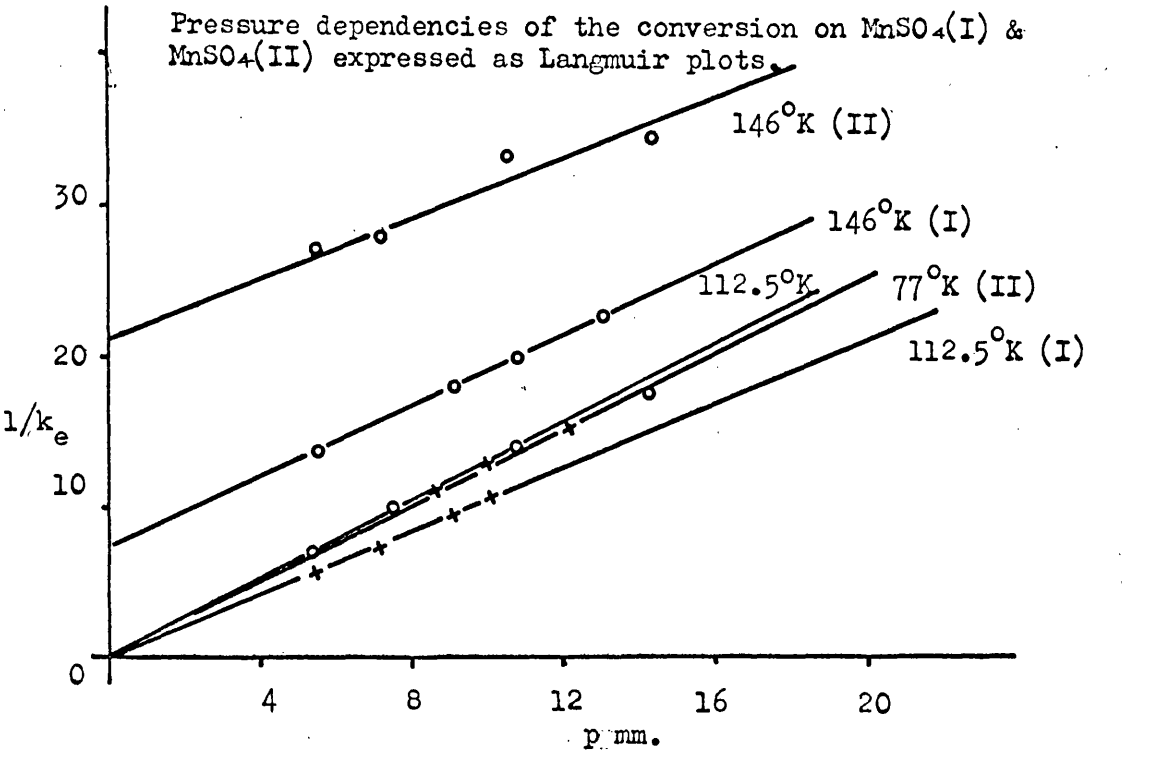

The Freundlich and Langmuir plots for $MnSO_4$(I) and (II) are given in FIG. 6.17 and 6.18 respectively. Since both the Langmuir and Freundlich isotherms are obeyed over the pressure region investigated

$n = (1 - \theta)$

TABLE 6.15 Variation of the Freundlich pressure exponent with temperature.

Temp.(°K)	77(II)	112.5(I)	112.5(II)	146(I)	146(II)	209.5	273
n	0	0	~0	0.79	0.87	1	1
θ	1	1	~1	0.21	0.13	0	0

TABLE 6.16 Adsorption of hydrogen on $MnSO_4$(II).

77°K				90°K			
Init. press. (mm)	Equil. press. (mm)	Vads (cc)	Vads (molecules/cm^2)	Init. press. (mm)	Equil. press. (mm)	Vads (cc)	Vads (molecules/cm^2)
3.63	2.32	0.157	8.4×10^{13}	3.42	2.12	0.101	5.4×10^{13}
5.64	3.66	0.211	11.3×10^{13}	3.97	2.76	0.129	6.9×10^{13}
7.16	4.75	0.255	13.7×10^{13}	6.92	4.11	0.171	9.1×10^{13}
8.31	5.61	0.271	14.5×10^{13}	8.25	5.91	0.191	10.2×10^{13}
9.12	6.07	0.312	16.7×10^{13}	9.16	7.62	0.210	11.2×10^{13}
11.03	7.81	0.284	15.3×10^{13}	11.77	8.67	0.225	12.1×10^{13}
14.58	10.14	0.323	17.3×10^{13}	12.01	8.91	0.203	10.9×10^{13}
15.20	10.37	0.301	16.1×10^{13}				

The isotherm is shown in FIG. 6.19

FIGURE 6-19

Adsorption Isotherms of Hydrogen on $MnSO_4$ (II)

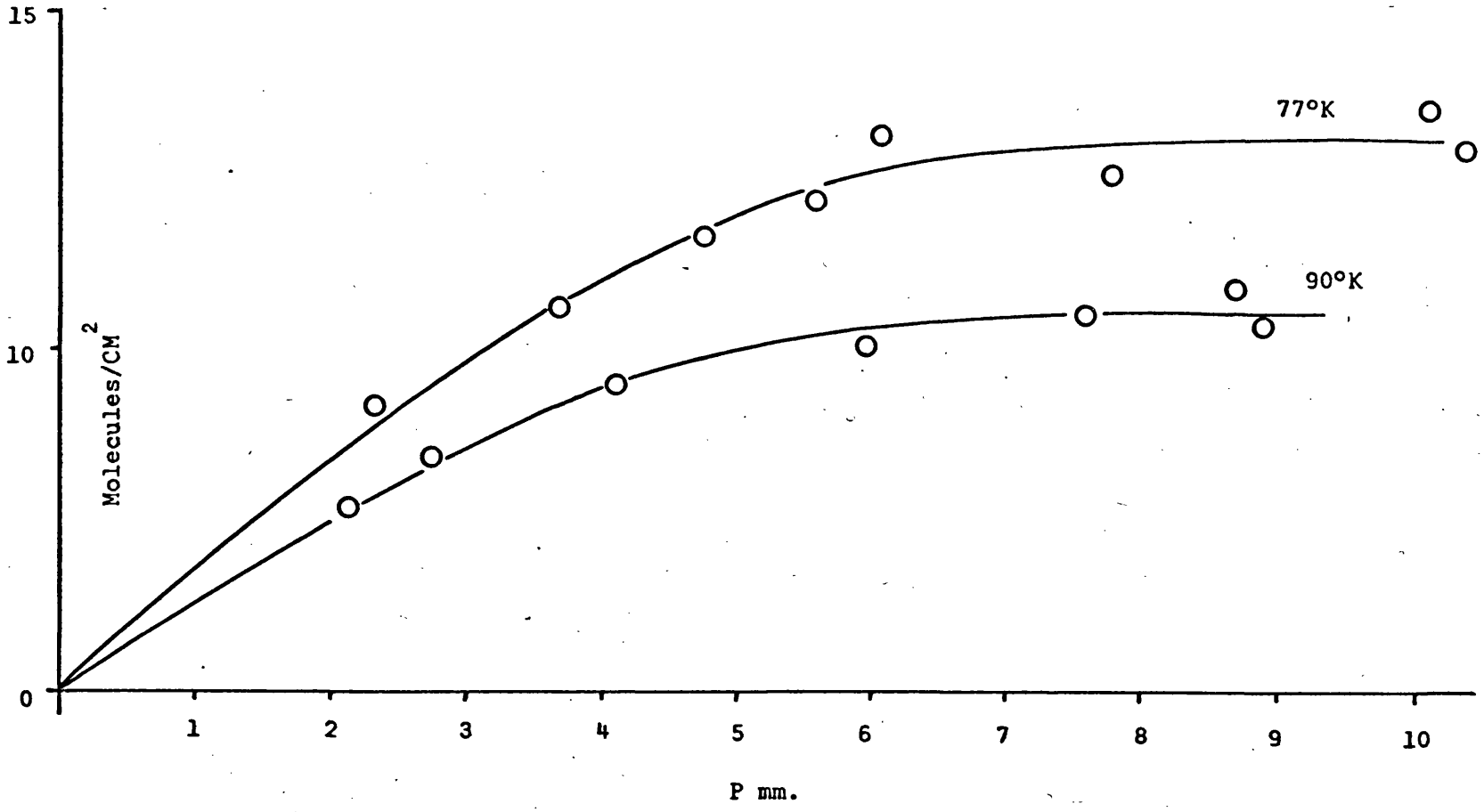

Hydrogen Deuterium Equilibration reaction.

Temp. (°K)	t (min)	p (mm)	ratio HD/D_2
77	15	7.3	1:7.4
146	20	7.2	1:7.4
298	60	7.1	1:7.5
Blank			1:7.4

(ii) Kinetic data obtained from the divalent oxides of the first row transition metal salts.

Cupric Oxide, CuO.

The sample of cupric oxide was heated to 650°K in a dynamic vacuum of 10^{-6} mm Hg. until constant activity was obtained. The sample of oxide used to determine the surface area was pretreated in an identical manner to that used in the catalytic work. Cupric oxide is unstable above 700°K in a vacuo this being due to the increasing dissociation pressure above this temperature, thus the intitial evacuation temperature and kinetic data was limited to temperatures below 650°K

Determination of surface of CuO.

p_o (mm)	p (mm)	Vads (cc)	Vads/g (v')	$p/v'(p_o-p)$	p/p_o
752.3	112.3	10.83	2.69	0.065	0.15
752.3	142.9	11.99	2.98	0.079	0.19
752.3	171.9	12.87	3.21	0.092	0.23

$S.A._{B.E.T} = 12.43\ m^2\ g^{-1}$

TABLE 6.17 Determination of catalytic activity of CuO.

Reaction volume 322 cc. Surface area 15.89 m^2

T (^oK)	Av.press. (mm)	k_e X 10 (min^{-1})	$\log_{10} k_e$	k_m (molecules $cm^{-2} sec^{-1}$)	$\log_{10} k_m$	$10^2/T$
increasing temperature						
77	5.3	12.50	$\bar{1}.10$	2.80×10^{12}	12.45	1.30
90	5.4	13.73	$\bar{1}.14$	2.68×10^{12}	12.43	1.11
112.5	5.5	14.10	$\bar{1}.15$	2.24×10^{12}	12.35	0.89
135	5.6	17.66	$\bar{1}.25$	2.38×10^{12}	12.38	0.74
146	5.2	10.64	$\bar{1}.03$	1.23×10^{12}	12.09	0.69
178	5.2	8.10	$\bar{2}.91$	7.70×10^{11}	11.89	0.56
209.5	5.5	5.25	$\bar{2}.72$	4.49×10^{11}	11.65	0.48
273 *	5.3	2.72	$\bar{2}.43$	1.72×10^{11}	11.24	0.37
decreasing temperature						
203.5	5.4	0.59	$\bar{3}.77$	4.95×10^{10}	10.69	0.48
146	5.3	2.57	$\bar{2}.41$	3.15×10^{11}	11.50	0.69
90	5.5	7.56	$\bar{2}.88$	1.50×10^{12}	12.18	1.11
77	5.5	10.82	$\bar{1}.03$	2.52×10^{12}	12.40	1.30

* The data at this temperature was taken from only one reading. The rate was found to decrease with subsequent additions of hydrogen. This is indicative of poisoning by irreversible adsorption of hydrogen on catalytic sites.

The Arrhenius plots of $\log_{10} k_e$ and $\log_{10} k_m$ against $1/T^oK$ are shown in FIG.6.20 and FIG.6.21. From the slopes and intercepts of FIG.6.21 the apparent activation energies (E_a) and frequency factors (B_m) can be found.

FIGURE 6.20

Arrhenius plot of log k_e against $1/T^oK$

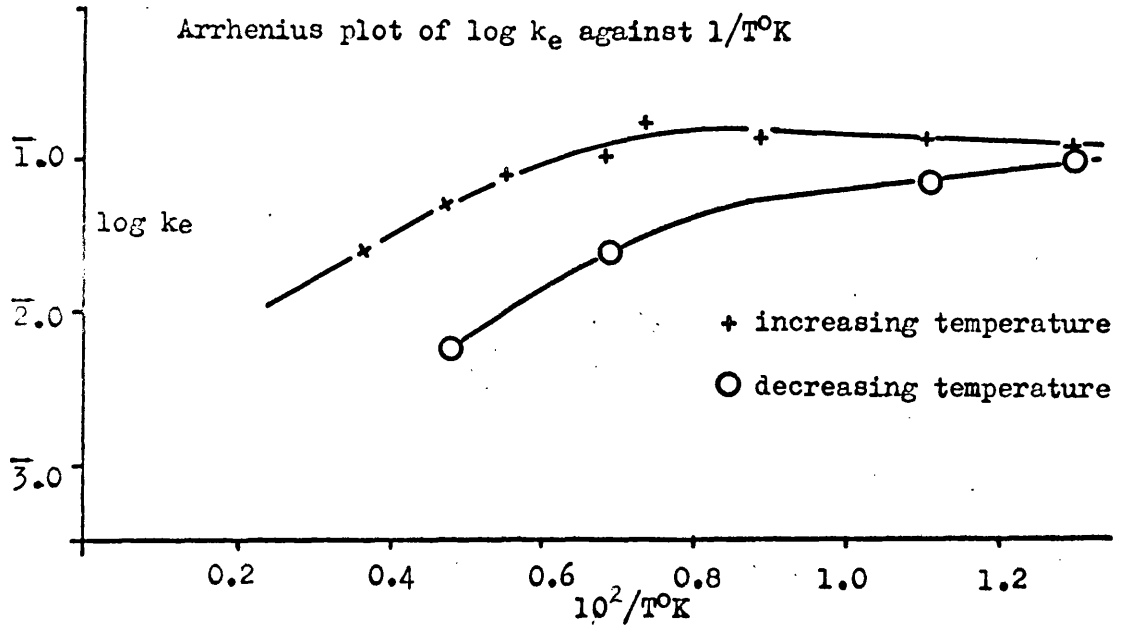

FIGURE 6.21

Arrhenius plot of log k_m against $1/T^oK$

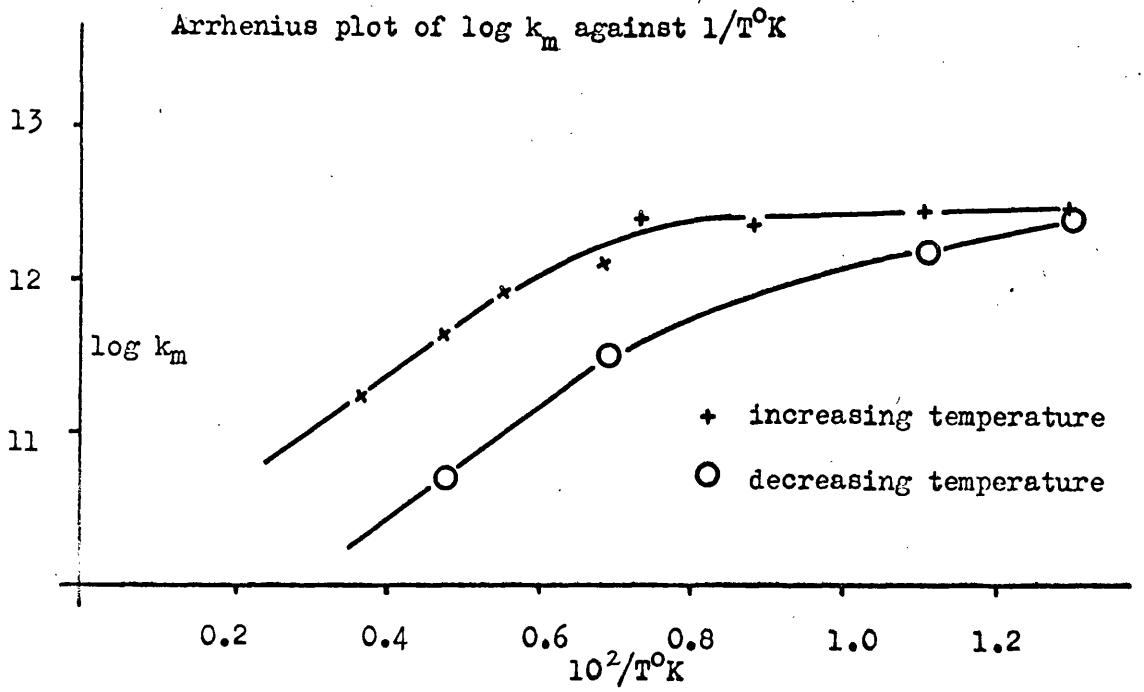

Increasing temperature

Temperature region 77°-150°K

E_a = -0.089 k cal/mol log B_m = 12.21 $B_m = 1.62 \times 10^{12}$

Temperature region 150°-300°K

E_a = -1.57 k cale/mol log B_m = 9.96 $B_m = 9.12 \times 10^{9}$

Decreasing temperature

Temperature region 77°-150°K

E_a = -0.55 k cal/mol log B_m = 10.8 $B_m = 6.31 \times 10^{10}$

Temperature region 150°- 300°K

E_a = -1.7 k cal/mol log B_m = 8.86 $B_m = 7.24 \times 10^{8}$

TABLE 6.18 Pressure dependence of the conversion.

Temp. (°K)	Press (mm)	$\log_{10} p$	time (min)	$\log \Omega_o/\Omega_t$	k_e	$1/k_e$	$\log_{10} k_e$
77	5.3	0.73	8	0.44	0.13	8.00	$\bar{1}.09$
77	7.9	0.89	6	0.22	0.09	11.63	$\bar{2}.93$
77	10.5	1.02	10	0.28	0.07	15.40	$\bar{2}.82$
77	6.0	0.78	10	0.49	0.11	8.77	$\bar{1}.06$
146	5.3	0.73	10	0.46	0.11	9.43	$\bar{1}.03$
146	6.3	0.80	10	0.39	0.09	11.11	$\bar{1}.00$
146	7.8	0.89	6	0.19	0.07	13.70	$\bar{2}.86$
146	11.3	1.05	7	0.15	0.05	20.80	$\bar{2}.69$
209.5	5.5	0.74	10	0.23	0.05	18.91	$\bar{2}.72$
209.5	6.9	0.84	10	0.19	0.04	22.22	$\bar{2}.65$
209.5	9.8	0.99	6	0.09	0.03	28.20	$\bar{2}.55$

The Langmuir and Freundlich plots are shown in FIG. 6.22 and 6.23 respectively. Since both the Langmuir and Freundlich isotherms are obeyed over the pressure region investigated $n = (1 - \theta)$

TABLE 6.19 Variation of the Freundlich pressure exponent with temperature.

Temp °K	77	146	209.5
n	0	0	0.3
θ	1	1	0.7

FIGURE 6.22

Pressure dependencies of the conversion at different temperatures expressed as Langmuir plots.

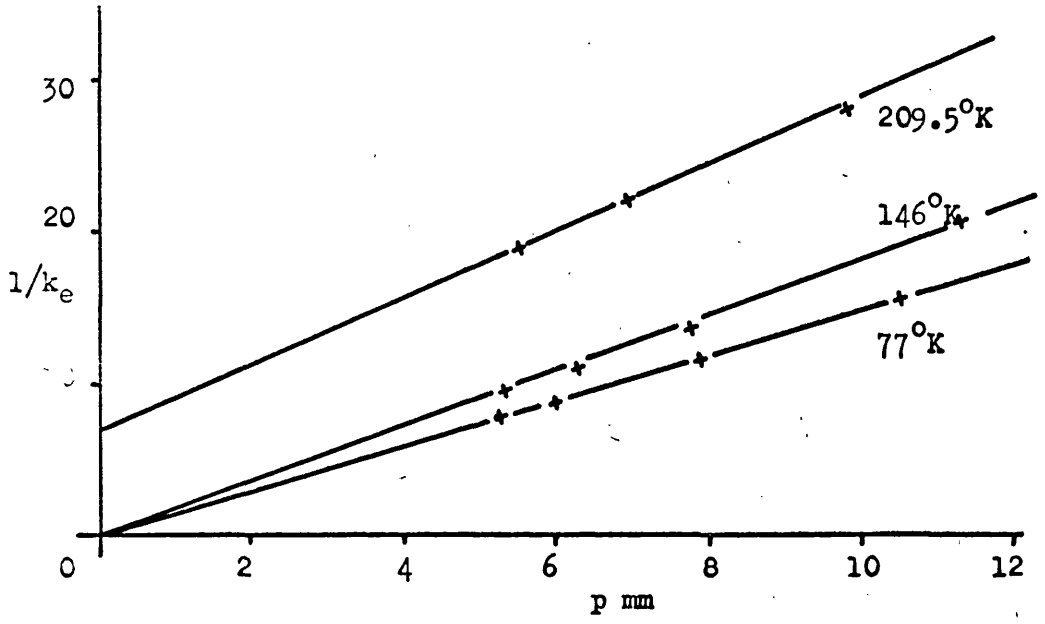

FIGURE 6.23

Pressure dependencies of the conversion at different temperatures expressed as Freundlich plots.

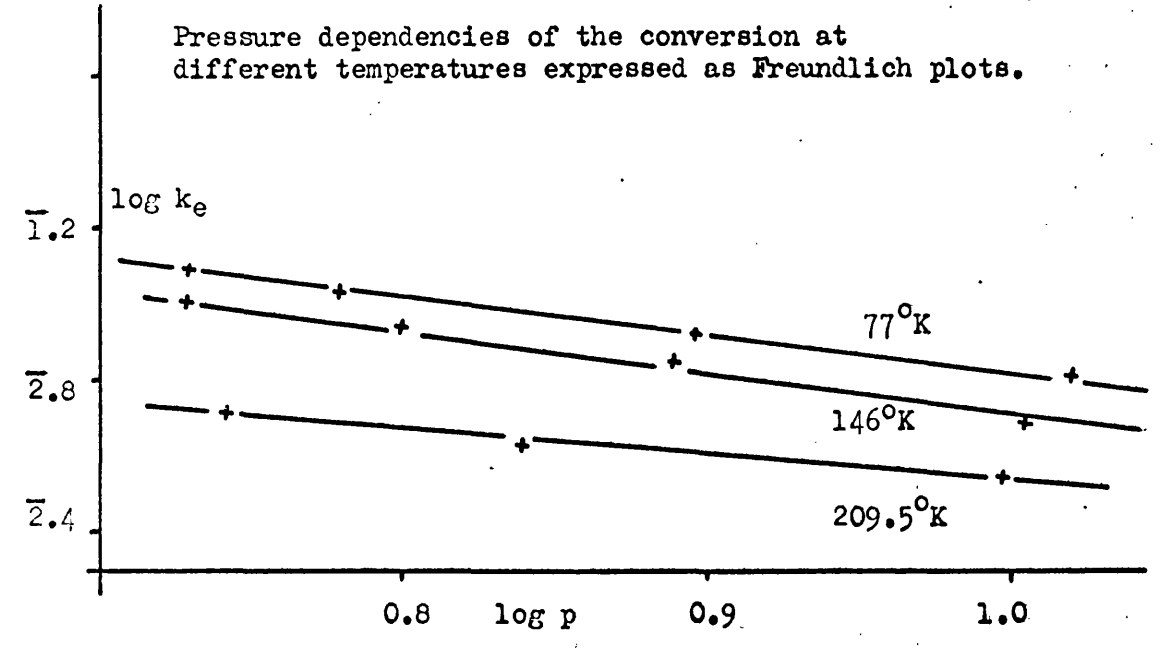

Nickel Oxide, NiO

Two samples of nickel oxide were studied. The samples are denoted by NiO (I) and NiO (II). Heat pretreatment of both samples involved heating to constant activity at 700°K in a dynamic vacuum of 10^{-6} mm.Hg. Technical limitations prevented similar pretreatment of the surface area sample.

Determination of surface area.

Since both NiO (I) and NiO (II) were from the same source and were pretreated in an identical manner it is assumed that their surface areas are identical

Determination	p_o (mm)	p (mm)	v_{ads} (cc)	v_{ads}/g (v')	$p/v'(p_o-p)$	p/p_o
A	759.6	110.6	0.83	0.067	2.53	0.15
	759.6	143.8	0.91	0.074	3.16	0.19
	759.6	179.1	0.97	0.079	3.88	0.24
B	755.1	95.6	0.82	0.066	2.20	0.13
	755.1	121.5	0.86	0.070	2.75	0.16
	755.1	149.5	0.91	0.074	3.32	0.20

$S.A_{B.E.T}$ (A) = 0.255 $m^2 g^{-1}$ $S.A_{B.E.T}$(B) = 0.255 $m^2 g^{-1}$

Mean surface Area = 0.255 $m^2 g^{-1}$

TABLE 6.20 Kinetic study of NiO(I).

Reaction volume 320cc Surface area 0.887 m^2

Temp (°K)	Av.press. (mm)	k_e X 10 (min^{-1})	$\log_{10} k_e$	k_m (molecules $cm^{-2} sec^{-1}$)	$\log_{10} k_m$	$10^2/T$
increasing temperature						
77	5.5	13.43	$\bar{1}.13$	5.56×10^{13}	13.74	1.30
90	5.5	15.78	$\bar{1}.20$	5.59×10^{13}	13.75	1.11
112.5	5.4	15.78	$\bar{1}.20$	4.39×10^{13}	13.64	0.89
135	5.4	15.78	$\bar{1}.20$	3.66×10^{13}	13.56	0.74
146	5.6	15.07	$\bar{1}.18$	3.35×10^{13}	13.53	0.69
178	5.5	17.22	$\bar{1}.24$	3.08×10^{13}	13.49	0.56
209.5	5.5	18.54	$\bar{1}.27$	2.82×10^{13}	13.45	0.48
273	5.4	21.28	$\bar{1}.33$	2.44×10^{13}	13.39	0.37

TABLE 6.21 Kinetic study of NiO(II).

Reaction volume 318cc Surface area 0.134 m^2

Temp (°K)	Av.press. (mm)	k_e X 10 (min^{-1})	$\log_{10} k_e$	k_m (molecules $cm^{-2} sec^{-1}$)	$\log_{10} k_m$	$10^2/T$
increasing temperature						
77	5.5	9.84	$\bar{2}.99$	2.68×10^{14}	14.43	1.30
90	5.5	10.72	$\bar{1}.03$	2.50×10^{14}	14.40	1.11
135	5.5	10.00	$\bar{1}.00$	1.55×10^{14}	14.19	0.74
209.5	5.6	10.48	$\bar{1}.02$	1.07×10^{14}	14.03	0.48
273	5.5	8.98	$\bar{2}.95$	6.90×10^{13}	13.84	0.37
372	5.5	20.72	$\bar{3}.32$	1.18×10^{14}	14.07	0.27
decreasing temperature						
273	5.6	15.08	$\bar{1}.18$	1.57×10^{14}	14.20	0.37
209.5	5.6	14.28	$\bar{1}.16$	1.45×10^{14}	14.16	0.48
146	5.5	11.75	$\bar{1}.07$	2.05×10^{14}	14.31	0.69
77	5.5	14.28	$\bar{1}.16$	3.85×10^{14}	14.59	1.30

The Arrhenius plots of $\log_{10} k_e$ and $\log_{10} k_m$ against $1/T^{\circ}K$ are shown in FIG. 6.24 and 6.25. From these plots the apparent activation energies (E_a) and frequency factors (B_m) for NiO(I) and NiO(II) can be found.

Temperature region 77°-$90^{\circ}K$

For both NiO(I) and NiO(II) $E_a \sim 0$ and

$B_m = 5.6 \times 10^{13}$ and 2.5×10^{14} respectively

Temperature region 90°-$300^{\circ}K$

$E_a = -0.224$ and -0.259 k cal/mole for NiO(I) and NiO(II) respectively and $B_m = 1.59 \times 10^{13}$ and 5.6×10^{13}

FIGURE 6.24

A comparison of the Arrhenius plots of NiO (I) & NiO (II).
log k_e against $1/T^oK$.

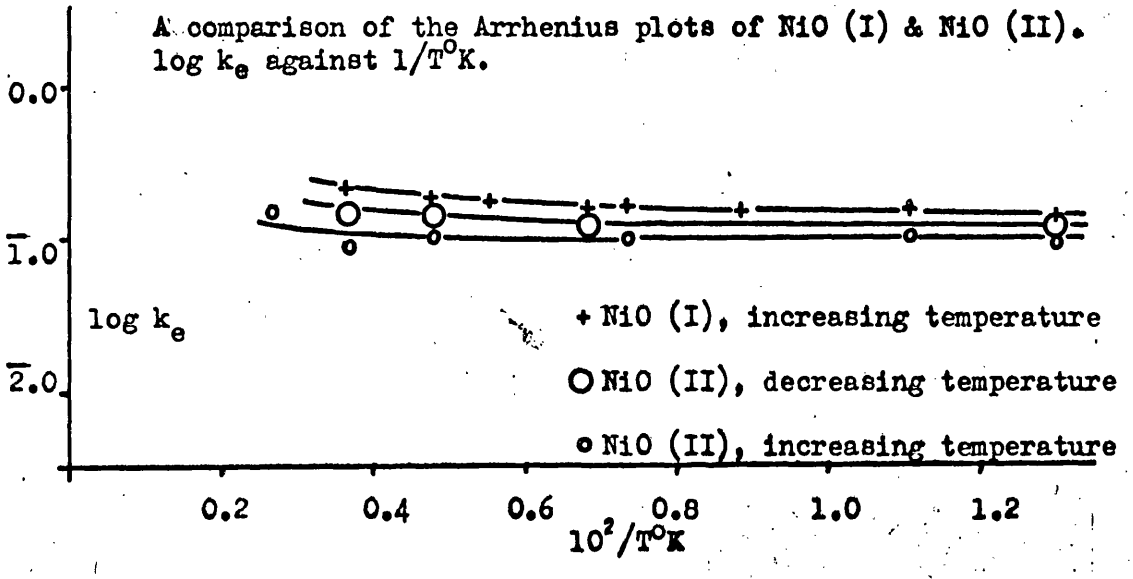

FIGURE 6.25

A comparison of the Arrhenius plots of NiO (I) & NiO (II).
log k_m against $1/T^oK$.

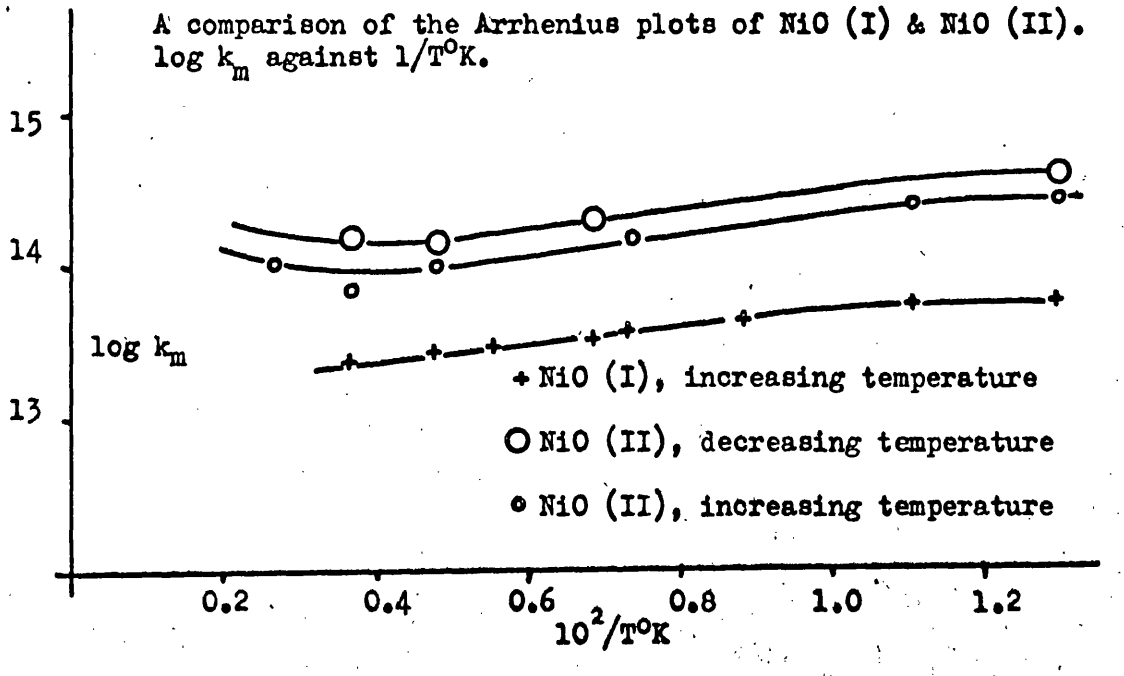

TABLE 6.22 Pressure dependence of the conversion on NiO(I)

Temp. (°K)	Press. (mm)	$\log_{10}p$	time (min)	log Ω_o/Ω_t	k_e (min^{-1})	$1/k_e$	$\log_{10}k_e$
77	5.40	0.73	10	0.58	0.135	7.41	$\bar{1}$.13
77	5.89	0.77	15	0.87	0.134	7.46	$\bar{1}$.13
77	7.19	0.86	10	0.45	0.105	9.52	$\bar{1}$.02
77	9.23	0.97	10	0.35	0.081	12.35	$\bar{2}$.91
77	11.03	1.04	10	0.30	0.069	14.49	$\bar{2}$.84
135	5.46	0.74	10	0.66	0.151	6.62	$\bar{1}$.18
135	6.31	0.80	10	0.60	0.139	7.19	$\bar{1}$.14
135	8.63	0.94	10	0.44	0.102	9.80	$\bar{1}$.01
135	10.43	1.02	10	0.36	0.082	12.02	$\bar{2}$.92
178	5.40	0.73	8	0.60	0.172	5.81	$\bar{1}$.24
178	6.07	0.78	10	0.70	0.160	6.25	$\bar{1}$.20
178	8.04	0.91	10	0.56	0.130	7.69	$\bar{1}$.11
178	10.35	1.02	10	0.40	0.093	10.75	$\bar{2}$.97

Since both the Langmuir and Freundlich isotherms are obeyed over the pressure region investigated $n = (1 - \theta)$

TABLE 6.23 Variation of the Freundlich pressure exponent with temperature.

Temp °K	77	135	178
n	0	0	0
θ	1	1	1

Hydrogen-Deuterium equilibration reaction

Temp (°K)	t (min)	p (mm)	ratio HD/D_2
77	20	7.1	1:6.8
178	20	7.3	1:5.6
372	15	7.3	1:4.3
Blank			1:7.4

Cobaltous monoxide, CoO

The sample of CoO was pretreated by heating to 700°K in a dynamic vacuum of 10^{-6} mm Hg., until constant activity was obtained. Technical limitations prevented similar pretreatment of the surface area sample.

Determination of surface area

Determination	p_o (mm)	p (mm)	v_{ads} (cc)	v_{ads}/g (v')	$p/v'(p_o-p)$	p/p_o
A	749.8	74.66	10.03	3.09	0.035	0.10
	749.8	96.32	10.27	3.17	0.046	0.13
	749.8	118.44	10.56	3.26	0.058	0.16
B	752.6	85.65	10.24	3.16	0.041	0.11
	752.6	110.00	10.58	3.26	0.052	0.15
	752.6	134.81	10.96	3.38	0.066	0.18

$S.A_{B.E.T}(A) = 11.36\ m^2\ g^{-1}$ $S.A_{B.E.T}(B) = 10.60\ m^2\ g^{-1}$

Mean surface area = $10.98\ m^2\ g^{-1}$

TABLE 6.24 Kinetics of the conversion

Reaction volume 320cc Surface area 8.72 m^2

Temp (°K)	Av.press (mm)	$k_e \times 10^2$ (min^{-1})	$\log_{10} k_e$	k_m (molecules) ($cm^{-2}\ sec^{-1}$)	$\log k_m$	$10^2/T$
			increasing temperature			
77	5.5	7.83	$\bar{2}.89$	3.30×10^{12}	12.52	1.30
90	5.6	3.85	$\bar{2}.59$	1.41×10^{12}	12.15	1.11
112.5	5.5	1.13	$\bar{2}.05$	3.78×10^{11}	11.58	0.89
146	5.7	0.73	$\bar{3}.86$	1.68×10^{11}	11.23	0.69
178	5.6	0.71	$\bar{3}.85$	1.32×10^{11}	11.12	0.56
209.5	5.5	0.72	$\bar{3}.86$	1.11×10^{11}	11.05	0.48
292	5.8	0.44	3.64	5.15×10^{10}	10.71	0.34
			decreasing temperature			
209.5	5.5	0.48	$\bar{3}.69$	7.43×10^{10}	10.87	0.48
178	5.4	0.69	$\bar{3}.84$	1.23×10^{11}	11.09	0.56
146	5.4	0.75	$\bar{3}.87$	1.64×10^{11}	11.21	0.69
90	5.5	3.45	$\bar{2}.54$	1.24×10^{12}	12.09	1.11
77	5.4	7.83	$\bar{2}.89$	3.24×10^{12}	12.51	1.30

The Arrhenius plots of $\log_{10} k_e$ and $\log_{10} k_m$ against $1/T°K$ are shown in FIGS.6.26 and 6.27. From these plots the apparent activation energies (E_a) and frequency factors (B_m) can be determined.

For the temperature region 77°-300°K $\underline{E_a = -0.895\ k\ cal/mole}$,

$\log B_m = 9.92$, $\underline{B_m = 8.3 \times 10^9}$

FIGURE 6.26

Arrhenius plot of log k_e against $1/T^oK$

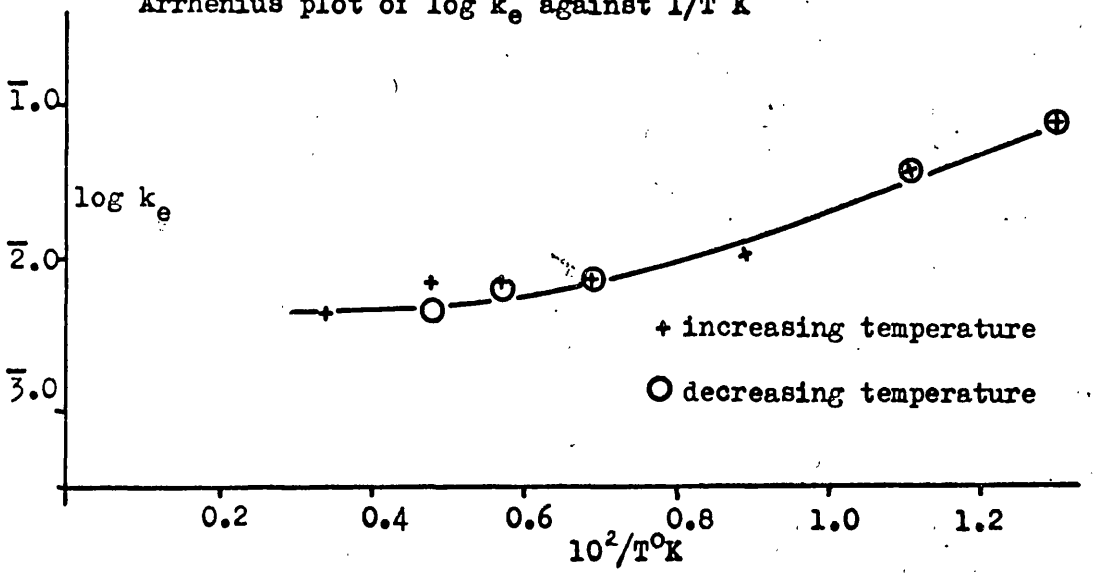

FIGURE 6.27

Arrhenius plot of log k_m against $1/T^oK$.

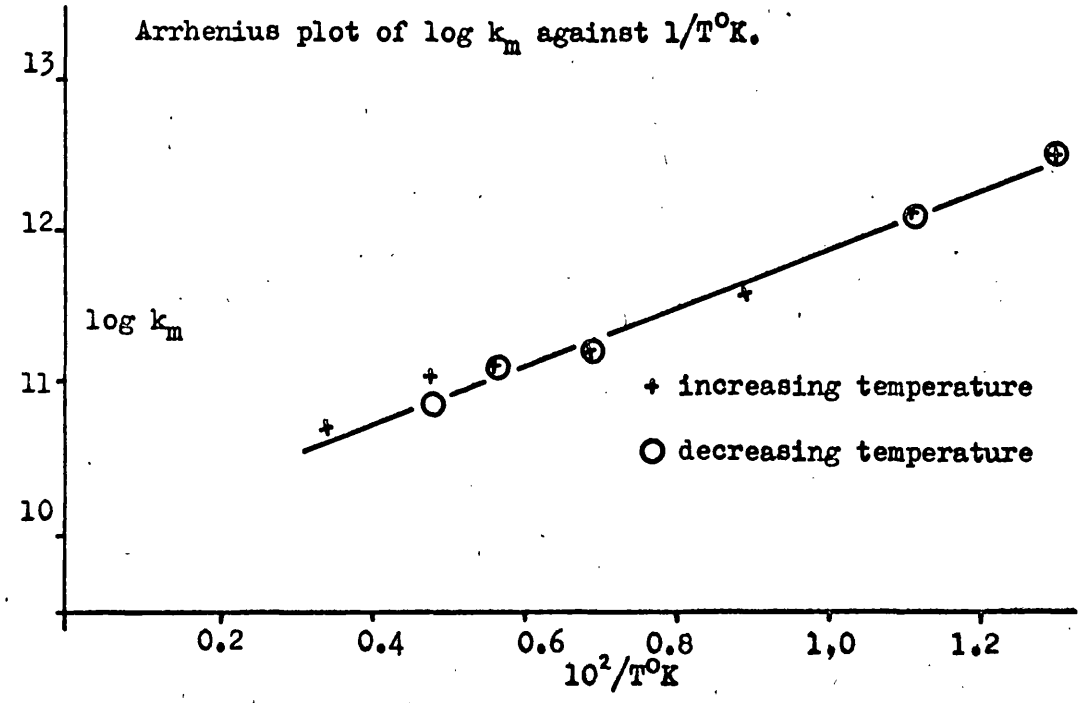

TABLE 6.25 Pressure dependence of the conversion.

Temp (°K)	Press (mm)	log p	time (min)	log Ω_o/Ω_t	k_e (min^{-1})	$1/k_e$	log k_e
77	5.52	0.74	10	0.34	0.078	12.82	$\bar{2}$.89
77	7.82	0.89	10	0.27	0.063	15.87	$\bar{2}$.80
77	9.06	0.96	10	0.25	0.056	17.86	$\bar{2}$.75
77	13.61	1.13	10	0.18	0.043	23.26	$\bar{2}$.63
90	5.52	0.74	17	0.28	0.038	26.32	$\bar{2}$.58
90	8.47	0.93	10	0.13	0.029	34.48	$\bar{2}$.46
90	12.51	1.10	12	0.13	0.024	41.67	$\bar{2}$.38
146	5.70	0.76	14	0.042	0.007	143.0	$\bar{3}$.84
146	7.19	0.86	15	0.043	0.007	151.0	$\bar{3}$.82
146	8.85	0.95	15	0.041	0.006	161.8	$\bar{3}$.79
146	10.93	1.04	15	0.039	0.006	167.0	3.78
209.5	5.52	0.74	18	0.057	0.007	139.1	$\bar{3}$.86
209.5	7.41	0.87	15	0.039	0.006	167.2	$\bar{3}$.78
209.5	9.52	0.98	15	0.036	0.006	181.4	$\bar{3}$.74
209.5	11.19	1.05	15	0.033	0.005	200.0	3.70

The Langmuir and Freundlich isotherms are shown in FIGS.6.29 and 6.28 respectively. Since both isotherms are obeyed over the pressure region investigated $n = (1 - \theta)$

TABLE 6.26 Variation of Freundlich pressure exponent with temperature.

Temp.(°K)	77	90	146	209.5
n	0.35	0.50	0.75	0.45
θ	0.65	0.50	0.25	0.55

Hydrogen-Deuterium equilibration reaction

Temp. (°K)	t (min)	p (mm)	ratio HD/D_2
77	15	7.2	1:6.9
146	20	7.3	1:5.4
292	18	7.1	1:4.7
Blank			1:7.4

FIGURE 6.28

Pressure dependencies of the conversion at different temperatures.

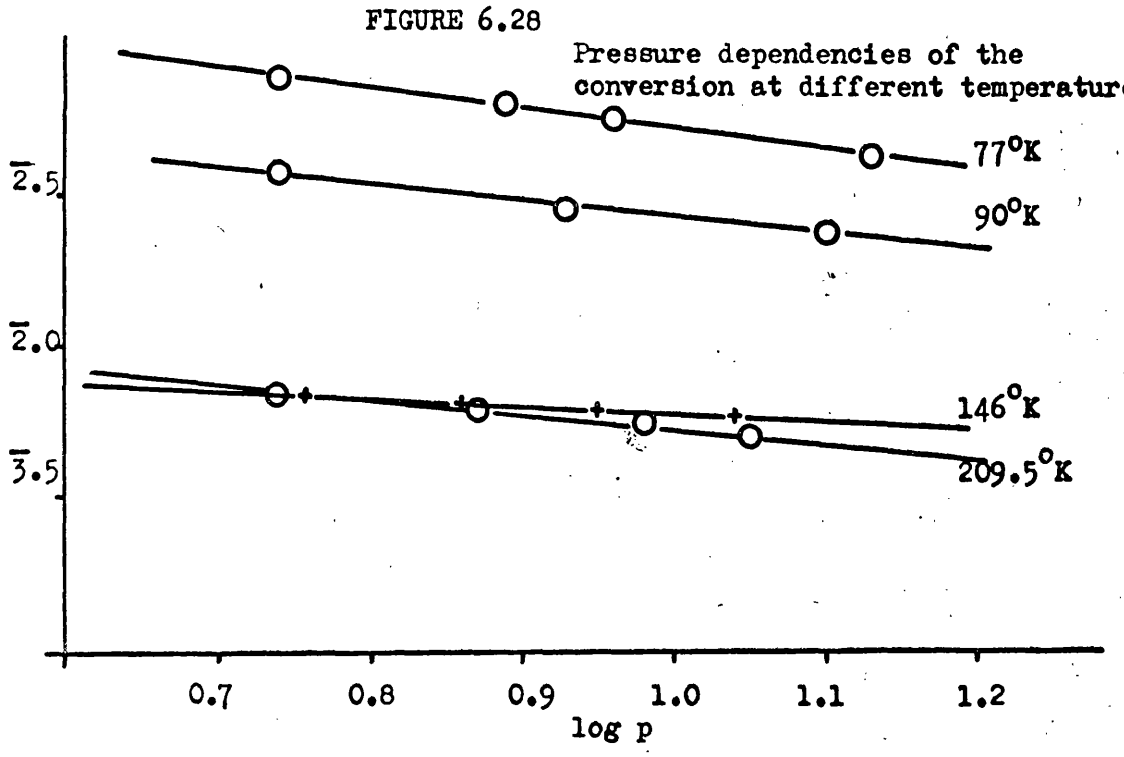

FIGURE 6.29

Pressure dependencies of the conversion at different temperatures, expressed as Langmuir plots.

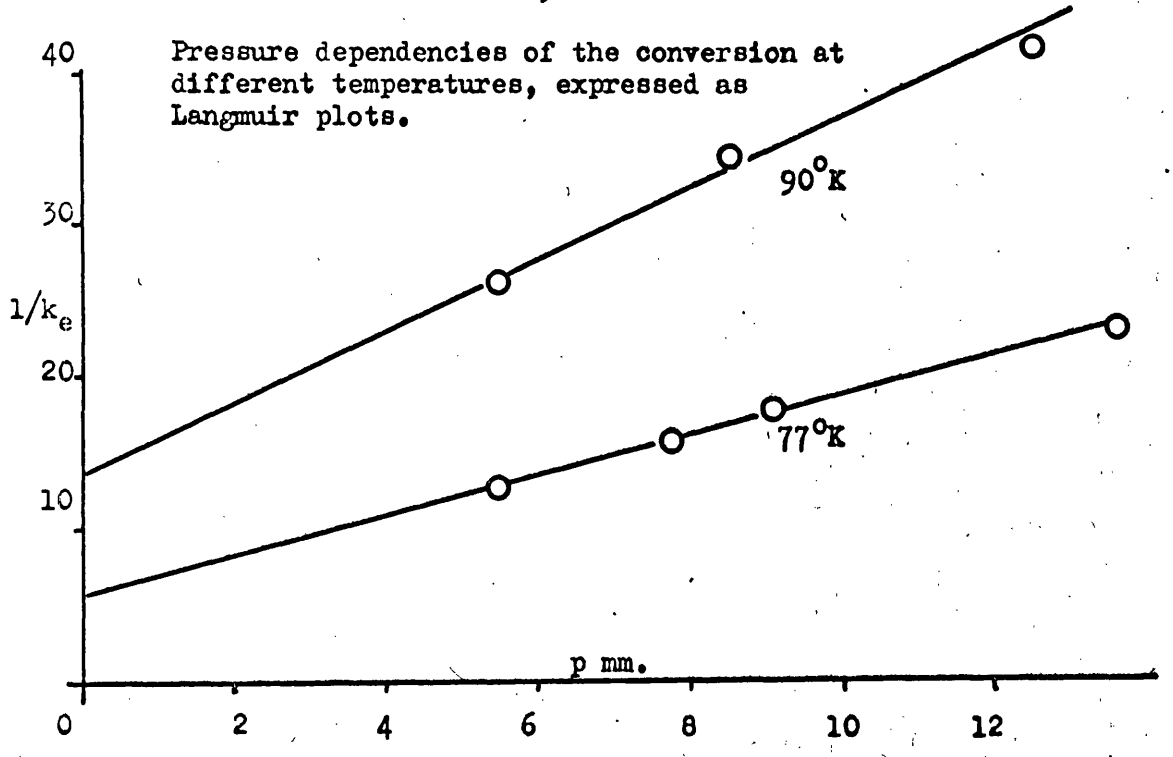

(iii) Kinetic data obtained from the divalent chlorides of the first row transition metal salts.

Cobaltous chloride, $CoCl_2$

The sample of $CoCl_2$ was pretreated by heating to 350°K in a dynamic vacuum of 10^{-6} mm. Hg., until constant activity was obtained. The sample used in the surface area determinations was pretreated in an identical manner.

Surface area determination

Determination	p_o (mm)	p (mm)	v_{ads} (cc)	v_{ads}/g (v')	$p/(p_o-p)v'$	p/p_o
A	754.4	132.0	3.53	1.12	0.189	0.18
	754.4	170.3	3.77	1.20	0.243	0.23
	754.4	209.0	4.03	1.28	0.299	0.28
B	755.1	114.5	3.39	1.08	0.162	0.15
	755.1	148.0	3.60	1.15	0.213	0.20
	755.1	181.5	4.04	1.28	0.251	0.24

$S.A._{B.E.T}$ (A) = 3.99 $m^2\ g^{-1}$ $S.A_{B.E.T}$ (B) = 4.085 $m^2\ g^{-1}$

Mean surface area = 4.04 $m^2\ g^{-1}$

TABLE 6.27 Kinetics of the conversion

Reaction volume 302cc. Surface area 1.6 m^2

Temp °K	Av.Press (mm)	k_e X 10^2 (min^{-1})	$\log_{10} k_e$	k_m (molecules / $cm^{-2} sec^{-1}$)	$\log_{10} k_m$	$10^2/T$
			increasing temperature			
77	5.6	5.30	$\bar{2}.72$	1.16×10^{13}	13.06	1.30
90	5.5	2.30	$\bar{2}.36$	4.26×10^{12}	12.63	1.11
146	5.5	0.11	$\bar{3}.04$	1.26×10^{11}	11.10	0.69
178	5.6	0.08	$\bar{4}.89$	7.44×10^{10}	10.87	0.56
209.5	5.5	0.02	$\bar{4}.38$	1.91×10^{10}	10.28	0.48
291	5.7	0.03	$\bar{4}.50$	1.90×10^{10}	10.28	0.34
411	5.7	0.02	$\bar{4}.40$	1.05×10^{10}	10.02	0.24
			decreasing temperature			
209.5	5.6	0.03	$\bar{4}.41$	2.10×10^{10}	10.32	0.48
90	5.6	2.26	$\bar{2}.35$	4.26×10^{12}	12.63	1.11
77	5.8	4.09	$\bar{2}.61$	9.34×10^{12}	12.97	1.30

The Arrhenius plots of log k_e and log k_m against $1/T^{\circ}K$ are shown in FIGS. 6.30 and 6.31 respectively.

The apparent activation energy and frequency factor were determined for the temperature range 90°-400°K

$E_a = -1.31$ k cal/mole log $B_m = 9.30$ $B_m = 2.0 \times 10^9$

FIGURE 6.30

Arrhenius plot of log k_e against $1/T^oK$

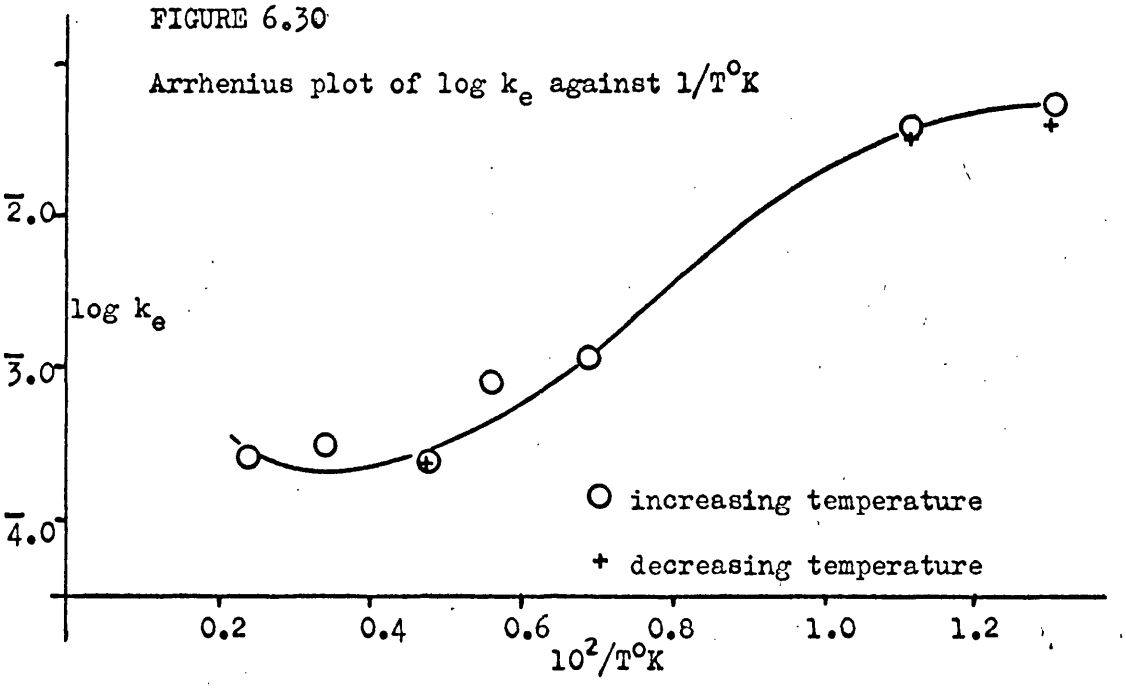

FIGURE 6.31

Arrhenius plot of log k_m against $1/T^oK$

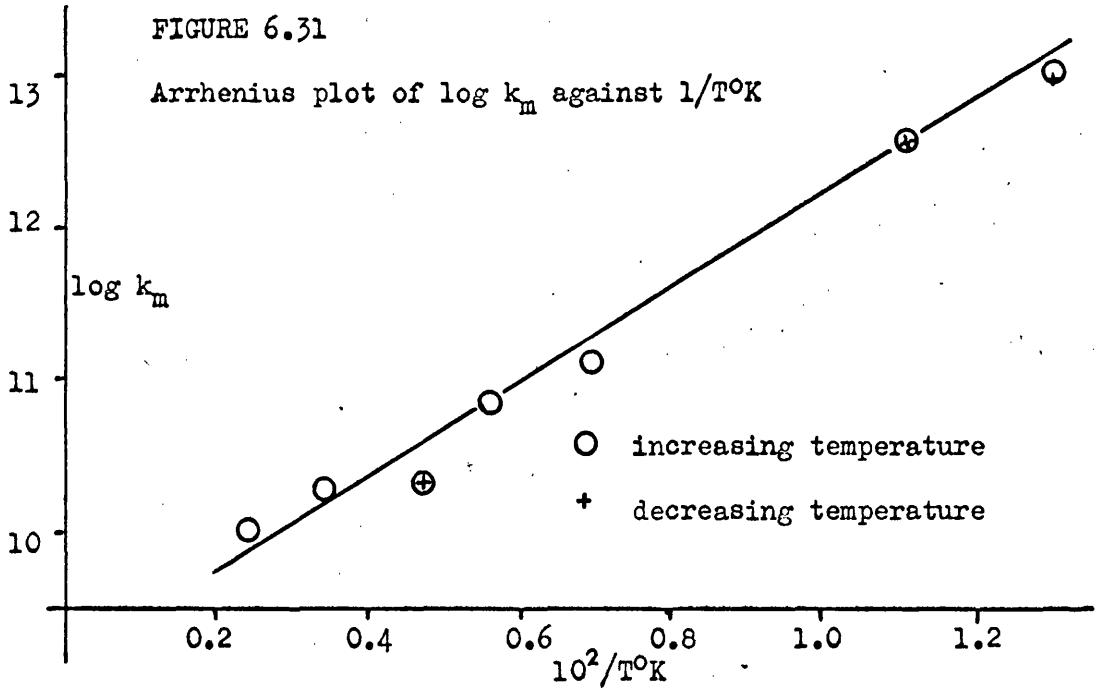

TABLE 6.28 Pressure dependence of the conversion.

Temp. (°K)	press. (mm)	$\log_{10}p$	time (min)	$\log \Omega_o/\Omega_t$	k_e (min^{-1})	$1/k_e$	$\log_{10}k_e$
77	5.58	0.75	15	0.34	0.054	18.52	$\bar{2}.73$
77	6.46	0.81	11	0.25	0.053	18.87	$\bar{2}.72$
77	8.47	0.93	10	0.18	0.041	24.39	$\bar{2}.61$
77	10.76	1.03	17	0.29	0.040	25.00	$\bar{2}.59$
90	5.64	0.75	12	0.13	0.025	40.00	$\bar{2}.39$
90	7.75	0.89	26	0.26	0.023	43.48	$\bar{2}.36$
90	8.47	0.93	25	0.20	0.022	45.45	$\bar{2}.35$
90	10.19	1.01	23	0.18	0.018	55.56	$\bar{2}.26$

The pressure dependency of the conversion is expressed as a Freundlich plot in FIG. 6.32. It was also found that the pressure dependency obeyed the Langmuir isotherm, thus $n = (1 - \theta)$

TABLE 6.29 Variation of Freundlich pressure exponent with temperature.

Temp °K	77	90
n	0.3	0.6
θ	0.7	0.4

FIGURE 6.32

Pressure dependencies of the conversion at different temperatures expressed as Freundlich plots.

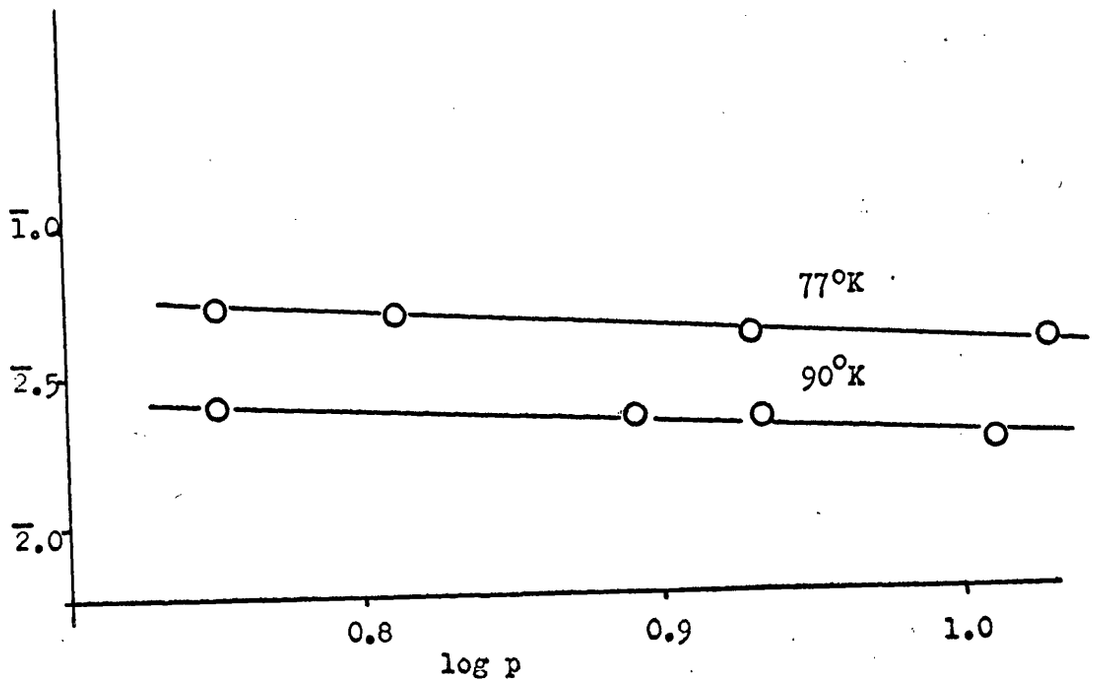

Manganous chloride, $MnCl_2$

The sample used was pretreated by heating to 450°K in a dynamic vacuum of 10^{-6} mm. Hg., until constant activity was obtained. The sample used in the surface area determination was pretreated in an identical manner.

Determination of surface area

Determination	p_o (mm)	p (mm)	v_{ads} (cc)	v_{ads}/g v'	$p/(p_o-p)v'$	p/p_o
A	762.7	109.31	6.99	1.24	0.14	0.14
	762.7	141.82	7.47	1.32	0.17	0.19
	762.7	175.75	7.80	1.38	0.22	0.23
B	760.2	113.29	6.94	1.23	0.14	0.15
	760.2	147.90	7.21	1.28	0.19	0.20
	760.2	182.80	7.68	1.36	0.23	0.24

$S.A._{B.E.T}$ (A) = 4.55 $m^2 g^{-1}$ $S.A_{B.E.T.}$ (B) = 4.39 $m^2 g^{-1}$

Mean surface area = 4.47 $m^2 g^{-1}$

TABLE 6.30 Kinetics of the conversion

Reaction volume 306 cc Surface area 5.28 m

Temp (^{o}K)	Av.press (mm)	$k_e \times 10^2$ (min^{-1})	$\log_{10} k_e$	k_m (molecules) ($cm^{-2}sec^{-1}$)	$\log_{10} k_m$	$10^2/T$
increasing temperature						
77	5.6	13.71	$\bar{1}.14$	9.28×10^{12}	12.97	1.30
90	5.7	11.47	$\bar{1}.06$	6.76×10^{12}	12.83	1.11
112.5	5.6	3.80	$\bar{2}.58$	1.76×10^{12}	12.25	0.89
146	5.5	1.13	$\bar{2}.05$	3.96×10^{11}	11.60	0.69
178	5.6	0.38	$\bar{3}.58$	1.11×10^{11}	11.04	0.56
209.5	5.5	0.23	$\bar{3}.36$	5.62×10^{10}	10.75	0.48
291	5.5	0.14	$\bar{3}.15$	2.46×10^{10}	10.39	0.34
412	5.7	0.08	$\bar{4}.92$	1.03×10^{10}	10.01	0.24

The Arrhenius plots of $\log_{10} k_e$ and $\log_{10} k_m$ against $1/T^{o}K$ are shown in FIG. 6.33 and 6.34 respectively. The apparent activation energy and freqency factor were determined for the temperature range 90^{o}-$400^{o}K$

$E_a = -1.57$ k cal/mole $\log B_m = 9.16$ $B_m = 1.45 \times 10^9$

FIGURE 6.33

Arrhenius plot of log k_e against $1/T^{o}K$.

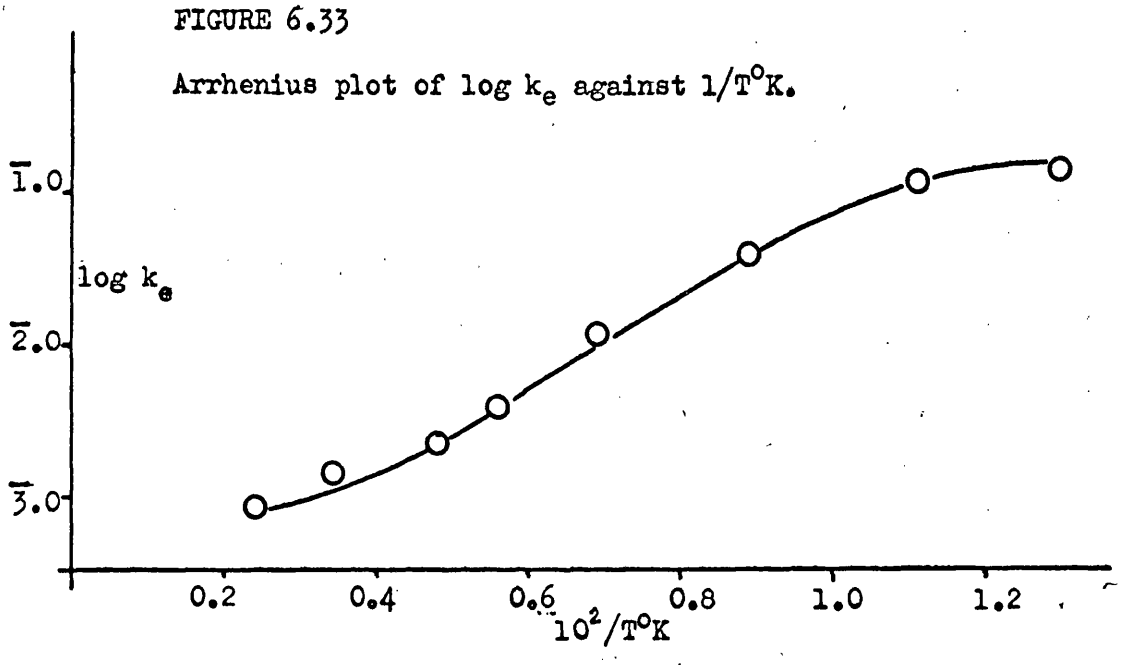

FIGURE 6.34

Arrhenius plot of log k_m against $1/T^{o}K$.

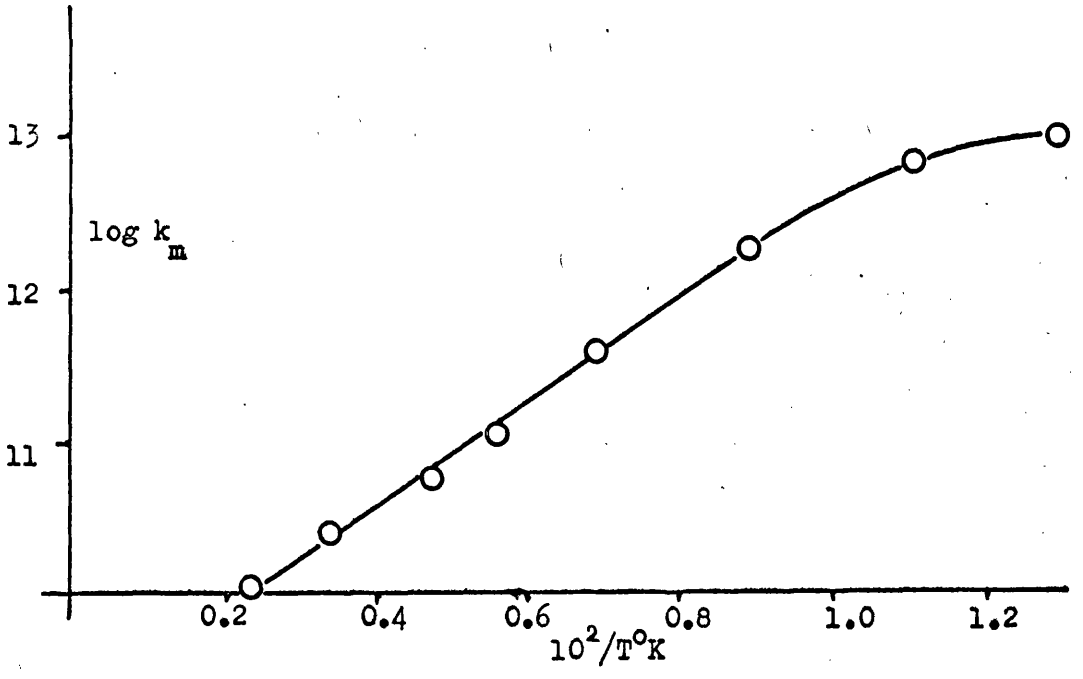

TABLE 6.31 Pressure dependence of the conversion

Temp (°K)	press (mm)	log p	time (min)	log Ω_o/Ω_t	k_e (min^{-1})	$1/k_e$	log k_e
77	5.40	0.73	10	0.63	0.149	6.71	$\bar{1}.17$
77	5.72	0.76	15	0.81	0.127	7.87	$\bar{1}.10$
77	9.23	0.96	10	0.34	0.078	12.82	$\bar{2}.89$
77	11.03	1.04	10	0.28	0.065	15.38	$\bar{2}.81$
90	5.58	0.75	10	0.50	0.116	8.62	$\bar{1}.06$
90	7.61	0.88	10	0.36	0.084	11.90	$\bar{2}.94$
90	9.87	0.99	10	0.27	0.061	15.39	$\bar{2}.79$
90	11.53	1.06	10	0.25	0.059	16.95	$\bar{2}.77$
146	5.40	0.73	11	0.05	0.011	90.9	$\bar{2}.03$
146	7.96	0.90	15	0.06	0.009	111.1	$\bar{3}.96$
146	9.63	0.98	15	0.06	0.009	114.2	$\bar{3}.94$
146	11.20	1.05	36	0.15	0.008	125.0	$\bar{3}.92$

The pressure dependencies are expressed as Freundlich and Langmuir plots in FIG. 6.35 and 6.36 respectively. Since both isotherms are obeyed over the pressure region investigated then $n = (1 - \theta)$

TABLE 6.32 Variation of Freundlich pressure exponent with temperature

T (°K)	77	90	146
n	0	0.05	0.65
θ	1	0.95	0.35

Hydrogen - Deuterium equilibration

Temp (°K)	t (min)	p (mm)	ratio HD/D_2
77	20	7.2	1:7.3
178	20	7.4	1:7.4
291	18	7.1	1:7.4
Blank			

FIGURE 6.35

Pressure dependencies of the conversion at different temperatures expressed as Freundlich plots.

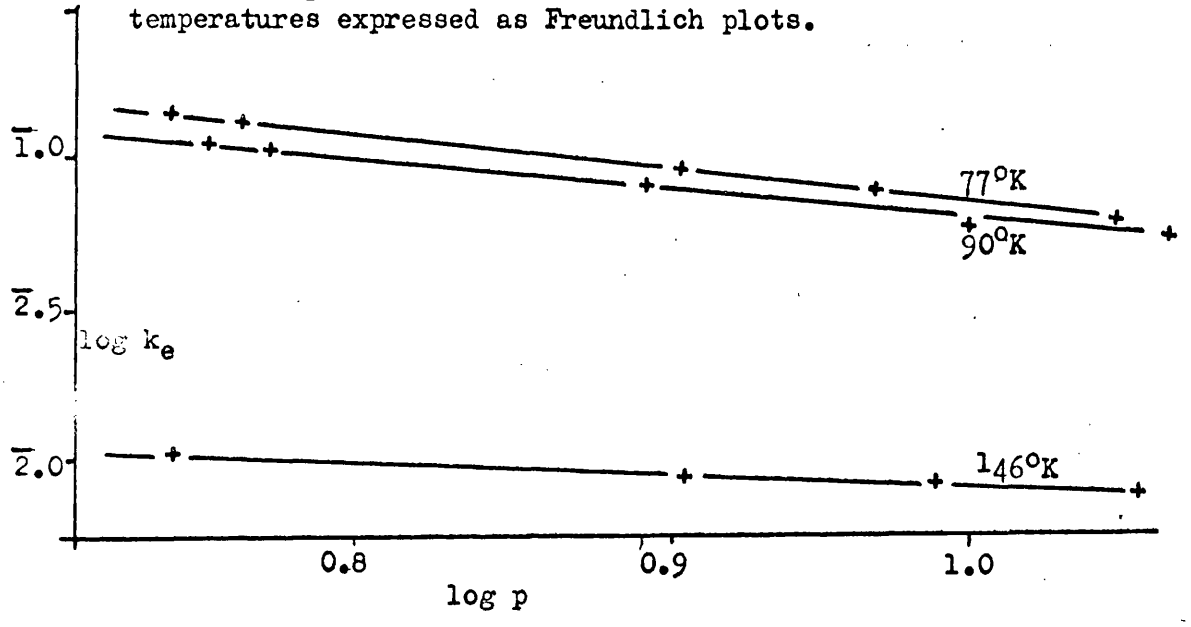

FIGURE 6.36

Pressure dependencies of the conversion at different temperatures expressed as Langmuir plots.

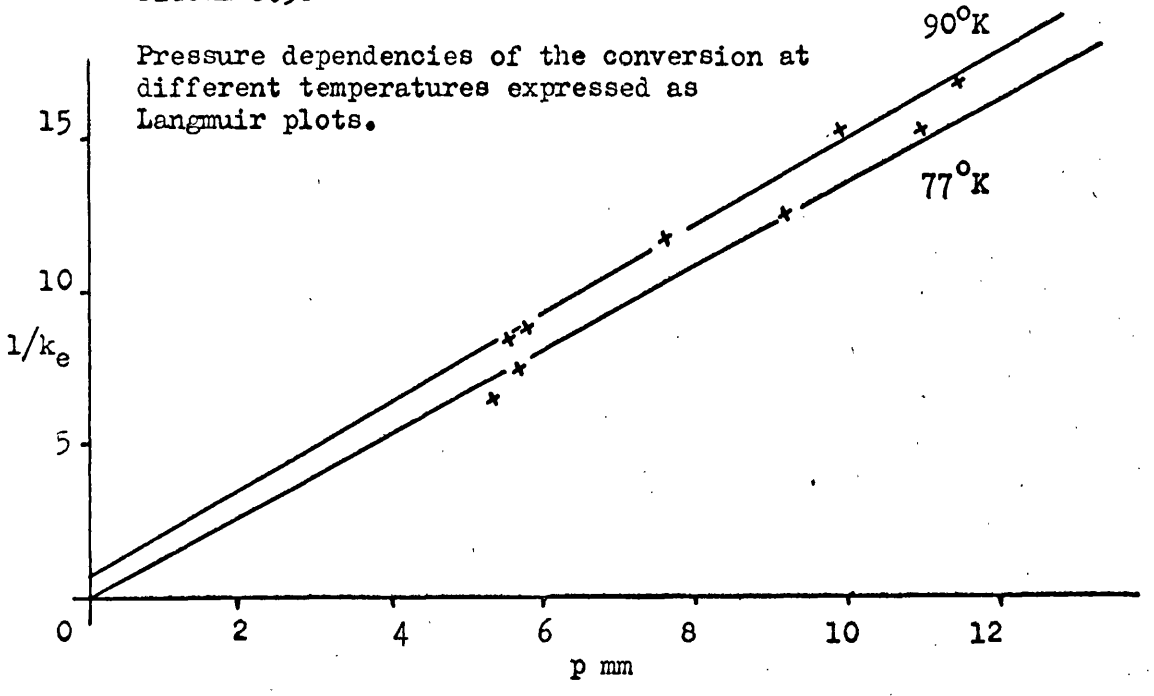

6·3 Discussion

(i) The effect of temperature

Sulphates

With most of the sulphates examined two series of kinetic studies were carried out, one with increasing temperature and one with decreasing temperature. It was found that the Arrhenius plots obtained from the two investigations were identical, which suggests that there is no irreversible adsorption of hydrogen or change in catalytic properties within the temperature range of the investigation. The collected plots of $\log_{10}k_e$ and $\log_{10}k_m$ against $1/T°K$, for increasing temperature only, are given in FIG. 6·37 and 6·38 respectively. As can be seen from the Arrhenius plots in FIG. 6·38 the conversion can best be considered in terms of two temperature ranges, a low temperature range where the apparent activation energy is ∿0 and a high temperature range where the activation energy is in the region of 2-3 k.cal/mole. The absence of any hydrogen-deuterium equilibration on $NiSO_4$ and $MnSO_4$ can be considered as evidence that the conversion goes via a physical mechanism over the whole temperature range of the kinetic investigation. The negative activation energies are also indicative of a physical mechanism where the reaction proceeds via surface paramagnetism. TABLE 6·33 gives the rates of conversion observed at 77°, 90° and 273°K on all the compounds examined in this work and also the apparent activation energies and

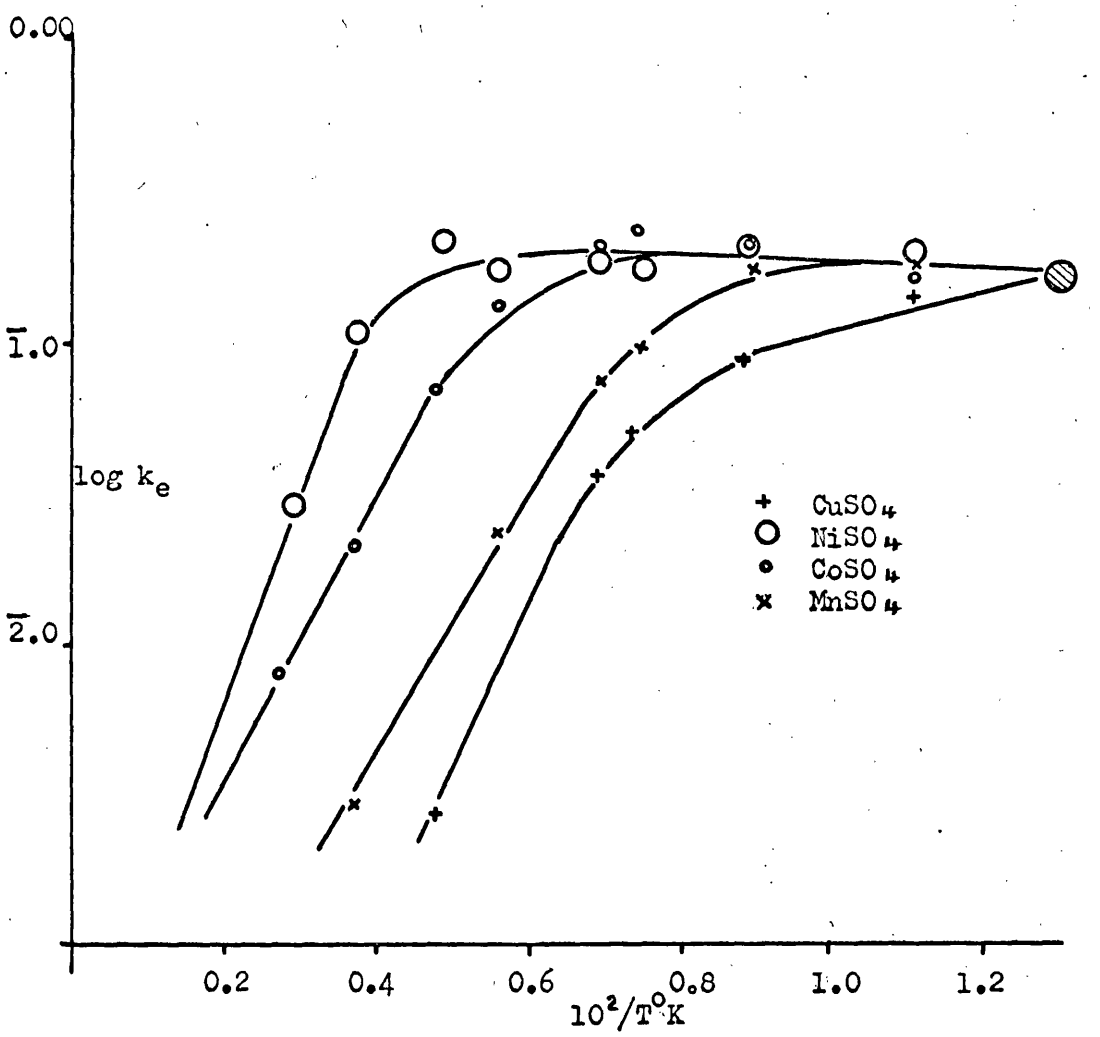

FIGURE 6.37

Collected plots of log k_e against $1/T^oK$ for the conversion with increasing temperature.

FIGURE 6.38.

Collected plots of log k_m against $1/T^oK$ for the conversion at increasing temperature.

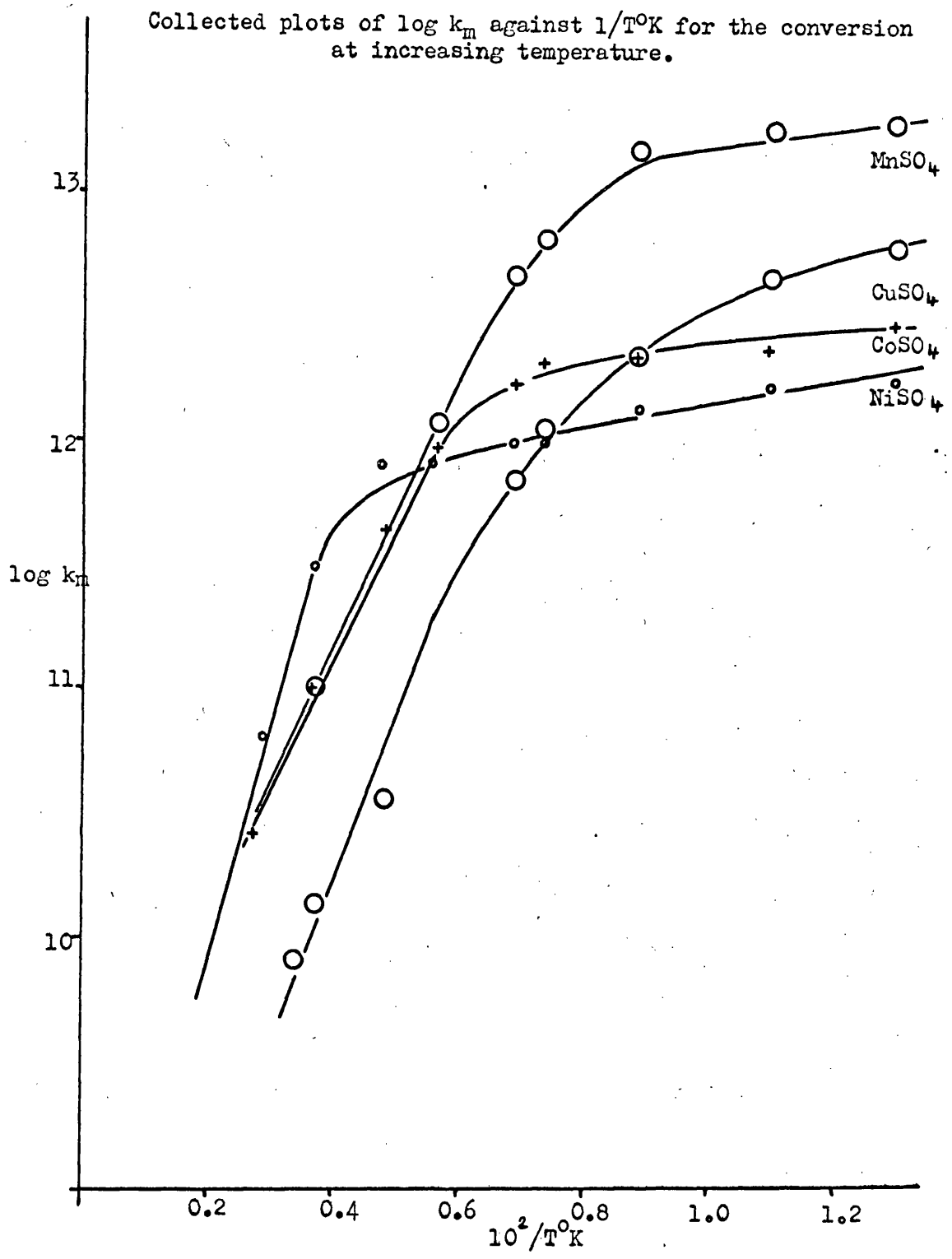

frequency factors in the two temperature regions.

TABLE 6·33 Kinetic data at p = 5–6 mm.

Parameter	$CuSO_4$	$NiSO_4$	$CoSO_4$	$MnSO_4$	CuO	NiO	CoO	$CoCl_2$	$MnCl_2$
E_a(low temp)	0·47	0·18	0·08	0·09	0·09	0	0·9	1·31	1·57
E_a(high temp)	2·56	3·21	2·50	2·64	1·57	0·22			
$\log_{10}B_m$(low temp)	11·42	11·73	12·14	12·98	12·21	13·75	9·92	9·30	9·16
$\log_{10}B_m$(high temp)	8·00	8·85	8·92	7·78	9·96	13·20			
$\log_{10}k_m$(77°K)	12·76	12·23	12·44	13·25	12·45	13·74	12·52	13·06	12·97
$\log_{10}k_m$(90°K)	12·64	12·21	12·34	13·23	12·43	13·75	12·15	12·63	12·83
$\log_{10}k_m$(273°K)	10·12	11·49	10·99	10·95	11·24	13·39	-	-	-

Oxides

A kinetic investigation similar to that done on the sulphates was carried out on the oxides and the collected plots of $\log_{10}k_m$ against $1/T°K$, for increasing temperature only are shown in FIG. 6·39. For both CuO and NiO there are numerical differences between the Arrhenius plot with increasing temperature and the same plot with decreasing temperatures (FIG. 6·21 and 6·25). The possible explanation of this difference is that the surface is free from chemisorbed hydrogen atoms when the temperature is increased, this not being the case when the temperature is decreased.[21] The data obtained for CuO

FIGURE 6.39

Collected plots of log k_m against $1/T^{o}K$ for the conversion with increasing temperature.

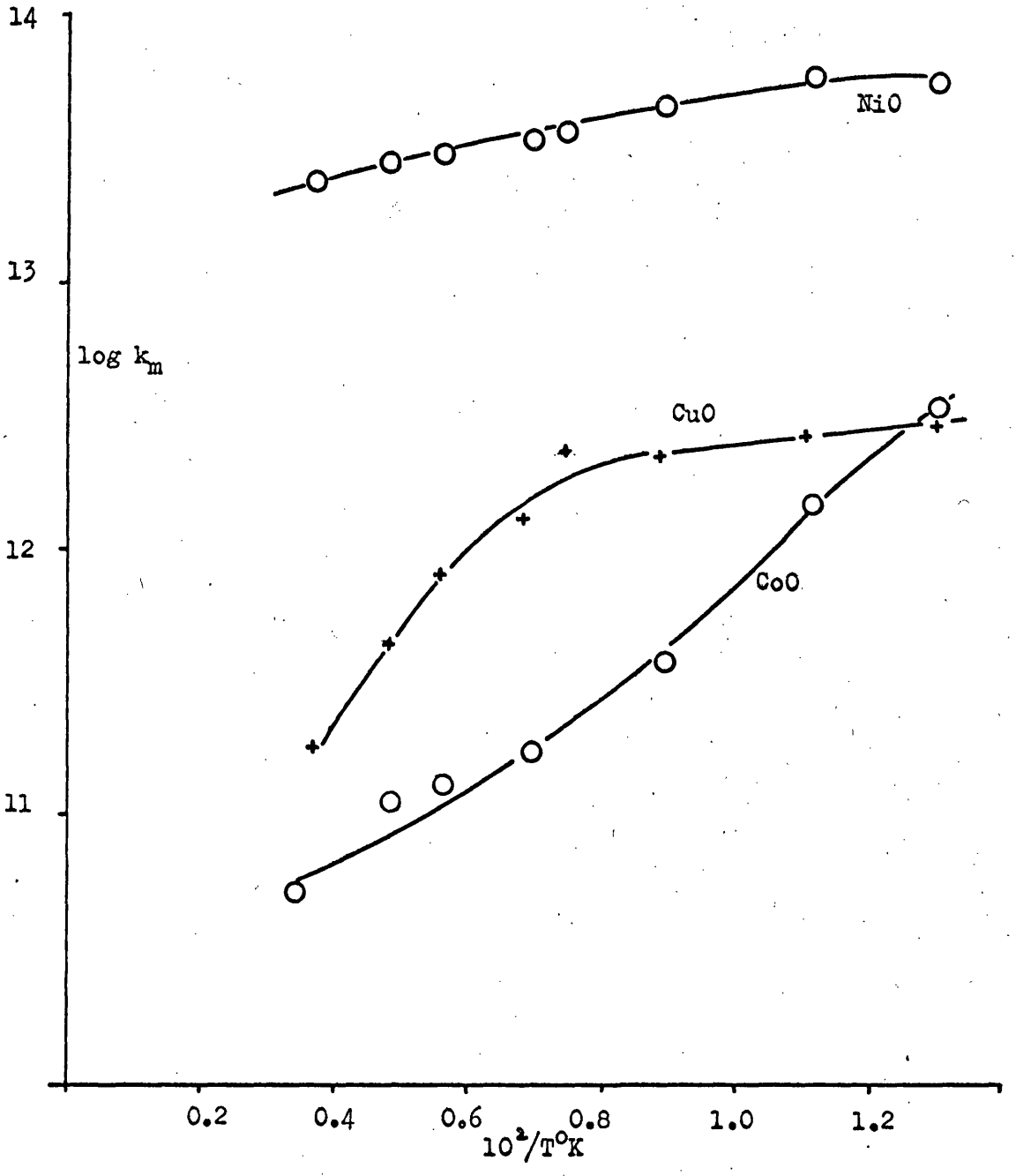

at 273°K tends to confirm this viewpoint. Experiments at this temperature established that if hydrogen was admitted to the catalyst at 273°K and then pumped out to 10^{-6} mm. Hg. for 15 minutes at the same temperature, the conversion rate on admitting further hydrogen was reduced by ~40%. Pumping for 6 hrs. at 500°K completely restored the original conversion rate. For temperatures below 273°K no poisoning effect was observable.

The results obtained for the hydrogen-deuterium equilibration reaction on NiO and CoO suggest that there is an exchange reaction occurring at 77°K as well as at higher temperatures, this agrees with earlier observations. Dowden et al.[34,35] suggest that the condition for high activity is that the oxide should possess some but not too many unpaired d-orbital electrons, thus high activity to the exchange reaction occurs, just after the beginning of the transition metal period and towards the end. Thus CuO should not show any appreciable activity towards the reaction, which is found to be the case.[34] This may be the reason for the close similarity of its Arrhenius plot to those of the sulphates, while the plots of NiO and CoO show only a small resemblance.

The difficulty of obtaining reproducible surfaces is more marked with the oxides than it is with the sulphates. This fact is illustrated by comparing the results obtained with NiO(I) and (II) and $MnSO_4$(I) and (II). It was originally considered[36] that outgassing

NiO at 650°K in vacuo was sufficient to free the surface of initially adsorbed oxygen, since it has been shown that the oxygen exchange reaction,

$$^{16}O_2 + {}^{18}O_2 \rightleftharpoons 2\,{}^{16}O\,{}^{18}O$$

takes place readily at that temperature. Other workers,[37] however, consider that a higher temperature of 800°K is necessary to remove oxygen from the surface. In this work an outgassing temperature of greater than 650°K was not possible due to technical limitations, therefore the surface of the NiO catalyst must be considered to be fractionally covered with adsorbed oxygen which will subsequently effect the kinetics of the ortho-parahydrogen conversion.

The presence of a significant exchange reaction on NiO at ∿300°K while it is absent on the corresponding sulphate, eliminates any possibility that oxide impurities are playing anything but a minor role in the conversion observed on the sulphates.

Chlorides

The main features of the Arrhenius plots given in FIG. 6·31 and 6·34 for $CoCl_2$ and $MnCl_2$ are the same. For $CoCl_2$ a kinetic investigation with decreasing temperature gives, within the limits of experimental error, a plot identical to that obtained with increasing temperature. It is therefore, reasonable to assume that

there is no catalyst poisoning within the temperature range of the investigation. The negative activation energy obtained for both the salts suggest that the conversion is via a physical mechanism. The absence of any hydrogen-deuterium exchange on $MnCl_2$, throughout the temperature range of the investigation, confirms that the conversion is proceeding via a physical and not a chemical mechanism.

(ii) The effect of pressure

The effect of pressure on the rate of conversion has been studied over the range 5-10 mm. It was not possible to obtain pressures of less than 5 mm due to technical limitations. In all cases it was found that both the Langmuir and Freundlich isotherms are obeyed over the pressure range investigated, thus $d\ln\theta/dp$ from both isotherms have the same value[23] and

$$n = (1-\theta)$$

The variation in reaction order, n, with change in temperature for all the compounds investigated are collected in TABLE 6·34.

TABLE 6·34 Variation of reaction order.

Reaction order for	Temp °K 77	90	112·5	135	146	178	209·5	273	350
$CuSO_4$	0·00	0·08	0·10	0·17	0·24	-	1·00	1·00	-
$NiSO_4$	0·00	-	-	-	-	0·00	-	-	0·77
$CoSO_4$	0·00	-	-	-	0·00	-	-	0·83	1·00
$MnSO_4$	0·00	-	0·00	-	0·79	-	1·00	-	-
CuO	0·00	-	-	-	0·00	-	0·03	-	-
NiO	0·00	-	-	0·00	-	0·00	-	-	-
CoO	0·35	0·50	-	-	0·75	-	0·45	-	-
$CoCl_2$	0·30	0·60	-	-	-	-	-	-	-
$MnCl_2$	0·00	0·05	-	-	0·65	-	-	-	-

When comparing the variation of n and the absolute rate as expressed by an Arrhenius plot for a particular compound a striking feature arises. When n = 0·00 (θ = 1) the rate remains approximately constant with change in temperature giving an apparent activation energy of $\sim$0. When n begins to approach unity ($\theta \rightarrow 0$) the rate begins to drop rapidly with increase in temperature and the apparent activation energy is in the region of 2 kcal/mole. Only with the oxides NiO and CoO do discrepancies arise, this being no doubt due to a chemical mechanism contributing to the conversion in addition to a physical mechanism.

Hydrogen adsorption isotherms have been measured on $MnSO_4$ at 77° and 90°K, this being shown in FIG. 6·19. The results show that at a pressure of 5 mm of hydrogen, saturation has been reached which is in keeping with the observed kinetics of the conversion which indicate that at these temperatures the fractional coverage of hydrogen, θ, is unity. Conversion, therefore, appears to take place on the whole surface. The isotherms yield a value of 2·3 k cal/mole for the isosteric heat of adsorption for coverage up to 10^{14} molecules cm^{-2}. These results however must be treated with a certain degree of scepticism as the hydrogen uptake measurements were obtained using an instrument not constructed for working at pressures of less than 10 mm and errors are, therefore, in the region of ±50%.

(iii) The mechanism of the conversion.

The investigation of the spin isomerisation on the transition metal sulphates suggest that the isomerisation takes place via a physical mechanism over the whole temperature range. This type of conversion arises from the interaction of the nuclear spins of the hydrogen molecule with the inhomogenous magnetic field at the surface of the catalyst. The possible mechanisms for this type of conversion have already been discussed in Chapter 4, and it is of interest to see how the experimental absolute rates compare to the theoretical absolute rates determined by the Wigner theory and

modifications thereof. For convenience the mechanisms discussed in 4·3 will be classified (a), (b) and (c).

(a) The Wigner[18] treatment which considers conversion to occur during simple collisions with the surface, a fraction F_a of which is paramagnetic. The equation for the absolute rate constant is given as :-

$$k_m = \frac{8\mu_a{}^2\mu_p{}^2 I\pi^2}{9r_s{}^6h^2kT} \quad G(T).Z.F_a \qquad \text{from (4·4)}$$

where $Z = P/(2\pi mkT)^{1/2}$

(b) The Eley[21] treatment, where an adsorbed hydrogen molecule is vibrating with frequency[42] $\nu = 4{\cdot}5 \times 10^{11}$ sec^{-1} over a sunken site. Each vibration is considered a collision and the absolute rate constant is given as:-

$$k_m = \frac{24\mu_a{}^2\mu_p{}^2 I\pi^2 t_s{}^2}{h^2m\, r_s{}^8} \quad n_o\, \theta\nu \qquad \text{from (4·15)}$$

(c) The Harrison and McDowell[20] treatment, where molecular hydrogen is mobile in a 2-dimensional film over the whole surface. At high surface coverages the absolute rate constant is given as:-

$$k_m = \frac{KG(T)l^2F_a\, n_o\, m^{1/2}}{r_s{}^8(2kT)^{1/2}l_m} \qquad \text{from (4·14)}$$

where $t_s{}^2 = \bar{l}^{\,2}/c^2 = 2r^2/c^2$ and $l_m = 4r/\pi$.

In the low temperature region (a) is eliminated immediately since it predicts that k_m should depend directly upon pressure, which is not the case with the sulphates. Both (b) and (c) predict that when the surface coverage is high the rate constant should be independent of pressure; this prediction fits the observed kinetics. Calculation of absolute rates using (a), (b) and (c) was done for $MnSO_4$ at 77°K. This salt was used because it was the only one for which gas adsorption data was available, this data suggests that the number of sites n_o cm^{-2} can be approximated to 10^{13}. If the whole surface is regarded as catalytically active, $F_a = 1$, and the surface coverage, θ, is assumed to be unity, then any value of k_m calculated from (a), (b) or (c) would be expected to give an upper value of k_m with respect to θ and F_a. Using (a), (b) and (c) values of k_m were calculated for $F_a = 1$, $\theta = 1$, $n_o = 10^{13}$, $\mu p = 2{\cdot}79/1840$ Bohr magneton, $\mu_a = 5{\cdot}7$ Bohr magneton, $r = 1\text{Å}$, $r_s = 2\text{Å}$, $T = 77°K$, $G(T) = 0{\cdot}218$ at 77°K and $I = 0{\cdot}467 \times 10^{-40}$. Observed and calculated values for k_m assuming that r_s does not alter with temperature are given below.

pH2, 77°K, 5 mm.

k_m (obs)	$1{\cdot}94 \times 10^{13}$	molecules	cm^{-2}	sec^{-1}
k_m (calc.a)	$2{\cdot}26 \times 10^{10}$	"	"	"
k_m (calc.b)	$7{\cdot}23 \times 10^{12}$	"	"	"
k_m (calc.c)	$4{\cdot}89 \times 10^{14}$	"	"	"

Although (b) gives a value of k_m close to that of the observed value, this is the maximum possible rate with respect to θ and F_a, therefore using (c) to describe the conversion would probably be more realistic since it is unlikely that the whole of the surface is catalytically active. Eley et al.[21] have shown that for Nd_2O_3 the conversion is confined to a relatively small fraction of the surface. The above calculations as a whole must not be regarded as exact owing to the uncertainty in the values of r, r_s, n_o and ν. The value of r_s, the distance of closest approach, occurs to the sixth and eighth power in (a), (b) and (c), and since its value is unknown for any particular case errors in k_m are easily introduced. Increasing the value of r_s to 3Å, which can still be considered to be a reasonable value for the distance of closest approach, decreases the k_m value determined for r_s = 2Å using (a) and (b) by a factor of 10 and (c) by a factor of 20. The value of (c) using r_s = 3Å is $2{\cdot}4 \times 10^{13}$ molecules cm^{-2} sec^{-2} which is very close to the observed value. Although the uncertainty in the calculated values of k_m is quite considerable they do show that the rate of conversion is considerably increased when adsorption occurs on the surface of the catalyst, compared to the Wigner approach where there is no gas adsorption.

It is of interest to see how the observed kinetics over the whole temperature range fit the postulated mechanisms of the conversion.

For the Wigner mechanism the rate should depend on the manner in which $G(T)/T^{3/2}$ varies with temperature, for the Eley mechanism the rate should depend on the manner $G(T)/T$ varies with temperature and for the Harrison and McDowell mechanism the rate should depend on the way $G(T)/T^{1/2}$ varies with temperature. The variation of these temperature dependent factors with temperature is given in TABLE 6·35.

TABLE 6·35

Variation of temperature dependent factors in mechanisms (a), (b) and (c).

Temp.(°K)	G(T)	$10^2 \times G(T)/T^{1/2}$	$10^4 \times G(T)/T^{3/2}$	$10^3 \times G(T)/T$
77	0·218	2·48	3·22	2·83
90	0·265	2·79	3·10	2·94
112·5	0·358	3·38	3·00	3·18
135	0·419	3·61	2·67	3·10
146	0·451	3·73	2·55	3·09
160·5	0·491	3·87	2·41	3·06
209·5	0·596	4·12	1·97	2·84
273	0·690	4·18	1·53	2·53

Calculations show that the apparent activation energy predicted for the conversion over the temperature range of the investigation are of the order

Wigner	-40 to -100 cal $mole^{-1}$
Eley	+50 to -150 cal $mole^{-1}$
Harrison and McDowell	+100 cal $mole^{-1}$

On the basis of activation energies none of these mechanisms appear to fit the observed kinetics which give apparent activation energies of -100 to -2000 cal $mole^{-1}$ over the same temperature range. The Harrison and McDowell treatment, however, considers two cases

(i) Where the fractional coverage of sites, θ, is unity;

(ii) where the fractional coverage of sites, θ, approaches zero.

For the condition $\theta=1$ it predicts that the rate should increase slowly and be independent of pressure with increasing temperature. For the condition $\theta \to 0$ it predicts that the rate should be dependent upon pressure and exhibit a "negative activation energy" equal to the heat of adsorption. Although this treatment does not agree with the observed kinetics at high surface coverages it appears to provide an explanation for the kinetics of the conversion at low surface coverages on the sulphates and chlorides of the

first row transition metals, where the activation energy is in the region of 2-3 k.cal/mole. An apparent activation energy of 2-3 k.cal/mole is reasonable in magnitude for physical adsorption (2 k.cal/mole is the maximum value permitted for the heat of physical adsorption of hydrogen by using the B.E.T equation). The adsorption data from $MnSO_4$ gives a value for the isosteric heat of adsorption of 2·3 k.cal/mole compared with 2·64 k.cal/mole for the apparent activation energy derived from kinetic data. The discrepancy at high surface coverages could possible be due to the fact that the values obtained for θ are only approximately equal to unity. If this is the case and the Harrison and McDowell treatment also applied to this region, then a negative contribution would be made to the total apparent activation energy, which could explain the results obtained at high surface coverage.

It might be expected that as the temperature increased then the adsorption layer should decrease and the absolute rate constant should approach that predicted by the Wigner theory, which considers conversion to take place via pure collisions with the paramagnetic surface. The conversion on $CuSO_4$ at 273°K is dependent on pressure, this is in accord with the Wigner theory. The rate constant calculated from the Wigner theory using $r_s = 2\text{Å}$ gives a value of $3{\cdot}2 \times 10^{8}$ molecules cm^{-2} sec^{-1} at 273°K and 12 mm, compared to an observed value of $1{\cdot}33 \times 10^{10}$ molecules

cm^{-2} sec^{-1} which suggests that even at this temperature the conversion is not occurring via pure collisions but via an adsorbed layer on the surface of the catalyst. Calculations using the Eley and Harrison and McDowell treatments at 273°K on $CuSO_4$ were not possible owing to the uncertainty of adsorption data and other parameters.

Since theory predicts that the rate of paramagnetic conversion varies with μ_a^2, k_m/μ_a^2 should be constant for the series of sulphates examined in this work. Eley et al.[21] found that for the rare earth oxides k_m/μ_a^2 was approximately constant and slowly increased with increasing atomic number of the cation which was attributed to the lanthanide contraction. TABLE 6·36 gives data for the rates of conversion at 77°K at pressures of 5 mm together with values of μ_a and k_m/μ_a^2 for the corresponding ion.

TABLE 6·36

Sulphate	$k_m \times 10^{-12}$ (molecules cm^{-2} sec^{-1})	μ_a of M^{2+} (Bohr magnetons)	$k_m/\mu_a^2 \times 10^{-11}$
$CuSO_4$	5·73	1·8	1·76
$NiSO_4$	1·68	3·1	0·18
$CoSO_4$	2·74	5·05	0·11
$MnSO_4$	19·40	5·70	0·55

The ratio k_m/μ_a^2 does not give a constant value as might be expected. The most probable explanation of the discrepancy is that the adsorptive properties of the four sulphates are disimilar. A comparison of the k_m/μ_a^2 values would be more meaningful if the number of adsorption sites and the fraction of them which are catalytically active could be accurately estimated for each compound. Another possible reason for the discrepancy is the variation in parameters of the d-block ions on going from one salt in the series to the next. These parameters will vary to a much greater degree in the first row transition metal ions than in the rare earths where the ions have a much more compact electronic structure. This could account for the lack of correlation in the values of k_m/μ_a^2 obtained for the transition metal sulphates compared to the values of k_m/μ_a^2 obtained by Eley et al.[21] for the rare earth oxides. Without a knowledge of these parameters and the adsorptive properties of the sulphates any correlation between their catalytic activity and 3d orbital electrons is unobtainable, although it seems reasonable that one should exist.

(iv) <u>The effect of changing the anion on the catalytic properties of the cation</u>.

The effect of changing the anion on the catalytic properties of the cation has been investigated for the Co^{2+} ion. The kinetics of the conversion were studied from 77° to 300°K on $CoSO_4$, $CoCl_2$ and CoO.

The general kinetics of the conversion over the whole temperature range for $CoCl_2$ and $CoSO_4$ appear to be both explained by the Harrison and McDowell treatment, CoO would not be expected to conform to this treatment because of the contribution of a chemical mechanism to the total conversion. The kinetic data obtained of 77°K and 5 mm for $CuSO_4$, $CoCl_2$ and CoO is given below.

$CoSO_4$	$2{\cdot}74 \times 10^{12}$	molecules	cm^{-2}	sec^{-1}
$CoCl_2$	$11{\cdot}60 \times 10^{12}$	"	"	"
CoO	$3{\cdot}30 \times 10^{12}$	"	"	"

For $CoSO_4$ and $CoCl_2$ the conversion of 77°K has been shown to be purely physical in nature. Such a conversion depends on the magnetic properties of the Co^{2+} ion and it might be expected that the rate of conversion on $CoSO_4$ and $CoCl_2$ at 77°K would be the same. The reason for such a difference in the observed rates on these two salts can be attributed to several factors. Firstly the magnetic moment of the Co^{2+} ion in $CoSO_4$ (5·05 Bohr magneton) has been shown to be different from that in $CoCl_2$ (5·47 Bohr magneton), since the rate of conversion depends on μ_a^2 this could account for small numerical differences in the rates obtained for $CoSO_4$ and $CoCl_2$. The distance of closest approach, r_s, may be changed due to the differing radii of the anions which may sterically hinder or assist the approach of a hydrogen molecule to the cation. Since the rate

is dependent on r_s to the eighth power a small difference in r_s can alter the absolute rate by a considerable amount, as has been shown previously. Another factor is that on going from $CoSO_4 \rightarrow CoO \rightarrow CoCl_2$ there is a change of structure from distorted rhombic → sodium chloride → layer structure. This will mean that the arrangement of the Co^{2+} ions on the surface will alter thus affecting the rate of conversion. A difference in the number of adsorption sites and the fraction of them which are catalytically active could also affect the rate of conversion.

PART TWO

REFERENCES

1. Heisenberg;
Z.F.physik, 41,239,(1927).

2. Hund;
Z.F.physik, 42,93,(1927).

3. Mecke;
Z.F.physik, 31,709,(1925).

4. Eucken;
Sitzber.Preuss.Akad.Wiss., 41,(1912).

5. Dennison;
Proc.Roy.Soc., A115,483,(1927).

6. Bonhoeffer and Harteck;
Naturwiss, 17,182,(1929).

7. Bonhoeffer and Harteck;
Sitzber,Preuss.Akad.Wiss., 103,(1929).

8. Bonhoeffer and Harteck;
Z.physik.Chem., B.4,113,(1929).

9. Farkas;
Z.physik.Chem., B.10 ,419,(1930).

10. Farkas;
Z.physik.Chem., B.22,344,(1933).

11. Eley;
J.Phys. & Coll.Chem., 55,1017,(1951).

12. Bonhoeffer and Farkas;
Trans.Far.Soc., 28,242,(1932).

13. Rideal;
Proc.Cambr.Phil.Soc., 35,130,(1939).

14. Roberts;
Trans.Far.Soc., 35,941,(1935).

15. Eley;
Trans.Far.Soc., 44,216,(1948).

16. Couper and Eley;
Proc.Roy.Soc., 211.A,536,(1952).

17. Boreskov and Vassilevith;
Actes.2nd.Cong.Int.Catalyse, Vol.1,1095,(1961).

18. Wigner;
Z.physik.Chem., 823,28,(1933).

19. Kalckar and Teller;
Proc.Roy.Soc., A.150,520,(1935).

20. Harrison and MacDowell;
Proc.Roy.Soc., A.220,77(1953).

21. Ashmead,Eley and Rudham;
Trans.Far.Soc., 59,207,(1963).

22. Sandler;
Can.J.Chem., 32,249,(1954).

23. Eley;
Nature, 194,1076,(1962).

24. Eley and Rossington;
Chemisorption(Ed. W.E. Garner, Methuen,1957).

25. Couper and Eley;
Disc.Far.Soc., 8,172,(1950).

26. Bolland and Melville;
Trans.Far.Soc., 33,1316,(1937).

27. Farkas;
Light and Heavy Hydrogen (Camb.Un.Press),(1935).

28. Ashmead and Rudham;
Chem. and Ind., 401,(1962).

29. Brunauer, Deming and Teller;
J.Am.Chem.Soc., 62,1723,(1940).

30. Brunauer, Emmett and Teller;
J.Am.Chem.Soc., 60,309,(1938).

31. Hill;
Adv. in catalysis, 4,242.

32. Boer;
Chem.Soc.Ann.Meetings, (1967).

33. Farkas and Sandler;
J.Chem.Phys., 8,248,(1940).

34. Dowden,Mackenzie and Trapnell;
Proc.Roy.Soc., A.237,245,(1957).

35. Dowden,Mackenzie and Trapnell;
Ad. in catalysis, 9,65,(1953).

36. Winter;
J.Chem.Soc., 3824,(1955).

37. Charman,Dell and Teale;
Trans.Far.Soc., 59,453,(1963).

38. De and Stone;
Nature, 194,570,(1962).

39. Ashmead;
Ph.D thesis, University of Nottingham.

40. Fajans;
Z.physik.Chem., B.28,239,252,(1935).

41. Bonhoeffer,Farkas and Rummel;
Z.physik.Chem., B.21,225,(1933).

42. Dewing and Robertson;
Proc.Roy.Soc., A240,423,(1957).

43. Selwood and Turkevich;
J.Am.Chem.Soc., 63,1072,(1941).

44. Tarama;
Yuki Gosei Kagaku Kyakai Shi, 16,433,(1958).

45. Harrison,Nicholls and Steiner;
J. of Catalysis, 7,359,(1967).

46. Tompkins;
Personal communication.

47. Ostroff and Sanderson;
J.Inorg.Nucl.Chem., 9,45,(1959).